Piotr Wiśniewski

Numerical modelling of phase-change processes in humid air transonic flows

Doctoral dissertation

Scientific discipline: Environmental Engineering, Mining and Energy

Silesian University of Technology

Faculty of Energy and Environmental Engineering

Department of Power Engineering and Turbomachinery

Gliwice, Poland, 2022

Silesian University of Technology

Author:

mgr inż. Piotr Wiśniewski

Silesian University of Technology

Faculty of Energy and Environmental Engineering

Department of Power Engineering and Turbomachinery

Konarskiego 18

44-100 Gliwice

Poland

e-mail: piotr.wisniewski@polsl.pl

Supervisor:

Prof. dr hab. inż. Sławomir Dykas

Silesian University of Technology

Faculty of Energy and Environmental Engineering

Department of Power Engineering and Turbomachinery

Konarskiego 18

44-100 Gliwice

Poland

e-mail: slawomir.dykas@polsl.pl

Polish title of the PhD dissertation:

Modelowanie matematyczne przemian fazowych w przepływach transonicznych powietrza wilgotnego

Acknowledgement

I would like to thank everyone without whom this work would not have been possible. I express my sincere gratitude to my supervisor, prof. dr hab. inż. Sławomir Dykas, for his guidance and tutelage.

I thank dr hab. inż. Mirosław Majkut, prof. of the SUT, for his help during the experimental measurements. I extend my gratitude to prof. Satoru Yamamoto and prof. Jens Friedrichs for invitation and support during my research-related stays abroad. Special thanks are directed to Tim Wittmann, whose help increased my understanding of the phase-change phenomenon on the one hand, but also my awareness of the need for international collaboration on the other.

I would also like to thank the European Union through the European Social Fund for financial support under the POWR.03.05.00-00-Z305 project and the Polish National Agency of Academic Exchange for financing my stay at Tohoku University under the NAWA 2021 BPN/BEK/2021/1/00011/U/00001 grant.

Last but not least, I wish to thank my parents, my brother, my closest family and friends for their unflagging support and motivation during the period of this challenge, which the doctorate undoubtedly is.

Nomenclature

Latin symbols

a	speed of sound, $m \cdot s^{-1}$
A	area, m^2
AoA	angle of attack, º
bf	blending parameter, -
c	chord length, m
C	Kantrowitz correction, -
C_d	drag coefficient, -
C_l	lift coefficient, -
c_p	specific heat at constant pressure, $J \cdot kg^{-1} \cdot K^{-1}$
C_p	pressure coefficient, -
D	turbulence kinetic energy cross-diffusion, -
d	diameter, m
E	energy, $J \cdot kg^{-1}$
$\mathbf{F}$	force vector, N
f	frequency, Hz
G	turbulence kinetic energy generation
$\mathbf{g}$	gravitational acceleration vector, $m \cdot s^{-2}$
h	enthalpy, $J \cdot kg^{-1}$
h	height, m

J	nucleation rate, $kg^{-1} \cdot s^{-1}$
k	turbulence kinetic energy
k_B	Boltzmann constant, $J \cdot K^{-1}$
Kn	Knudsen number, -
L	latent heat, $J \cdot kg^{-1}$
l	length, m
l	specific work, $J \cdot kg^{-1}$
l_S	mean free path, m
M	Mach number, -
m	mass, kg
m	molecular mass, $g \cdot mol^{-1}$
$\dot{m}$	mass steam, $kg \cdot s^{-1}$
n	number of droplets, kg^{-1}
p	pressure, Pa
p	amplitude, Pa
$\dot{P}$	expansion rate, s^{-1}
Pr	Prandtl number, -
q_c	condensation correction coefficient, -
R	individual gas constant, $J \cdot kg^{-1} \cdot K^{-1}$
r	radius, m
r^*	critical radius, m

Re	Reynolds number, -
s	entropy, $J \cdot kg^{-1} \cdot K^{-1}$
S	source term, -
S	supersaturation, -
t	temperature, ºC
T	temperature, K
v	velocity vector, $m \cdot s^{-1}$
x	humidity, -
x, y	coordinates in the Cartesian coordinate system, -
y	mass humidity degree, -
Y	turbulence kinetic energy dissipation, -
y	liquid water mass fraction, -
y^+	non-dimensional wall distance, -
z	position along the blade, m

Greek symbols

α_c	correction coefficient, -
α	mass fraction, -
α	correction coefficient, -
γ	heat capacity ratio, -
δ	Kronecker delta
η	efficiency, -

λ	conductivity, $W \cdot m^{-1} \cdot K^{-1}$
μ	dynamic viscosity, $kg \cdot m^{-1} \cdot s^{-1}$
ρ	density, $kg \cdot m^{-3}$
σ	surface tension, $J \cdot m^{-2}$
υ	correction coefficient, -
φ	relative humidity, %
ω	turbulence energy dissipation rate, -
$\boldsymbol{\tau}$	stress tensor, $N \cdot m^{-2}$
ζ	entropy loss coefficient, -

Acronyms and abbreviations

CFD	computational fluid dynamics
con	Continuous
DPET	Department of Power Engineering and Turbomachinery
DPM	discreet particle model
EXP	Experiment
FS	Fuchs-Suttugin
GY	Gyarmathy
HK	Hertz-Knudsen
HS	solid particles
HW	liquid droplets
IAPWS	International Association for the Properties of Water and Steam

IWSMP	International Wet Steam Modelling Project
NASA	National Aeronautics and Space Administration
PDE	partial differential equation
PM	respirable and fine suspended particles
SF	single-fluid
SST	shear stress transport
SUT	Silesian University of Technology
UDF	user defined function
YO	Young

Subscripts

0	total parameters
1-4	position along the flow
∞	free stream
a	Air
a	Adiabatic
b	Back
E	Energy
eff	Effective
het	Heterogeneous
hom	Homogeneous
i, j	matrix position

inv	Inviscid
l	Liquid
max	Maximum
p	Particle
s	Saturation
v	Vapour

Introduction

Multiphase flows with phase transition are ubiquitous both in the environment and in engineering. The phase transition from steam (also called water vapour) to liquid water is the best-known case of condensation. It occurs when a decrease in pressure or temperature causes steam to cross the saturation line. Condensation is important for efficient design of machinery and equipment in many industries. Traditionally, research on condensation has focused on pure steam flows. Recently, however, there has been a significant increase in the interest in the condensation of air-steam mixtures. For example, the operation of turbines in fuel-cell turbochargers involves condensing air-steam mixtures. Condensation may also occur in present and future aircraft engines with transonic fans. For these and other applications, numerical methods are an important design process tool. However, the existing numerical methods are only reliable for pure steam flows. They require further development to account for condensation in air-steam mixtures.

In nature, expansion and condensation occur slowly. This allows steam to condense on pre-existing surfaces such as dust particles. Such a process is called heterogeneous nucleation. In expanding flows in engineering, the drop in pressure or temperature is much faster, and the number of particles available for heterogeneous nucleation is usually insufficient. Therefore, the flow supercools and a thermodynamic non-equilibrium is established. When the supercooling is strong enough, homogeneous nucleation occurs. In this case, nuclei form directly from steam, without any pre-existing surfaces. Once these nuclei reach the critical radius, they grow rapidly as the surrounding supercooled steam condenses onto the droplets. Homogeneous nucleation and subsequent condensation of steam can thus be viewed as a spontaneous reversal from a metastable state to a stable state. However, it has to be remembered that in many engineering applications there is a transition from the sonic to the subsonic flow. The transition involves flow discontinuities in the form of a shock and a sudden change in flow properties. The question is whether the supercooled droplets will evaporate on collision with the shock, or whether they will be thrown off the metastable state and form ice crystals. Homogeneous nucleation, condensation and evaporation pose a number of challenges to numerical calculation. The spontaneity of nucleation makes condensation sensitive to even smallest changes in flow and substance properties. Moreover, the dispersive nature of the droplet phase and the wide range of relevant sizes in engineering applications require extensive modelling instead of direct calculations. As a result, models typically rely on calibration with

validation cases such as supersonic nozzle flows. Such validation cases have been published for a number of pure steam flows, as well as for a few cases with humid air at ambient conditions. Other than that, no research has been published on condensation in a wide range of other possible temperatures, pressures and mass fractions of air-steam mixtures.

In order to meet the challenges of improving the efficiency of turbomachinery, it is necessary to develop robust and reliable numerical tools. State-of-the-art commercial and academic codes give the information needed for design and operation. Nevertheless, there are still phenomena that have to be taken into account and validated to provide a reliable solution. One of these is the phase change in multi-species transonic flows, which is a crucial aspect for future turbomachinery, such as fuel-cell turbochargers or compressor rotors, and fans of aviation turbines. However, in order to create a reliable numerical model, extensive validation is needed. And for this, experimental testing is a must.

1.1 Objectives and scope

This work aims to develop a robust numerical tool for the study of the phase change occurring in humid air and evaluation of its importance in energy machines. This goal will be achieved in the following stages:

1) in-depth analysis and selection of condensation models for the numerical study of humid air transonic flows;

2) experimental study of atmospheric air expansion in symmetric and asymmetric nozzles with a low expansion rate;

3) evaluation of the phase-change impact on the performance of future machinery;

4) a proposal for a substantial improvement in numerical methods intended for condensing flows.

The detailed aim of each stage is as follows:

The first goal of this work is a thorough analysis of the reliability of available condensation models for the humid air flow. In the past condensation was considered mostly in pure steam and was neglected in the case of humid air flows. Although recently there has been a growing interest in condensation occurring in humid air, or generally in mixtures containing steam, the applicability of the findings for atmospheric air is poorly recognized. This is mainly due to the background of the research, i.e. the focus on the condensation model for pure steam flows.

Therefore in this work, the applicability of the presented condensation models is analysed thoroughly to find a reliable approach for the numerical modelling of humid air condensing flows.

The second goal of this work is to fill the gap in the experimental study of the expanding flow. For this purpose, the existing experimental facility at the SUT was extended to perform nozzle experiments with condensing flows with a low expansion rate. It was expected that the results would provide a solid basis during the numerical model validation process, especially with regard to the impact of the phase change on the position of the shock wave in the transonic flow. The obtained results enabled further development of the existing thermodynamic models for accurate calculation of condensing flows of multicomponent mixtures. Additionally, an open test case was created. In general, all research teams working on numerical methods related to condensation rely on test cases to validate and calibrate their models. No other experiments have been published for the operating conditions studied in this project. Therefore, it is expected that an open test case using experimental data and numerical meshes, along with the results obtained herein, will have a lasting impact on the field.

The next goal is to study the influence of condensation on the performance of modern turbomachinery. After a reliable tool is obtained to investigate condensation in internal and external flows, a comprehensive study is to be carried out with a focus on the work of the first stage of the compressor of a turbine and the fan of a turbofan engine. The aim of this research is to investigate numerically the influence of condensation, as well as evaporation, on the performance of turbomachinery working on atmospheric air containing solid and liquid suspended particles.

An additional effect of this work is a comparison of modelling approaches to substantially improve numerical methods for the calculation of condensing flows. So far, mostly monodisperse Euler approaches have been used, which consider not only the gas phase but also the droplet phase as a continuum [1]. These approaches are quite robust and fast. However, most of them introduce simplifications, such as the omission of the full droplet spectrum or slip velocities between phases. These aspects are particularly important in flows with a high swirl or when droplets reach a size of the order of micrometres. An alternative is the Euler-Lagrange approach which represents the droplet phase with discrete particles. It is capable of resolving the entire droplet spectrum, individual droplet trajectories, and also interphase slip velocities. However, the Euler-Lagrange approach is computationally expensive and less robust,

especially if discontinuities appear in the fluid in the form of shock waves. This work aims to compare the two approaches and develop a technique that will benefit from both, while maintaining adequate stability and robustness. The combination of the Euler and the Euler-Lagrange approach will make it possible to make use of the advantages of the two methods. The concept for this is a one-way coupling, where the Euler mixture results are post-processed using the Euler-Lagrange method.

1.2 Literature review

Flows with a phase change are certainly omnipresent in both nature and engineering. Cloud formation, rain, blizzards, etc. are the effect of a phase change. Phase-change processes can be utilized for example in steam generation in power stations and in processes related to iron solidification in iron casts. These processes have attracted researchers' attention for ages. One of the most common flow mediums in engineering is air. Unless pre-dried, air always contains a certain amount of water vapour. The influence of the phase change on the flow structure and operating conditions of machines is particularly interesting.

The presence of water or steam in atmospheric air exerts a significant influence on flow parameters in elements of any devices or machines. In the conditions of the wet steam flow, it can be assumed that it affects their durability, accuracy and efficiency [2]. If unfiltered or wet, atmospheric air always contains a certain amount of suspended solid particles, water droplets (fog, rain, etc.) or steam. Air cleaning or drying is not feasible in many technical applications, e.g. in turbine engines. Therefore the impact of such impurities on the flow in turbomachinery needs to be investigated.

In the case of transonic flows, phase-change phenomena can be divided into homogeneous and heterogeneous processes depending on the condensation trigger. Spontaneous nucleation occurs due to the process of rapid supersaturation (or supercooling) of gas when the appearing condensation nuclei reach the critical radius triggering the homogeneous condensation phenomenon. If the air contains suspended particles, condensation may occur on them. This process is referred to as heterogeneous condensation. The tiny droplets formed due to nucleation or on the suspended particles grow further. In favourable conditions, they can reach significant sizes and form so-called coarse droplets. The condensation process can be rapid, especially during gas expansion in the convergent-divergent nozzle (CD nozzle), where supersonic conditions are reached in the nozzle divergent part. The phase-change phenomena are related

to the interphase latent heat exchange. During the condensation process, latent heat is released from condensing steam to the gaseous phase. This affects the flow structure by changing the gas pressure, temperature and, thereby, velocity. The influence of the latent heat release is of major importance during the occurrence of rapid homogeneous condensation. The so-called condensation wave then appears, followed by a sudden release of a high amount of energy. On the other hand, if the air contains suspended particles, heterogeneous condensation becomes the major phase-change process, which has a more gradual character but results in the formation of droplets with a relatively large size, depending on the initial size of the foreign nuclei.

Evaporation is a process opposite to condensation. If the droplet evaporates, latent heat is absorbed from the gaseous phase in the phase-change process, leading to a local drop in the fluid temperature, pressure, and therefore – in its density, velocity, entropy, etc. If the flow is supersonic, shock waves arise and the liquid droplets interacting with the shock wave tend to evaporate. This process is particularly interesting if the liquid fraction (e.g. fog or rain) is significant because it then results in the absorption of a relatively large amount of latent heat.

Most often homogeneous and heterogeneous condensation processes appear together. Only their share in the liquid phase formation may change depending on the air parameters. The parameter usually used to define the content of steam in humid air is called relative humidity, which is the relative value of the ratio of the mass of steam in the air to the total mass of steam the air can hold. Typical humidity values range from 40% to 50%. However, due to a change in weather conditions, the relative humidity level can reach as much as 100%. If the mass of steam in atmospheric air exceeds the mass of steam the air can hold, the excess steam condenses creating fog. It has to be emphasized that the mass of steam that the air can hold, and therefore the air relative humidity, is strictly related to the air temperature and pressure. If the air temperature rises, the steam saturation pressure increases and, as a result, air can hold more steam. Therefore, the impact of temperature is crucial if condensation occurs. Another air parameter that has a major impact on phase-change phenomena is the number and diameter of the particles suspended in the air. If the number of particles is significant, heterogeneous condensation might become the major phase-change phenomenon, weakening the influence of homogeneous condensation and weakening the condensation wave. Taking account of the impact of phase-change phenomena on the most crucial parameters of the transonic moist air flow, it must be stressed that the aforementioned factors (i.e. humidity, air parameters, presence

of suspended solid or liquid particles) should be taken into consideration in CFD modelling of such flows.

Internal and external condensing flows have been investigated intensively for over 50 years and are still of great interest to researchers all over the world [3]. They were initiated with a view to increasing the reliability and efficiency of steam turbines. In the 1960s Gyarmathy proposed one of the most popular models of the droplet growth to model the steam condensing flow in the turbine. Gyarmathy's model [4] was further modified by Young [5,6] and by Fuchs and Suttugin [7] in the 1970s, and provides slightly better predictions of the growth of nanosized droplets. Despite the fact that research in this field was initiated a long time ago, experimental studies on steam condensation are still continued; they are also complemented with numerical research [8,9,10,11]. The research conducted at the DPET of the SUT as part of the International Wet Steam Experimental Project (IWSEP) focuses on the experimental study of the pressure distribution in the condensing flow, as well as on the size of the condensate droplets for a wide range of steam parameters [12]. State-of-the-art condensing flow numerical investigation is described in the paper summing up the International Wet Steam Modelling Project (IWSMP). The aim of the project was to compare the numerical approaches adopted by world-renowned research groups and provide reliable reference for further research [1].

So far the use of experimental techniques has resulted in significant progress in the research on transonic flows of atmospheric air. For example, at an aerodynamics congress in 1935 Prandtl demonstrated a *schlieren* picture of two crossing oblique shock waves near the throat of a nozzle with a flow with no back pressure. It was concluded that the presented structure was dependent on the air initial humidity. The disturbance was called a condensation shock wave, which in the case of a nozzle flow has an X-shaped structure. In the 1990s Schnerr performed CFD calculations on different types of supersonic nozzles, confirming numerically the presence of an X-shaped condensation wave in nozzle flows [13,14,15]. The process of water vapour condensation in the atmospheric air flow is still topical and concerns both external [13,16] and internal flows [15,17].

The condensation phenomena in internal and external transonic humid air flows have been the focus of a lot of research, with studies initiated over 30 years ago and continuing to present times [15]. The experimental and numerical studies regarding humid air internal flows through CD nozzles conducted by Schnerr et al. [18,14,13] became the reference for researchers for the modelling of both moist air and pure steam condensing flows. Adam investigated, both

experimentally and numerically, the non-stationarity of the flow, especially the impact of relative humidity on the interaction between condensation and shock waves and the oscillation frequency in a nozzle with parallel walls downstream of the throat [19]. A 3D academic in-house code was developed by Dykas et al. [20,21,22,23]. It treats the air-steam mixture as a homogeneous fluid and was validated against in-house experimental studies. The code enables robust computation of condensation in internal and external flows [24,25]. Recently, it became the basis for the model external implementation in commercial software [26,27,28,29]. The functionality of the model implemented in commercial software was extended by allowing slip velocity consideration, i.e. investigation of the difference between liquid- and gaseous-phase velocities, which is especially important if droplets reach a relatively large size or if the flow has a significant swirl [30,21,31]. Valuable techniques of condensation simulation in complex 3D structures were introduced by Yamamoto [32,33,34]. The numerical study of condensation is extremely demanding in terms of computing power, but the latest advancements have led to attempts to simulate the entire compressor rotor with a non-uniform circumferential distribution of wetness at the inlet [35]. The liquid water content at the jet engine inlet was studied by Moriguchi et al., who proved a significant change in air parameters at the compressor rotor outlet due to water evaporation [36]. Wiśniewski et al., studied the impact of suspended liquid and solid particles on the expansion phenomena in low expansion rate nozzle and on the efficiency of turbomachinery [37,38]. Most numerical studies regarding condensation are performed based on the single-fluid approach, using the assumption of a continuous fluid for the mixture of air, steam and water. This approach gives reliable results if the droplet inertia and temperature between the phases are negligible. However, if the swirl of the flow of droplets is significant or if the droplets are relatively large, air and water should be considered as separate phases using the two-fluid approach [39]. Some attempts have been made to model multi-phase humid air and wet steam flows [40,41], which is especially important in future propulsion systems using fuel cells. Wittmann et al. developed a Lagrangian model for the study of the condensation impact on fuel-cell turbochargers [42,43,44].

Condensation is not only present in humid air. In fact, the described models were developed based on the wet steam condensing flow, which is still an open research issue. Therefore, similar models have been adjusted to simulate condensation in pure steam [41,45] or other gases, such as CO_2 [46,47]. Condensation is considered in many branches of industry, starting from steam energy systems, thorough modern propulsion systems and ending with evaluation of the condensation potential for sea water distillation [21,48,49].

This brief literature review shows the importance of and the need for further both experimental and numerical studies to improve the understanding of phase-change phenomena in multi-species expanding flows. A better understanding of the phenomena related to evaporation and condensation in transonic flows will make it possible to design highly efficient and reliable devices and turbomachinery for state-of-the-art engineering solutions.

Atmospheric air

Like any substance, water can exist in three basic states. It is a single-species substance which can exist in up to three phases simultaneously, depending on pressure and temperature (see Figure 2.1). However, when considering a mixture of different substances, the mixture phases are determined by physical properties of all the substances involved. One of the most common multi-species mixtures in nature is atmospheric air, which is a solution (mixture) of dry air and water that takes the form of vapour, liquid droplets (e.g. fog, cloud) or ice crystals (e.g. ice mist, snow). The occurrence of individual water phases is determined by the mixture properties, such as temperature, pressure, saturation properties, water partial pressure, dew point, etc. When such a thermodynamic system crosses the saturation line, saturation is reached and a phase change may occur. Crossing at a temperature above the triple point causes condensation; below the triple point, sublimation occurs. At constant pressure, the temperature at which humid air reaches saturation is called the dew point. When humid air is cooled below the dew point, the vapour enters a metastable state of supercooling. Depending on the supercooling, the temperature, and the presence of a sufficient number of nuclei, the case is either condensation or sublimation. In nature, condensation often occurs through isobaric cooling by means of an external heat sink.

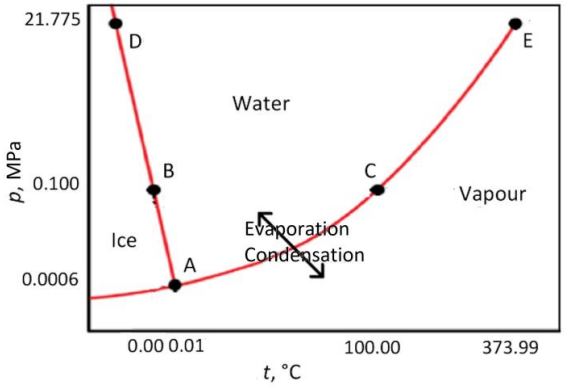

Figure 0.1. Water phase diagram, A – triple point, B – normal freezing point, C – normal boiling point, D – critical pressure, E – critical point

In engineering, condensation is often triggered in adiabatic systems with rapid expansion, such as accelerated flows. It is particularly important for transonic flows, i.e. flows with Mach numbers in the range of ~0.8 to ~1.2. As the fluid temperature and pressure drop due to the flow acceleration, saturation pressure decreases and falls below the vapour partial pressure. This

causes the flow to supercool and thermodynamic non-equilibrium conditions are established. When sufficient supercooling is achieved, droplets form by nucleation. Their further growth by condensation is caused by the impingement of water molecules on the droplet. This phase change can have a very abrupt character, leading to significant changes in the flow structure. Due to the rapid condensation process, a large amount of latent heat is locally transferred to the fluid. As a result, the so-called condensation wave is formed, which is accompanied by a local increase in pressure and temperature. In the case of transonic flows, the droplets encounter a shock wave on which they evaporate, which results in a local drop in pressure and temperature. Moreover, a transient condensation wave in the presence of pressure waves in the transonic flow, such as shock waves or expansion waves, can cause complex interaction phenomena. In particular, the unsteady character of pressure waves and condensation waves can lead to symmetric and asymmetric flow oscillations [19].

1.3 Thermodynamic description

Both in nature and in industrial applications gases occur in the form of a mixture. If a mixture of dry air (or another inert gas) and water in the form of vapour occurs, the case is a moist gas. If water is in the liquid form, the case is wet air. Moist air mass m is defined as the sum of the mass of air m_a and the total mass of water vapour m_v:

$$m = m_{\mathrm{a}} + m_{\mathrm{v}} \tag{2.1}$$

The water content in the gas is determined by specifying its absolute humidity, i.e. the ratio between the mass of water vapour to the mass of dry air:

$$x = \frac{m_{\mathrm{v}}}{m_{\mathrm{a}}} \tag{2.2}$$

Customarily, relative humidity φ is used as the quantity to define the water content in air. Relative humidity defines the ratio of the real amount of water to the maximum amount of water that can take the gaseous form for certain thermodynamic parameters. Using Dalton's law, governing moist gases at a not very high pressure, water vapour pressure p_v and dry gas pressure p_a give the pressure of the mixture – p.

$$p = p_{\mathrm{a}} + p_{\mathrm{v}} \tag{2.3}$$

The water vapour pressure component must not exceed the maximum value established through the state of equilibrium in the mixture, where vapour would occur in the non-saturated state. This means that the vapour pressure value cannot exceed saturation pressure, and the ratio between the two quantities is referred to as relative humidity. In practice, the relative moisture value is given for total, i.e. stationary parameters, and it is expressed in percentages:

$$\varphi_0 = \frac{p_{\mathrm{v},0}}{p_{\mathrm{s}}(T_0)} \cdot 100\% \tag{2.4}$$

where $p_s(T_0)$ is the steam saturation pressure depending on temperature. Knowing the mixture relative humidity, pressure and temperature, the absolute humidity value can be determined using the following equation:

$$x = \frac{R_{\mathrm{a}}}{R_{\mathrm{v}}} \frac{1}{\frac{p_{\mathrm{v},0}}{\frac{\varphi_0}{100} p_{\mathrm{s}}(T_0)} - 1} \tag{2.5}$$

where R_{a} and R_{v} are individual gas constants of dry air and water. If air contains liquid water, the mass degree of humidity y is often defined apart from humidity; the degree of humidity is the ratio of the condensate mass (liquid water) to the mass of moist air.

$$y = \frac{m_{\mathrm{l}}}{m} \tag{2.6}$$

The humidity degree maximum value is defined in the case of complete condensation of all the water contained in air. The relation between the maximum mass degree of humidity y_{max} and absolute humidity is expressed in the following way:

$$y_{\max} = \frac{x}{1 + x} \tag{2.7}$$

In the case of moist air, the temperature equilibrium is often assumed for the mixture:

$$T = T_{\mathrm{a}} = T_{\mathrm{v}} = T_{\mathrm{l}} \tag{2.8}$$

The assumption can be justified easily in cases where the phase change occurs slowly. If the phase change occurs abruptly and fast, the temperature difference between the phases can be essential with a substantial effect on the process of nucleation and the droplet growth. However,

if numerical models are used, the phenomenon is often omitted to simplify the applied mathematical models and its impact is taken into account in the form of correction factors. Introducing thermal equilibrium between the phases, it is possible to use Dalton's law and calculate the partial pressure of vapour in wet air from the following relation:

$$p_{\mathrm{v}} = p\frac{(y_{\max} - y)}{\frac{R_{\mathrm{a}}}{R_{\mathrm{v}}}(1 - y_{\max}) + (y_{\max} - y)} \tag{2.9}$$

The derived relations and the adopted simplifications enable determination of the gas constant, specific heat at constant pressure c_{p} and the adiabatic exponent γ. These properties are calculated using mass fraction α of each gas contained in the mixture, omitting water in the liquid form. However, it should be noted that in phase-change flows the properties vary:

$$R = (1 - \alpha)R_{\mathrm{a}} + \alpha R_{\mathrm{v}} \tag{2.10}$$

$$c_{\mathrm{p}} = (1 - \alpha)c_{\mathrm{p,a}} + \alpha c_{\mathrm{p,v}} \tag{2.11}$$

$$\gamma = (1 - \alpha)\gamma_{\mathrm{a}} + \alpha\gamma_{\mathrm{v}} \tag{2.12}$$

Air and water vapour density ρ_{a} and ρ_{v}, respectively, are calculated in the following way:

$$\rho_{\mathrm{a}} = (1 - \alpha)\rho \tag{2.13}$$

$$\rho_{\mathrm{v}} = \alpha\rho \tag{2.14}$$

Quantities such as enthalpy h, and entropy s for the mixture, considering liquid water, take the following form:

$$h = (1 - y)((1 - \alpha)h_{\mathrm{a}} + \alpha h_{\mathrm{v}}) + yh_{\mathrm{l}} \tag{2.15}$$

$$s = (1 - y)((1 - \alpha)s_{\mathrm{a}} + \alpha s_{\mathrm{v}}) + ys_{\mathrm{l}} \tag{2.16}$$

Physical parameters of water vapour and air, i.e. specific heat, surface tension, viscosity, evaporation heat, etc. are calculated in two ways. They are mainly found from empirical relations derived based on experimental data and available in the libraries of the International Association for the Properties of Water and Steam (IAPWS). It should be noted, however, that

these libraries have a limited range. Therefore, beyond the area of their correctness, analytically derived relations should be used [50,19].

1.4 Moist air expansion

Phase changes can occur in flows with no participation of an external heat source. Expansion is an example of such a phenomenon. During expansion the fluid pressure and temperature fall due to a rise in the fluid velocity. Physical parameters of the fluid determine its state of aggregation. If the steam parameters drop below the parameters of saturation, condensation occurs. This is especially important in the case of transonic and supersonic flows. In such flows, due to acceleration, temperature and pressure fall to very low values causing supercooling of steam, which leads to a violent phase change. It should be noted that in supersonic flows the water created due to condensation is supercooled. In other words, it is in a metastable state, which is highly unstable because, due to collisions with walls limiting the flow or with other droplets, the droplets of supercooled water may transform into ice. This phenomenon is particularly dangerous in aircraft engineering. The icing of the plane wings, fuselage or instrumentation may cause a malfunction or, at worst, an aviation disaster.

A flow is referred to as transonic if its velocity oscillates around the local value of the speed of sound. It is accepted that transonic flows occur in the range of velocities reaching the Mach number (M) values of 0.8 to 1.2, where the Mach number is expressed as the ratio between the air velocity and the local speed of sound. In fact, however, any flow in which transition occurs from the subsonic to the supersonic flow and vice versa can be called transonic.

In some engineering applications it may be assumed that a change in the fluid density and temperature due to a change in velocity is negligible. A flow of this kind is referred to as incompressible. Such a simplification can be used for low-velocity flows with the Mach number $M<0.3$. If the velocity values are high, the flow should each time be treated as compressible. Moreover, this simplification may not be used in analyses of non-stationary or acoustic effects because these are related to local changes in the fluid density.

The most common cases of the occurrence of a transonic flow are expansion in the de Laval nozzle and the flow around an aerodynamic airfoil profile. In an internal diabatic flow, such as the moist air flow through a convergent-divergent nozzle, the fluid temperature and pressure fall due to a rise in the fluid velocity. This leads to a heat exchange between the liquid and the gaseous phase on the condensation wave and on the shock wave. In the case of an external

diabatic flow, such as the flow around a plane wing, the condensation phenomenon may already occur for flight velocities of M~0.7, especially at high angles of attack. This is related to local acceleration of the fluid, which on the suction face of the wing can reach velocity values close to or higher than the speed of sound. Like in the internal flow, a drop in the fluid parameters causes local and abrupt condensation. The described type of the external flow with local velocity values exceeding the speed of sound involves the occurrence of a shock wave on which water evaporates. The phenomenon of condensation and evaporation is due to evaporation heat being supplied and carried away abruptly. It changes the nature of the flow around the profile and results in a change in the aerodynamic perfection characteristic.

Condensation can be spontaneous in character. Steam supercooling, i.e. a drop in saturation pressure and temperature below partial-property values, triggers the nucleation process. Nucleation consists in the formation of nuclei due to supercooling and fluctuations in density. If the nuclei reach a size bigger than critical, they may grow further; if the critical size is not achieved, they disintegrate. At high supercooling values, a great number of nuclei are created abruptly in the nucleation process, which causes abrupt condensation. This phenomenon is referred to as homogeneous condensation. Homogeneous condensation is triggered by particles suspended in the fluid. Both in internal and external flows air filtering or drying is often technically impossible. This means that the fluid contains water vapour and solid or liquid impurities. As there is no nucleation, heterogeneous condensation is less violent than homogeneous condensation, but it may result in the formation of droplets with a considerable size. The two condensation types usually occur in parallel, but if the number of suspended particles is very high, heterogeneous condensation may become the main source of the phase change.

The liquid created due to condensation forms a mist with a large number of tiny droplets. Depending on the phenomenon intensity and the environment of its occurrence, the droplets arising due to homogeneous condensation have the dimensions ranging from several to a few dozen nanometres. In the case of heterogeneous condensation, the size of the droplets is related to initial dimensions of the nuclei present in the fluid. If the flow is transonic, water droplets evaporate during the transition through the shock wave on which a violent rise in temperature and pressure occurs. The evaporation of the droplets results in an abrupt drop in the fluid temperature due to absorption of evaporation heat, and this has an effect on the location of the shock wave. It should be noted that condensation usually occurs at low temperatures and low

pressures, the values of which point to the solid form of water, whereas the water in the droplets is in the supercooled liquid phase form. This can be explained by high pressure values, of the order of megapascals, inside the droplet due to the work of the droplet surface. In the supercooled state, the liquid may easily transform into a solid body (ice). Such a phenomenon occurs if the liquid is thrown off its metastable state, for example due to a collision with another droplet or with a wall limiting the flow. The phenomenon of water freezing due to contact with the walls limiting the flow is called icing. It is extremely undesirable and in fact dangerous in aviation. The icing of the plane wings, fuselage or measuring instruments may result in malfunctions and pose an aviation disaster hazard. Additionally, a question arises whether a phase transition from the liquid to the solid state is possible due to the droplet being thrown off the state of equilibrium on aerodynamic (expansion and compression) waves. The answer to this and other questions can be found by means of experimental, numerical and analytical studies.

1.5 Basic flow parameters of moist air

The modelling of flows involving phase changes is particularly challenging. Due to the transport of mass, momentum and energy from the gas to the liquid or to the solid body, the properties determining the flow tend to change. One of such varying quantities is the speed of sound – in water it is about four times higher than in air. The speed of sound is a quantity determining the rate of propagation of density fluctuations. It depends on the elasticity and density of the fluid or the solid body and is defined as:

$$a^2 = \left.\frac{\partial p}{\partial \rho}\right|_s \tag{2.17}$$

The above relation can be simplified introducing the ideal gas assumption:

$$a^2 = \gamma RT \tag{2.18}$$

where the speed of sound depends only on temperature and on the medium under consideration.

The density of water contained in a mixture has a substantial impact on the density of the whole mixture and as such should not be omitted. Taking account of the density of air, water vapour and water, the following relation can be derived:

$$\frac{1}{\rho} = (1-y)\left((1-\alpha)\frac{1}{\rho_a} + \alpha\frac{1}{\rho_v}\right) + y\frac{1}{\rho_l} \tag{2.19}$$

In the case of a moist air flow with a phase change, the heat exchange phenomenon occurs. The latent heat release or absorption due to condensation or evaporation has an impact on the gaseous phase, the enthalpy of which can be written as:

$$h = (1-y)\big((1-\alpha)h_a + \alpha h_v\big) + yL \tag{2.20}$$

where L is latent heat. Considering the temperature equilibrium of the gaseous phase in the mixture (equation 2.8) and the moist air specific heat (equation 2.11), its enthalpy can be written as:

$$h = (1-y)c_p T + yL \tag{2.21}$$

According to the energy conservation law, the adiabatic flow total enthalpy must be constant:

$$h_0 = h + \frac{u^2}{2} = c_p T + \frac{u^2}{2} = const \tag{2.22}$$

However, if the flow involves a phase change, the equation should be extended with term yL, which results from the release and absorption of latent heat due to condensation and evaporation:

$$h_0 = h + \frac{u^2}{2} = c_p T + \frac{u^2}{2} + yL \tag{2.23}$$

It should be noted that the gas specific heat due to the mass content of air and water vapour in atmospheric air varies in the range of less than 3% (see the Figure 2.2). Taking account of the considerable increment in temperature and of the fact that the velocity value at which abrupt condensation occurs is about 400m/s, which in the total enthalpy equation is raised to the second power, it may be assumed that the impact of changes in specific heat is negligible. This reasoning leads to the following relation:

$$\Delta T_0 = T_{0,2} - T_{0,1} = \frac{yL}{c_p} \tag{2.24}$$

Figure 2.2 shows the increment in total temperature in a moist air flow due to condensation under the assumption that during the condensation process all the water vapour contained in air is transformed into a liquid form. As illustrated by the figure, a rise in temperature and relative humidity is accompanied by a higher increment in temperature due to condensation. This is related to a bigger content of water vapour in air, which means a bigger amount of released latent heat.

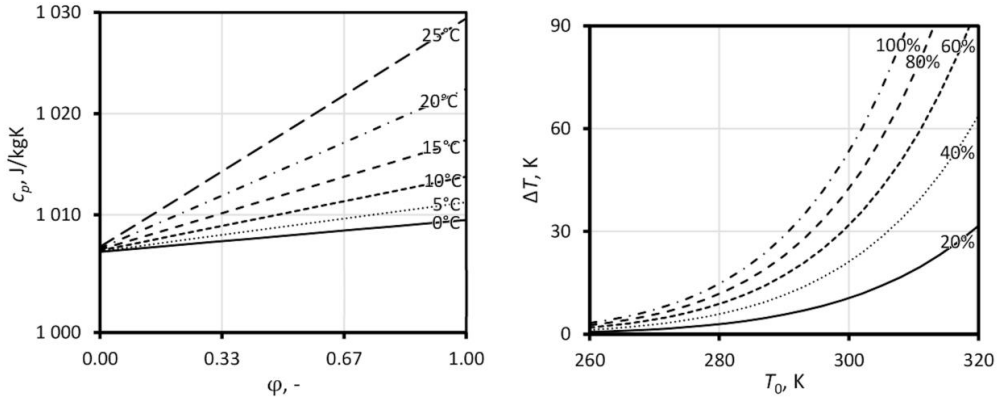

Figure 0.2. The impact of relative humidity on the value of specific heat at constant pressure (left) and the impact of total temperature and relative humidity on the temperature increase on the condensation wave (right)

It has to be mentioned that during the condensation process very small droplets appear in the flow, which has a significant impact on the pressure inside it. The molecules on the surface of the droplet are forced inwards due to surface tension. Therefore the pressure inside the drop must rise to achieve force equilibrium. The resultant pressure inside the droplet, p_l, can be computed as follows:

$$p_l = p + \frac{\sigma}{r} \tag{2.25}$$

where p is the continuous fluid pressure, σ is the surface tension and r is the droplet radius. If the droplet is very small, the pressure inside the droplet can reach values of the order of 10^9 Pa, which in the case of water can justify the phase transition from vapour to a liquid instead of a solid form, in other words, condensation instead of sublimation.

Figure 2.3 presents the effect of condensation on expansion in the convergent-divergent nozzle. If the flow through the nozzle is adiabatic, assuming that there are no viscosity-related losses, the expansion line is straight. This is marked in the figure as the $0\text{-}1_a$ transition. The occurrence

of a shock wave in the flow involves a flow discontinuity characterized by a sudden rise in pressure and temperature, which results in an increase in the fluid entropy and static enthalpy. This case is illustrated in the figure as the 1_a-2_a transition. If moist air expansion is considered, it is initially identical with the expansion of dry air until point 1, where due to water vapour supercooling, droplet nuclei are created violently and condensation occurs, which is accompanied by a release of latent heat. The fluid absorbs the evaporation heat, which causes a rise in its pressure and temperature and a drop in its velocity. This is represented in the figure by the 1-2 transition. It is worth noting that the transition results in the fluid total temperature $T_{0,2}$. The 2-3 transition is further expansion of the mixture of gas and liquid in the form of droplets. If a shock wave occurs in the flow – transition 3-4 – the liquid phase evaporates on it partially or entirely. The gaseous phase thus gives away the evaporation heat and this results in a drop in the fluid total temperature $T_{0,4}$. It should also be noted that due to condensation, the expansion process is accompanied by a bigger increment in entropy compared to the adiabatic flow, which in practice translates into lower efficiency. In industrial applications this means a decrease in the efficiency of machines.

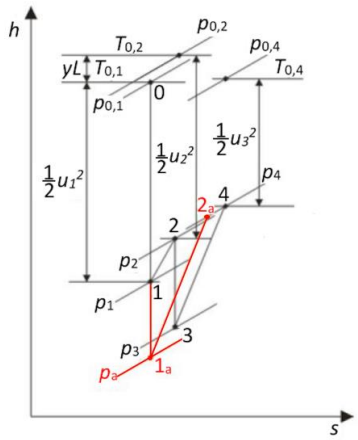

Figure 0.3. Adiabatic (red) and diabatic (black) expansion curves

Flow condensation may have a different character depending on the fluid parameters and on the acceleration process itself. In internal flows, oblique or normal condensation waves may occur. Their nature may be stationary or non-stationary, causing symmetric or non-symmetric oscillations. Both in internal and external flows, condensation and pressure waves may interact with each other. Considering the above-mentioned aspects and the condensation impact on the

efficiency of machines, it is not surprising that the phenomenon has become the focus of research for many scientists.

Silesian University of Technology
Department of Power Engineering and Turbomachinery
44 -100 Gliwice, ul. Konarskiego 18

Physical and mathematical model

The most popular strategy adopted in studies on condensation is to use the so-called single-fluid (SF) approach, wherein the mixture of gas and liquid phases is treated as a homogeneous fluid. This approach is justified in cases where droplets do not reach a considerable size. Due to their small dimensions, the condensate particles do not affect the flow field and therefore their influence on the pressure field can be omitted. It is applicable for humid air, as the mass fraction of vapour in the mixture is low, so even if it condenses entirely, its impact on the fluid properties is slight and the main change of the flow character is due to the latent heat release. Despite the advantages of the single-fluid approach (e.g. high robustness and a low computational time), it is based on some simplifications and neglects several issues, such as the spectrum of the size of droplets or their mutual collisions. It also takes no account of the temperature difference between the liquid and the gas phase and finally of the interphase slip velocity. These aspects can to some extent be represented by introducing correction factors, e.g. based on the droplet size, the temperature of liquid droplets is computed from the Clausius equation. Correction factors increase the accuracy of mathematical models, but their physical explanation can be dubious.

The two-fluid approach extends the single-fluid model with another Eulerian phase. In the two-fluid approach, the gaseous and liquid phases are treated as separate continua, which makes it possible to take into account some of the phenomena which the SF approach neglects. By the introduction of another fluid, a set of governing equations is added. Adding the continuity equation, the fluid properties are influenced by the presence of the liquid, and the physical properties of the fluid (specific heat, viscosity, etc.) are thus computed with higher accuracy. Owing to an additional set of momentum equations, the interphase slip velocity can be computed and the energy equation for the liquid phase enables precise computation of the dispersed phase temperature, which is crucial for the droplet growth rate computation. Despite the importance of these aspects, the two-fluid approach is seldom used in its full form due to the need for much more computational power and poorer stability of the solver. A possible solution is a hybrid model where only additional energy or momentum equations are implemented to identify the phenomena that are considered to have a major impact on the flow.

Another method is the implementation of the so-called Discrete Phase Model, i.e. a model based on the Eulerian-Lagrangian approach, where droplets are not treated as a continuous phase but their motion is computed individually. Due to the large number of droplets, they are considered

as “packages” to reduce the computational time. This approach provides a precise solution regarding trajectories of droplets and their mutual collisions. However, due to its negative impact on the solver stability and computational time, it is not popular.

In the work presented herein, the working fluid properties (viscosity, thermal conductivity, specific heat etc. of steam or humid air (air-steam mixture)) are based on the IAPWS properties in the range of their validity. Therefore, if the fluid properties drop to a considerably low-temperature region, which occurs in humid air expansion, the properties are based on analytical correlations. The properties of air and steam are considered to satisfy the ideal-gas law; surface tension, water density, saturation pressure and latent heat are computed based on the relations proposed by Dohrmann [51], Pruppacher et al. [50] and Sonntag et al. [52], which are considered to be accurate enough when applied for condensation in humid air [19,53]. It should be noted that due to the phase change, the fluid properties vary. Therefore, they are computed based on the mass fraction of steam and air in the mixture using the species approach or the User-Defined Real Gas Model [54].

1.6 Single-fluid model

The RANS model for the compressible flow and the transport equations can be expressed as:

$$\frac{\partial}{\partial t}\rho + \frac{\partial}{\partial x_j}\rho \mathbf{v}_j = 0 \tag{3.1}$$

$$\frac{\partial}{\partial t}\rho \mathbf{v}_i + \frac{\partial}{\partial x_{ij}}\left(\rho \mathbf{v}_i \mathbf{v}_{ij} + \delta_{ij} p - \boldsymbol{\tau}_{ij}\right) = 0 \tag{3.2}$$

$$\frac{\partial}{\partial t}\rho E + \frac{\partial}{\partial x_j}\left(\mathbf{v}_j \rho E + \mathbf{v}_j p\right) = \frac{\partial}{\partial x_j}\left(\lambda_{\text{eff}} \frac{\partial}{\partial x_j} T + \boldsymbol{\tau}_{ij} \mathbf{v}_j\right) + S_E \tag{3.3}$$

where ρ is density, t is time, $\mathbf{v}$ is the velocity vector, δ is the Kronecker delta, p is pressure, $\boldsymbol{\tau}$ is the stress tensor, E is energy, λ_{eff} is effective conductivity, T is temperature, and S_E is the source term due to condensation with the following form:

$$S_E = \left(S_{y_{hom}} + S_{y_{het}}\right) \cdot L \tag{3.4}$$

where L is latent heat, $S_{y_{hom}}$ and $S_{y_{het}}$ are mass sources due to homogeneous and heterogeneous condensation, see equations 3.10 and 3.12.

The *k*-ω shear stress transport (SST) model was adopted as the eddy-viscosity turbulence model [55]:

$$\frac{\partial}{\partial t}\rho k + \frac{\partial}{\partial x_\mathrm{j}}\rho \mathbf{v}_\mathrm{j} k = \frac{\partial}{\partial x_\mathrm{j}}\left(\Gamma_\mathrm{k}\frac{\partial k}{\partial x_\mathrm{j}}\right) + \tilde{G}_\mathrm{k} - Y_\mathrm{k} \tag{3.5}$$

$$\frac{\partial}{\partial t}\rho \omega + \frac{\partial}{\partial x_\mathrm{j}}\rho \mathbf{v}_\mathrm{j} \omega = \frac{\partial}{\partial x_\mathrm{j}}\left(\Gamma_\omega\frac{\partial \omega}{\partial x_\mathrm{j}}\right) + \tilde{G}_\omega - Y_\omega + D_\omega \tag{3.6}$$

where k is turbulence kinetic energy and ω is the specific dissipation rate, Γ is effective diffusivity, $\tilde{G}$, Y and D stand for turbulence kinetic energy generation, dissipation and cross-diffusion, respectively. A detailed description of the turbulence model can be found in the ANSYS Fluent Theory Guide [54].

Additional transport equations were required to model the phase change due to homogeneous and heterogeneous condensation. Partial differential equations (PDEs) were included that describe the number of droplets per kilogram (n), created due to the nucleation process, and the liquid mass fraction (y), due to homogeneous (hom) and heterogeneous (het) condensation. These additional transport equations were introduced using the ANSYS Fluent UDFs. In total, there are three additional PDEs, which in the case of a 3D flow, together with the RANS model, create a system of 10 PDEs to solve. The number of solid particles in the heterogeneous process is constant and it is based on the literature data [56,20,57]. The additional transport equations for the liquid phase take the following form:

$$\frac{\partial \rho y_\mathrm{hom}}{\partial t} + \frac{\partial}{\partial x_\mathrm{j}}\left(\rho \mathbf{v}_\mathrm{j} y_\mathrm{hom}\right) = S_{\mathrm{y_{hom}}} \tag{3.7}$$

$$\frac{\partial \rho n_\mathrm{hom}}{\partial t} + \frac{\partial}{\partial x_\mathrm{j}}\left(\rho \mathbf{v}_\mathrm{j} n_\mathrm{hom}\right) = S_{\mathrm{n_{hom}}} \tag{3.8}$$

$$\frac{\partial \rho y_\mathrm{het}}{\partial t} + \frac{\partial}{\partial x_\mathrm{j}}\left(\rho \mathbf{v}_\mathrm{j} y_\mathrm{het}\right) = S_{\mathrm{y_{het}}} \tag{3.9}$$

where S represents the source term: for eq. 3.7 – the source of mass of the condensed liquid due to homogenous condensation, for eq. 3.8 – the source of droplets per kilogram of air generated due to the nucleation process, for eq. 3.9 – the source of mass of water resulting from the heterogeneous condensation process. The source terms are defined by the following formulae:

$$S_{\mathrm{y_{hom}}} = \frac{4}{3}\pi\rho\rho_{\mathrm{l}} r^{*3} J_{\mathrm{hom}} + 4\pi\rho\rho_l n_{\mathrm{hom}} r_{\mathrm{hom}}^2 \frac{\mathrm{d}r_{\mathrm{hom}}}{\mathrm{d}t} \tag{3.10}$$

$$S_{\mathrm{n_{hom}}} = \rho J_{\mathrm{hom}} \tag{3.11}$$

$$S_{\mathrm{y_{het}}} = 4\pi\rho\rho_{\mathrm{l}} n_{\mathrm{het}} r_{\mathrm{het}}^2 \frac{\mathrm{d}r_{\mathrm{het}}}{\mathrm{d}t} \tag{3.12}$$

where J is the nucleation rate presenting the number of nuclei with critical radius r^* formed in one kilogram of moist air in one second; r is the droplet radius calculated based on the water mass fraction and the number of droplets:

$$r = \left(\frac{3y}{4\pi\rho_{\mathrm{l}} n}\right) \tag{3.13}$$

It has to be mentioned that in the case of heterogeneous condensation triggered by the presence of foreign nuclei, the radius of the droplet accounts also for the radius of the suspended particle.

1.7 Nucleation

The homogeneous condensation process is triggered by spontaneous nucleation, whereby nuclei, reaching the critical radius, form in the fluid due to rapid supercooling. In this model, the critical radius was based on the Kelvin equation:

$$r^* = \frac{2\sigma}{\rho_{\mathrm{l}} R_{\mathrm{v}} T_{\mathrm{v}} \ln(\mathrm{S})} \tag{3.14}$$

where σ is the steam surface tension, R_{v} is the individual gas constant, T_{v} is the steam temperature and $S = p_{\mathrm{v}}/p_{\mathrm{s}}$ is supersaturation, the ratio of steam partial pressure to saturation pressure. Assuming an equilibrium distribution of motionless clusters multiplied by the collision rate based on the kinetic theory of gases, the Volmer equation is formulated to describe the formation of condensation nuclei in one kilogram of moist air in one second:

$$J_{\mathrm{hom}} = C\sqrt{\frac{2\sigma}{\pi m_{\mathrm{v}}^3}}\frac{\rho_{\mathrm{v}}}{\rho_{\mathrm{l}}} \mathrm{e}^{\left(-\frac{4\pi r^{*2}\sigma}{3k_{\mathrm{B}}T_{\mathrm{v}}}\right)} \tag{3.15}$$

where γ is the ratio of specific heat capacities, m_{v} is the mass of one vapour molecule, ρ_{l} is the liquid density at temperature T_{v}, k_{B} is the Boltzmann constant and α_{c} represents the

condensation coefficient, which is equal to one. C is the Kantrowitz correction factor [58] defined as:

$$C = \frac{\alpha_c}{1 + \frac{2(\gamma - 1)}{(\gamma + 1)} \frac{L}{R_v T_v} \left(\frac{L}{R_v T_v} - \frac{1}{2} \right)} \tag{3.16}$$

The so-called non-isothermal Kantrowitz correction is based on the assumption that all growing droplets have the same excess temperature. In the presence of a large volume of the gaseous phase, such as moist air, the isothermal assumption is justified because collisions of condensing molecules with inert gas molecules are much more common than those with condensing droplets. Finally, it reduces nucleation by a factor of 50–100.

1.8 Droplet growth

Once a cluster of nuclei is formed in supercooled vapour, their further growth can be described as a function of supersaturation, the droplet size and thermodynamic properties. According to the gas dynamics theory, the frequency of the collision of steam molecules with condensation nuclei is related to the mean free path of steam molecules and the radius of water droplets. The larger the Knudsen number (Kn), the smaller the diameter of the droplet. The equation for calculating Kn is:

$$\mathrm{Kn} = \frac{l_s}{d} = \frac{\frac{\mu_l}{p} \sqrt{\frac{\pi RT}{2}}}{d} \tag{3.17}$$

where l_s is the mean free path of the steam molecule, μ is the moist air dynamic viscosity, T is temperature, R is the gas constant; p is the moist air pressure, d is the droplet diameter. If Kn < 0.01, the droplet growth process can be described as a continuous flow region. If Kn > 4.5, the droplet growth is governed by the free molecular flow. If $0.01 \leq \mathrm{Kn} \leq 4.5$, the transition region is the case.

1.8.1 Continuous model

Assuming the Nusselt number equal 2 the continuous model is derived for very large droplets and is given by the following equation:

$$\frac{\mathrm{d}r}{\mathrm{d}t} = \frac{2\lambda_\mathrm{v}}{d} \cdot \left(1 - \frac{r^*}{r}\right) \cdot \left(\frac{R_\mathrm{v} T_\mathrm{v}{}^2}{\rho_\mathrm{l} L^2}\right) \cdot \ln(S) \tag{3.18}$$

where λ_v is the thermal conductivity of vapour. Considering that the droplet growth model should be applicable for small droplets, several models which take account of the Knudsen number were derived. The most popular and the one most often used by researchers is the continuous droplet growth model extension developed for steam by Gyarmathy [4], which is applied for a smaller size of droplets:

$$\frac{\mathrm{d}r}{\mathrm{d}t} = \frac{2\lambda_\mathrm{v}}{d} \cdot \frac{\left(1 - \frac{r^*}{r}\right)}{(1 + 3.18\mathrm{Kn})} \cdot \left(\frac{R_\mathrm{v} T_\mathrm{v}{}^2}{\rho_\mathrm{l} L^2}\right) \cdot \ln(S) \tag{3.19}$$

Another correction for the continuous model was proposed in [3] and is known as the Fuchs-Suttugin model:

$$\frac{\mathrm{d}r}{\mathrm{d}t} = \frac{2\lambda_\mathrm{v}}{d} \cdot \frac{(1 + 2\mathrm{Kn})\left(1 - \frac{r^*}{r}\right)}{(1 + 3.42\mathrm{Kn} + 5.32\mathrm{Kn}^2)} \cdot \left(\frac{R_\mathrm{v} T_\mathrm{v}{}^2}{\rho_\mathrm{l} L^2}\right) \cdot \ln(S) \tag{3.20}$$

Finally, a modification of Gyarmathy's model was proposed by Young, who, drawing on the experience from the nozzle flow modelling, introduced the following correction [5,6]:

$$\frac{\mathrm{d}r}{\mathrm{d}t} = \frac{2\lambda_\mathrm{v}}{d} \cdot \frac{\left(1 - \frac{r^*}{r}\right)}{\left(1 + 3.78(1 - \upsilon)\frac{\mathrm{Kn}}{\mathrm{Pr}}\right)} \cdot \left(\frac{\lambda_\mathrm{v} R_\mathrm{v} T_\mathrm{v}{}^2}{\rho_\mathrm{l} L^2}\right) \cdot \ln(S) \tag{3.21}$$

where Pr is the Prandtl number, and υ is computed as follows:

$$\upsilon = \frac{R_\mathrm{v} T_\mathrm{v}}{L}\left(\alpha - 0.5 - \frac{2 - q_\mathrm{c}}{2q_\mathrm{c}} \cdot \left(\frac{\gamma + 1}{2\gamma}\right)\left(\frac{c_\mathrm{p} T_v}{L}\right)\right) \tag{3.22}$$

where coefficients α and q_c are correction factors. It has to be said that these factors were introduced to enable the model calibration in a wide range of flows. However, in the research presented herein they were set to 1.

In continuous droplet growth models, the temperature of the droplets (T_l) can be determined by the capillarity effect using the expression given by Gyarmathy [4]:

$$T_{\mathrm{l}} = T_{\mathrm{s}} - (T_{\mathrm{s}} - T_{\mathrm{v}})\frac{r^*}{r}v \tag{3.23}$$

where T_{s} is the steam saturation temperature for given pressure. Here, steam temperature is equal to the temperature of the air-steam mixture. It is worth mentioning that with an increase in the droplet size, the ratio of the critical radius to the droplet radius $\left(\frac{r^*}{r}\right)$ and the Knudsen number decrease, which diminishes the impact of the GY, FS and YO corrections on the continuous model.

1.8.2 Kinetic model

If water droplets are small in relation to the mean free path, Kn>4.5, the growth of the droplets should be governed by considering the molecular and macroscopic transport process. Assuming that there is no significant change in the droplet temperature, $\frac{dT}{dt} \approx 0$, and that the temperature of the droplets, steam and air is the same: $T_{\mathrm{v}} = T_{\mathrm{l}} = T$, which was proposed by Hill [59], an approximation of the droplet growth can be obtained independently of the droplet size. This assumption introduced into the model proposed by Hertz and Knudsen results in the droplet growth equation for the free-molecular regime in the following form [13,14,18]:

$$\frac{\mathrm{d}r}{\mathrm{d}t} = \frac{\alpha_{\mathrm{c}}}{\rho_{\mathrm{l}}} \cdot \frac{p_{\mathrm{v}} - p_{\mathrm{s}}}{\sqrt{2\pi R_{\mathrm{v}} T}} \tag{3.24}$$

where α_{c} is a condensation coefficient describing how many steam molecules collide with the water droplet surface. The value of 1 for this coefficient means that all steam molecules are captured by the water droplet surface. If this value equals 0, none of the steam molecules is captured by the water droplet surface, all are deflected. This model is customarily referred to as the Hertz-Knudsen droplet growth model.

1.8.3 Blend model

The predictive performance of the mentioned model in humid air transonic flows has not been studied sufficiently enough. The HK model was derived based on the molecular-kinetic theory. Therefore it provides a physical explanation considering the growth rate for small droplets. However, the model implies some significant simplifications, such as the interphase temperature equality. On the other hand, the GY, FS and YO models are empirical extensions for the continuous model and they consider the influence of the interphase temperature

inequality. It has to be mentioned that the continuous model is derived for the droplet growth in the macroscopic and free molecular region. These correlations were created to meet the predictions of the droplet growth rate in steam, and therefore their application for humid air had to be studied.

As discussed above, the Knudsen number, i.e. the mean free path of the steam molecule over the droplet diameter, decides the type of the droplet growth process. Therefore it seems rational to create a blending function, e.g. of the following linear type:

$$\frac{dr}{dt} = bf\frac{dr}{dt_{\mathrm{CON}}} + (1-bf)\frac{dr}{dt_{\mathrm{HK}}} \tag{3.25}$$

where bf is the blending factor, from 0 to 1, related to the Knudsen number in the following way:

$$\begin{cases} bf = 1; & \mathrm{Kn} \le 0.01 \\ bf = -0.2227 \cdot \mathrm{Kn} - 0.0015; & 0.01 \le \mathrm{Kn} \le 4.5 \\ bf = 0; & 4.5 \le \mathrm{Kn} \end{cases} \tag{3.26}$$

The proposed blend model is considered to benefit from the strengths of the continuous and the kinetic model and to be applicable for a wide range of condensing flows.

1.9 Discrete phase model

The approach referred to as the Discrete Phase Model (DPM) was developed based on a mix of Eulerian and Lagrangian approaches, i.e. the Eulerian method is employed for the continuous phase and the Lagrangian approach is used to track the particles suspended in the flow. The trajectories of the particles are computed by integrating the force balance on the particle, which in the Lagrangian reference frame is written as:

$$m_{\mathrm{p}}\frac{d\mathbf{v}_{\mathrm{p}}}{dt} = m_{\mathrm{p}}\frac{\mathbf{v}-\mathbf{v}_{\mathrm{p}}}{\tau_{\mathrm{r}}} + m_p\frac{\mathbf{g}\left(\rho_{\mathrm{p}}-\rho\right)}{\rho_{\mathrm{p}}} + \mathbf{F} \tag{3.27}$$

where m_{p} is the particle mass, computed based on density and the droplet diameter, $\mathbf{v}$ and $\mathbf{v}_{\mathrm{p}}$, respectively, are the continuous and the discrete phase velocity vectors, ρ and ρ_{p} are densities of the continuous and the discrete phase, τ_{r} is the droplet relaxation time, $\mathbf{g}$ is gravitational acceleration and $\mathbf{F}$ is a force vector. The DPM model was extended with the condensation model

by means of UDFs and is identical with the model used with the single-fluid model. Like in the SF model, the temperature balance is assumed between droplets and the continuous fluid.

The DPM is used to investigate behaviour from the discrete perspective. The main advantage of the DPM is that it makes it possible to carry out a complex study of the interaction of particles with walls and one another, as well as to compute the full spectrum of particle diameters. The main disadvantage of the DPM is that it is not applicable in cases where the secondary phase volume fraction is not negligible. Despite its advantages, the model is rarely used in condensing flows. This is mainly because of the fact that due to low inertia forces, the slip velocity and the wall interaction can be omitted. As a result, the single-fluid approach is sufficient. However, in some future applications which are now under development, e.g. fuel cells [44,43], these simplifications will be irrelevant and the DPM model is viewed as the best approach for condensing flow considerations. The main weakness of the DPM is the correlation of the required computational power with the number of tracked particles. This is a major issue considering that the number of droplets appearing during spontaneous nucleation is large. The problem is usually reduced by packing particles into so-called packages representing droplets with a specific diameter. Another issue is the DPM stability, especially if the particles interact with aerodynamic waves.

The above-mentioned advantages and disadvantages of the DPM are somehow contrary to the advantages and disadvantages of the single-fluid model. Therefore in this study superposition of both models is proposed. The idea is to compute the flow based on the SF approach, which ensures a robust and reliable solution with regard to the continuous phase flow as well as to the impact of condensation, and then to post-process this solution further using the DPM to obtain a solution regarding the spectrum of the droplet diameters and the slip velocity. This is a novel approach developed by the author of this work and by Tim Wittmann. It makes it possible to benefit from the advantages of both models.

Experimental study

Experimental studies not only give a valuable insight into considered phenomena but also provide a basis for the validation of numerical models. In this work dry air-, steam- and humid air-flow experiments are used to validate the condensation model. The consideration of the dry air flow is based on the literature, i.e. the NASA benchmark test, whereas the Sajben transonic converging-diverging diffuser was selected for the dry air flow validation. The geometry and the experimental results can be found in the literature [60]. The study of the flows of steam and humid air combines the literature data with the in-house experimental results. Sections 4.1 and 4.2 below describe the experimental testing of selected flows of steam and humid air. Subsection 4.2.2 provides a detailed description of the experiment carried out for the purpose of this work regarding expansion in the symmetric and the asymmetric nozzle with a low expansion rate.

1.10 Steam flow

Experimental studies on condensing flows were taken up with a view to using them to improve the efficiency and reliability of steam turbines. In the last stages of low-pressure steam turbines, low steam parameters favour condensation and the turbine operates in the wet steam region. This has an unfavourable impact not only on expansion efficiency but also on the turbine failure rate due to erosion occurring as an effect of the collision of water droplets with the blades of the rotor and the stator ring.

A standard benchmark for the steam condensing flow is the Moses-Stein nozzle 252 and 257 [1,61]. It includes the results of experiments carried out by Moses and Stein in 1978 to measure the pressure distribution and the size of droplets in a convergent-divergent nozzle with the flow of water vapour. Static pressure was measured in the nozzle axis and the size of water droplets arising due to water vapour condensation was established by means of Light Scattering measurements.

Another, much newer example of research focused on steam condensation is the series of experiments carried out in the steam tunnel of the Department of Power Engineering and Turbomachinery of the SUT under the International Wet Steam Experimental Project (IWSEP). The quantities investigated within the project were the static pressure distribution on the nozzle wall and the droplet size. The testing was carried out for different inlet parameters of steam. A detailed description of the test stand and the applied measuring techniques can be found in [12].

The geometries of the nozzles analysed in the Moses and the IWESEP experiments, together with their main dimensions, are presented in Figure 4.1. Attention should be drawn to the dimensions because the IWSEP nozzle is considerably bigger compared to the nozzle investigated by Moses et al., both in terms of the flow direction and the critical cross-section. Table 0-1 presents the experimental testing results based on the literature data [1,12].

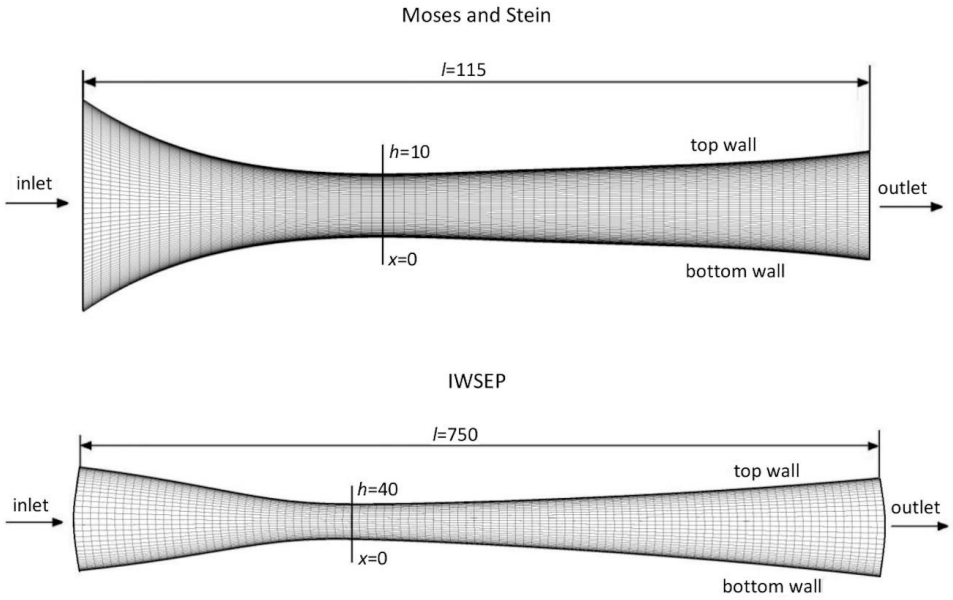

Figure 0.1. Geometries of the Moses and Stein and the IWSEP nozzle

Table 0-1. Experiment results for the Moses and Stein and the IWSEP nozzle

x, m	*p*, kPa	*d*, nm	*x*, m	*p*, kPa		*d*, nm	
	IWSEP	IWSEP		Moses252	Moses257	Moses252	Moses257
0	43.513	-	0.020	16.212	27.064	-	-
0.01	40.469	-	0.022	15.639	26.387	-	-
0.02	38.424	-	0.025	14.791	-	-	15.5
0.03	39.344	-	0.028	13.940	25.711	-	-

0.04	44.152	-	0.030	13.067	-	-	-
0.05	41.216	-	0.035	12.215	-	10.6	-
0.06	38.355	-	0.037	11.898	-	11.9	-
0.07	35.983	-	0.038	11.874	-	12.9	-
0.08	33.998	-	0.040	11.963	24.358	13.8	30.0
0.09	32.484	-	0.042	12.005	-	14.6	-
0.1	30.839	-	0.044	11.845	22.328	15.3	-
0.11	29.389	-	0.046	11.619	-	15.8	-
0.12	27.988	-	0.048	11.232	-	16.4	-
0.13	26.821	-	0.051	10.688	19.621	16.8	-
0.14	25.501	-	0.052	10.373	-	17.1	-
0.15	24.478	131	0.054	10.069	-	17.5	-
0.16	23.423	-	0.055	9.813	-	17.8	-
0.17	22.430	-	0.058	9.251	-	18.1	-
0.18	21.646	-	0.060	8.995	-	18.2	34.5
0.19	20.743	-	-	-	-	-	-
0.20	-	139	-	-	-	-	-
0.25	-	144	-	-	-	-	-

1.11 Humid air flow

When at an aerodynamics congress in 1935 Prandtl presented a schlieren photograph of two crossing oblique shock waves close behind the de Laval nozzle throat, it was concluded that this structure was dependent on the air initial humidity. Since atmospheric air is always moist, the wetness fraction cannot be eliminated without air drying. The X-shaped shock is very well visible for the nozzle with a high expansion ratio, higher than $3000s^{-1}$ [62]. In the case of a nozzle with a low expansion ratio, additional oblique shock waves may coexist that are induced aerodynamically and not thermodynamically like the X-shock (the condensation shock).

In the case of the moist air diabatic flow with the participation of external heat sources, condensation of water vapour contained in the air starts if the air temperature reaches a value lower than the dew point temperature. The dew point is approximately equal to the water vapour saturation temperature value defined for the water vapour partial pressure [18]. However, if water vapour condensation occurs during rapid expansion of atmospheric air, the process starts when air reaches speeds close to the speed of sound, i.e. around the Mach number equal to 1 ($M=u/a\sim1$), and the air temperature threshold for spontaneous condensation is usually by 30-50K lower than the dew point temperature calculated for total inlet parameters. This temperature value and the increment in pressure on the condensation wave depend on two factors – relative humidity, φ_0, and expansion rate, $\dot{P}$.

Expansion rate $\dot{P}$ expresses the logarithmic rate of the flow static pressure drop, which can be described using the following equation [62]:

$$\dot{P} = -\frac{d\ln p}{dt} - \frac{1}{p}\frac{dp}{dt} = -\frac{1}{p}\frac{dp}{dx}\frac{dx}{dt} = -\frac{a}{p}\frac{dp}{dx} \approx \frac{a_0}{p_0}\cdot\frac{p_1 - p_2}{l} \tag{4.1}$$

where a_0 – the sound speed at the inlet calculated from total pressure and temperature (p_0, T_0), p_1 – pressure at the inlet, p_2 – pressure at the outlet; l is a characteristic length, here – the length of the nozzle.

1.11.1 High-expansion rate nozzle

The subject of this research is a linear convergent-divergent nozzle with walls with the circular profile of 100 mm and the expansion rate of $\sim5000s^{-1}$. The nozzle width and the throat height are 20 mm each. The phenomena occurring in the nozzle are assumed to be two-dimensional. Figure 4.2 shows the shape of the nozzle and the main dimensions.

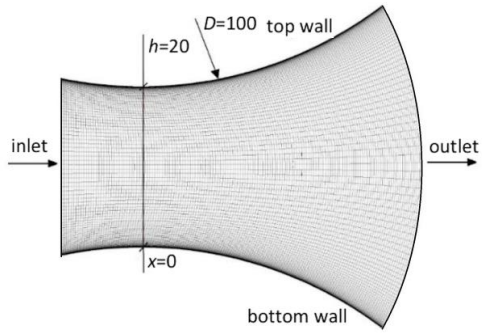

Figure 0.2. Dykas nozzle geometry with the numerical mesh

The experimental study was performed by Dykas et al. on a test rig dedicated for steam testing customized for the testing of moist air, which made it possible to obtain very low back pressure at the nozzle outlet. The steam facility is placed in the Department of Power Engineering and Turbomachinery of the SUT. Two measuring techniques were adopted here, i.e. the static pressure measurement on the nozzle bottom wall and schlieren photography for the flow field visualization. These two measuring techniques have been used at the DPET for many years and are described in detail in the literature [63,64]. The moist air flow through the de Laval nozzle was analysed for four boundary conditions at the nozzle inlet and outlet (see Table 0-2). Two groups of data can be distinguished here: the data for the flow with a normal shock wave induced by elevated back pressure and the data with a supersonic outlet. For all the cases under consideration it can be assumed that the inlet total pressure and temperature are the same and correspond to ambient conditions.

Table 0-2. Testing conditions for the D1 nozzle

	p_0, kPa	T_0, K	$\Phi, \%$	p_{out}, kPa
Normal Shock Wave				
D1.0BP			0.0	55
D1.1BP	98.8	297.15	43.0	55
D1.2BP			68.0	55
Supersonic				

D1.0SS			0.0	–
D1.1SS	98.8	297.15	43.0	–
D1.2SS			68.0	–

1.11.2 Low-expansion rate nozzle

This research concerns two linear convergent-divergent nozzles designed according to Witoszyński's curve [65] with the resulting expansion rate of ~1000s^{-1}. The nozzles differ in symmetry: the W1 nozzle is symmetric, whereas nozzle W2 has the top wall shifted linearly by 20 mm downstream the flow. The physical phenomena occurring in these nozzles are considered to be two-dimensional. Figure 4.3 shows the shape of the W1 nozzle and its main dimensions. The nozzle width is 20 mm.

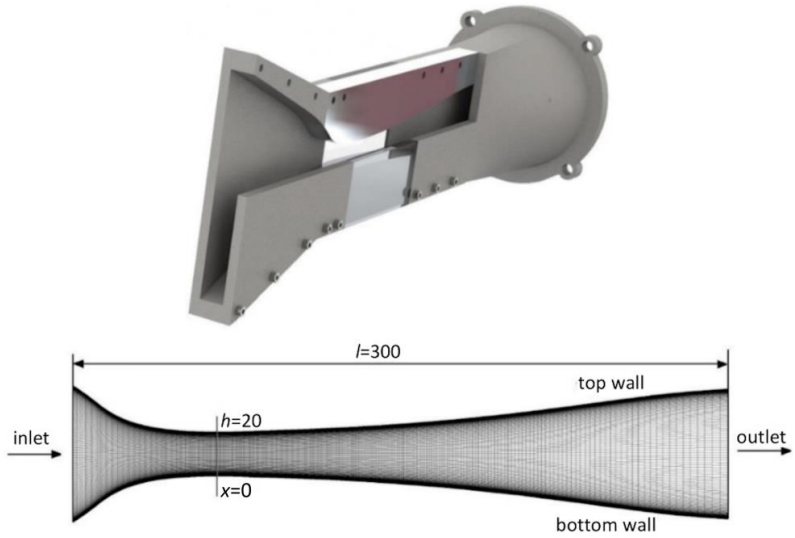

Figure 0.3. Experimental nozzle geometry (top) and numerical domain with the mesh (bottom)

The nozzle geometry, i.e. the top wall and the bottom wall with the pressure holes, was made of aluminium by means of CNC machining. Glass windows were used for the lateral walls. The whole was assembled on a frame made of a PLA filament using the 3D printing technique.

Figure 4.4 shows a diagram of the test rig available in the Department of Power Engineering and Turbomachinery of the SUT which was used to perform the experimental testing. Two measuring techniques were applied here, i.e. the static pressure measurement on the nozzle bottom wall and schlieren photography for the flow field visualization. These two measuring

techniques have been used by us for many years and are described in detail in our previous works [63,64].

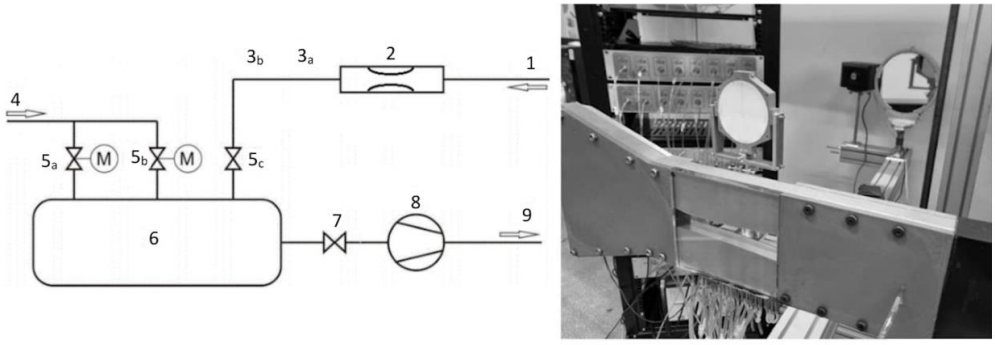

Figure 0.4. Diagram of the vacuum system for the nozzle test. 1 – test rig inlet (T_0, p_0, φ_0 evaluation), 2 – test section, 3_a – HWA probe, 3_b – ISA orifice plate, 4 – secondary air inlet, 5_a – DN 100 valve, 5_b – DN 50 valve, 5_c – valve, 6 – 3m^3 pressure vessel, 7 – cut-off valves, 8 – Roots air blower, 9 – exhaust to the environment (left) and the assembled test section (right)

1.11.2.1 Symmetric nozzle

The moist air flow through the de Laval nozzle was analysed for eight boundary conditions at the nozzle inlet and outlet (see Table 0-3). Two groups of data can be distinguished here: the data for the flow with a normal shock wave induced by elevated back pressure and the data with a supersonic outlet. For all the cases under consideration it can be assumed that the inlet total pressure and temperature are the same and correspond to ambient conditions.

Table 0-3. Testing conditions for the W1 nozzle

	p_0, kPa	T_0, K	$\Phi, \%$	p_b, kPa
Normal Shock Wave				
W1.0BP			0.0	78
W1.1BP	99.7	296.65	25.0	78
W1.2BP			37.5	78

W1.3BP			51.5	78
Supersonic				
W1.0SS			0.0	–
W1.1SS			25.0	–
	99.7	296.65		
W1.2SS			37.5	–
W1.3SS			51.5	–

Table 0-4 shows the nozzle geometry data and gathers all the static pressure values measured on the nozzle bottom wall for the considered test cases. The pressure measurement data are available for 4 cases with different resolutions. This is due to the availability of pressure transducers during the experiments. The *x* and *y* values define the position of points and the position of the pressure tap holes along the nozzle bottom wall while keeping $x = 0$ at the nozzle throat and $y = 0$ at the nozzle axis.

Table 0-4. Geometrical data of the nozzle and experimental data of pressure measured at the bottom wall of the W1 nozzle

x, m	*y*, m	*p*, kPa			
		W1.1BP	W1.2BP	W1.3BP	W1.1SS
-0.050	-0.020345	-	-	-	-
-0.025	-0.011726	-	-	-	-
-0.006	-0.010080	57.937	57.369	57.715	57.884
-0.003	-0.010020	55.316	-	-	-
0.000	-0.009996	52.694	52.187	52.530	52.610
0.003	-0.010002	50.179	-	-	-

0.006	-0.010034	47.664	47.242	47.596	47.540
0.009	-0.010089	45.202	-	-	-
0.012	-0.010161	42.739	42.354	44.269	42.507
0.015	-0.010248	41.776	-	-	-
0.018	-0.010348	40.812	41.111	47.297	40.266
0.021	-0.010457	40.008	-	-	-
0.024	-0.010574	39.204	41.497	47.740	37.560
0.027	-0.010697	39.956	-	-	-
0.030	-0.010825	40.708	43.142	42.649	34.130
0.033	-0.010956	44.473	-	-	-
0.036	-0.011090	48.237	43.265	40.803	36.046
0.039	-0.011226	50.529	-	-	-
0.042	-0.011363	52.821	46.290	40.858	33.523
0.045	-0.011502	54.115	-	-	-
0.048	-0.011643	55.409	55.627	52.228	32.263
0.051	-0.011785	56.927	-	-	-
0.054	-0.011929	58.445	57.729	54.807	30.570
0.057	-0.012076	59.769	-	-	-
0.060	-0.012225	61.092	60.438	57.959	28.351
0.063	-0.012377	62.270	-	-	-

0.066	-0.012533	63.448	62.820	60.804	26.860
0.069	-0.012694	64.514	-	-	-
0.072	-0.012859	65.580	64.861	63.208	27.493
0.075	-0.013031	66.496	-	-	-
0.078	-0.013209	67.412	66.691	65.250	34.155
0.090	-0.013999	-	-	-	-
0.120	-0.016680	-	-	-	-
0.150	-0.020357	-	-	-	-
0.200	-0.026678	-	-	-	-
0.235	-0.029933	78.067	78.490	77.916	-
0.250	-0.031885	-	-	-	-

1.11.2.2 Asymmetric nozzle

The moist air flow through the de Laval nozzle was analysed for 3 boundary conditions at the nozzle outlet gathered in Table 0-5. Two groups of data can be distinguished: the data for the flow with a supersonic outlet and for the cases with normal shock waves induced by elevated back pressure. For all the cases under consideration it can be assumed that the inlet total pressure and temperature are the same and correspond to ambient conditions.

Table 0-5. Testing conditions for the W2 nozzle

	p_0, Pa	T_0, K	φ, %	p_b, Pa
		Normal Shock Wave		
W2.0PB1	99.7kPa	296.65	0	74kPa

W2.0PB2	99.7kPa	296.65	0	78kPa
W2.1PB1	98.7kPa	295.65	26.1	74kPa
W2.1PB2	98.7kPa	295.65	26.1	78kPa
		Supersonic		
W2.0SS	99.7kPa	296.65	0	3kPa
W2.1SS	99.7kPa	296.65	26.1	3kPa

Table 0-6 presents the nozzle geometry data and all the static pressure values measured on the nozzle bottom wall for the considered test cases. The pressure measurement data are available for 3 cases. The x and y values define the position of points and the position of pressure tap holes along the nozzle bottom wall while keeping $x = 0$ at the nozzle throat and $y = 0$ at the nozzle axis; the top wall is shifted linearly by 20 mm downstream the flow.

Table 0-6. Geometrical data of the nozzle and experimental data of pressure measured at the bottom wall of the W2 nozzle

x, m	y, m	p, kPa		
		W2.1BP1	W2.1BP2	W2.1SS
-0.050	-0.020345	-	-	-
-0.025	-0.011726	-	-	-
-0.006	-0.010080	68.44272	68.42139	68.3993
-0.003	-0.010020	-	-	-
0.000	-0.009996	62.8656	62.82023	62.78188
0.003	-0.010002	-	-	-
0.006	-0.010034	57.18278	57.10682	57.04555

0.009	-0.010089	-	-	-
0.012	-0.010161	51.87952	51.7383	51.62148
0.015	-0.010248	-	-	-
0.018	-0.010348	51.03455	50.75272	50.5379
0.021	-0.010457	-	-	-
0.024	-0.010574	46.76733	46.4758	46.29117
0.027	-0.010697	-	-	-
0.030	-0.010825	43.31043	42.48492	42.12767
0.033	-0.010956	-	-	-
0.036	-0.011090	42.7925	39.7941	39.20345
0.039	-0.011226	-	-	-
0.042	-0.011363	44.70823	37.48936	36.11015
0.045	-0.011502	-	-	-
0.048	-0.011643	55.13923	39.03598	33.30837
0.051	-0.011785	-	-	-
0.054	-0.011929	56.57665	48.84807	33.62938
0.057	-0.012076	-	-	-
0.060	-0.012225	58.73442	52.10011	33.5093
0.063	-0.012377	-	-	-
0.066	-0.012533	61.23048	53.37402	30.54525

0.069	-0.012694	-	-	-
0.072	-0.012859	63.55615	55.75611	28.60825
0.075	-0.013031	-	-	-
0.078	-0.013209	65.5783	58.23669	27.12425
0.090	-0.013999	-	-	-
0.120	-0.016680	-	-	-
0.150	-0.020357	-	-	-
0.200	-0.026678	-	-	-
0.235	-0.029933	78.101	74.085	-
0.250	-0.031885	-	-	-

1.12 NASA rotor 37 and rotor 67

Experimental testing of aircraft engines is both extremely complex and expensive. The most common experiments used to validate mathematical models intended for computations of aircraft engines are the NASA rotor 37 and the NASA rotor 67 benchmarks [66,67,68,69,70]. The NASA rotor 37 is the experimental testing of the first stage of an aircraft turbine compressor, whereas the NASA rotor 67 is the experimental testing of the fan of a turbofan engine. During the experiments the engine performance characteristic was developed and the radial pressure distribution was measured at the blade channel outlet. Table 0-7 presents the testing conditions and the basic geometrical parameters of the two rotors.

Table 0-7. Testing conditions for the NASA rotors

	p_0, Pa	T_0, K	f, rad/s	blade length, m	number of blades
rotor 37	101325	288.15	1800	0.0749	36
rotor 67	101325	288.15	1680	0.1320	22

Figure 4.5 presents the geometry of the two rotors together with the experimental results of the pressure distribution at the rotor outlet. The outlet absolute total pressure of rotor 37 was measured at the section located 10.67 cm downstream of the blade hub leading edge. The inlet control plane was located 4.19 cm upstream of the blade hub leading edge. The outlet total pressure for rotor 67 was measured at the section placed 11.01 cm downstream of the blade hub leading edge, while the inlet control plane was located 2.47 cm upstream of the blade hub leading edge. For better visualization of the blade shape, the casing was partially removed from the geometry. It should be noted that the rotor 37 blade is almost straight, whereas the rotor 67 blade is twisted clearly in the radial direction.

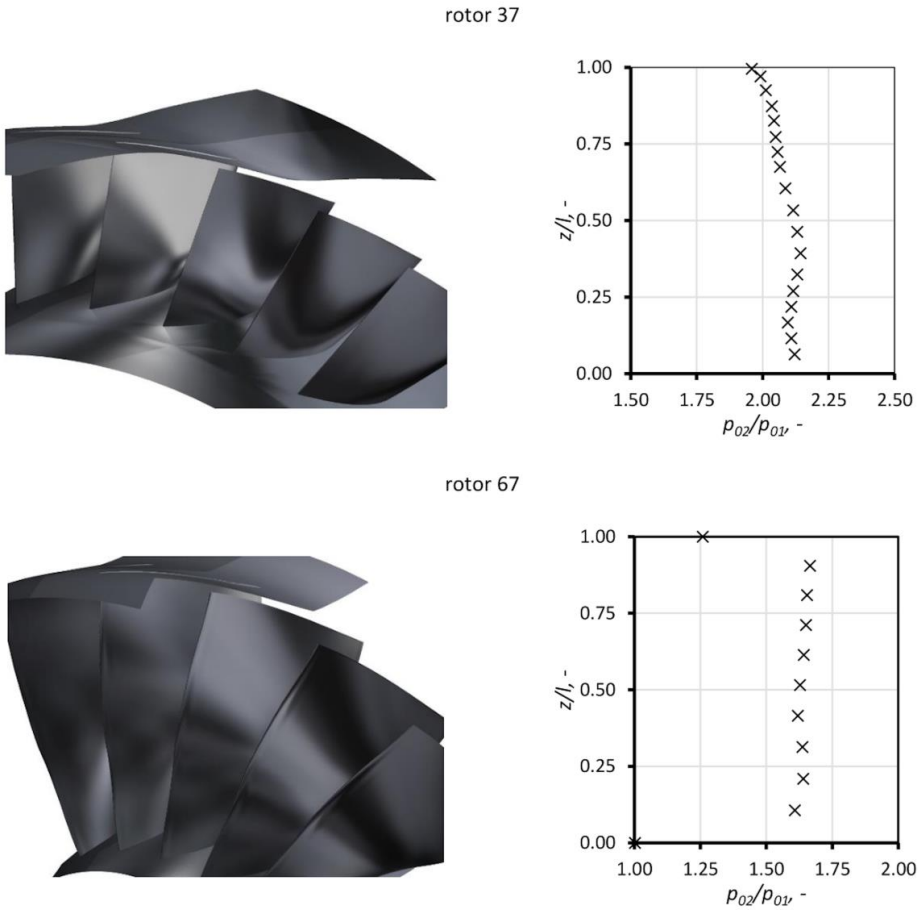

Figure 0.5. Geometry and pressure distribution at the blade channel outlet – rotor 37 and rotor 67

Numerical modelling

1.13 Mesh study

The rapid development of computing machines, the low prices of RAM chips and the use of advanced multicore processors have made it possible to perform calculations using large computational models. Using the finite volume method for viscous fluid-flow computations, the nonlinear term of transport equations can be found. For this purpose, the domain has to be divided into a finite number of elements, i.e. a numerical mesh has to be built. The smaller the mesh elements, the more accurate the solution of transport equations. However, more refined meshes involve longer computational times. In order to optimize the accuracy of the results in relation to the utilized computational power, the numerical analysis must include a study of the influence of the mesh element on the results. The mesh analysis was herein conducted for each of the applied geometries using the adiabatic model, the steam condensing model and the moist air condensing model. As a result, for each case under analysis meshes were obtained that, taking account of the selected turbulence model, guarantee a solid solution while maintaining a reasonable computational time.

1.13.1 Dry air flow

1.13.1.1 Sajben diffuser

The Sajben diffuser is a typical benchmark for the validation of the transonic dry air flow in an asymmetric nozzle. To ensure a mesh-independent CFD solution, the mesh-independence study was conducted. The CFD calculations were performed using three mesh resolutions. The numerical mesh was refined in the flow direction only (Table 0-1). The number of elements in the Y direction was set to ensure the y^+ value of ~1 while keeping the growth rate of about 1.1.

Table 0-1. Numerical mesh resolutions for the Sajben diffuser

Mesh statistics		
Case	X number of elements	Y number of elements
mesh1	150	130
mesh2	300	130

mesh3	600	130

Figure 5.1 shows the numerical schlieren photos and the static pressure distributions along the diffuser bottom (black line) and top (red line). The comparison of the results for the condensation flow model with a normal shock wave indicated mesh2 as the candidate for further simulations.

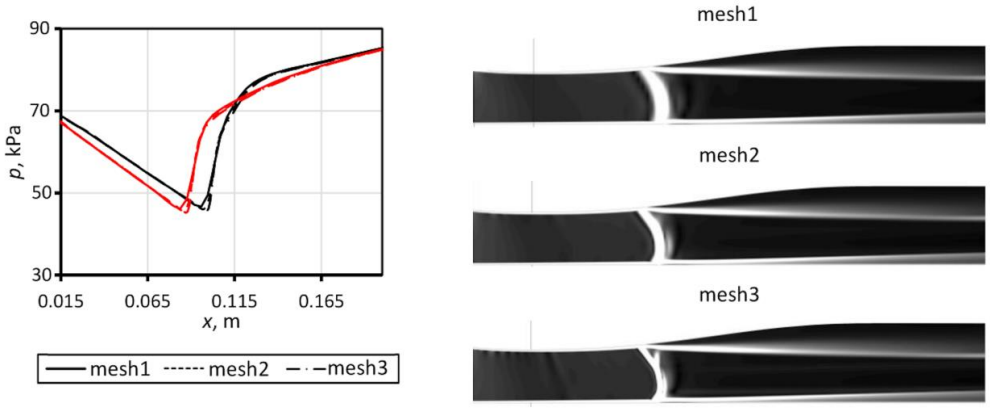

Figure 0.1. Mesh-independence study for the Sajben diffuser

1.13.1.2 Compressor rotor

The objective was to investigate the effect of phase-change phenomena on the performance of the turbine compressor rotor (NASA rotor 37) and the fan of a turbofan engine (NASA rotor 67). For this purpose, a mesh-independence study was performed first. Three numerical meshes were generated for each rotor in accordance with the literature guidelines and a mesh-independence study was performed [71]. The meshes, named mesh1, mesh2 and mesh3, are made of 0.25, 0.6 and 1.3 million elements for rotor 37 and 0.5, 1 and 1.7 million elements for rotor 67, respectively. The tip clearance was omitted because the study is focused on condensation phenomena. Even though mesh2 already gives a reasonable solution, and a further increase in the mesh density does not affect the spanwise pressure distribution (Figure 5.2), mesh3 was selected for the target studies of rotor 37 and rotor 67 due to better discretization near the wall. It is of major importance to keep good discretization of the boundary layer regions, because it plays a crucial role in the modelling of the interaction of the condensation shock or the shock wave with a solid wall. It has to be mentioned that, using the the k-ω SST turbulence model, the boundary layer was introduced to ensure $y^+ \approx 1$. Figure 5.2 presents the computational domain, the numerical mesh and the comparison of the ratio of the pitch-wise

averaged absolute total pressure at the control plane downstream of the blade (p_{02}) to the absolute total pressure at the inlet (p_{01}), obtained numerically. It may be concluded that even for the coarser numerical mesh (mesh2) the results are satisfactory. However, in the modelling of the condensing flow, a fine mesh is required to capture the condensation wave properly. Therefore mesh3 was selected for further investigations of the two rotors.

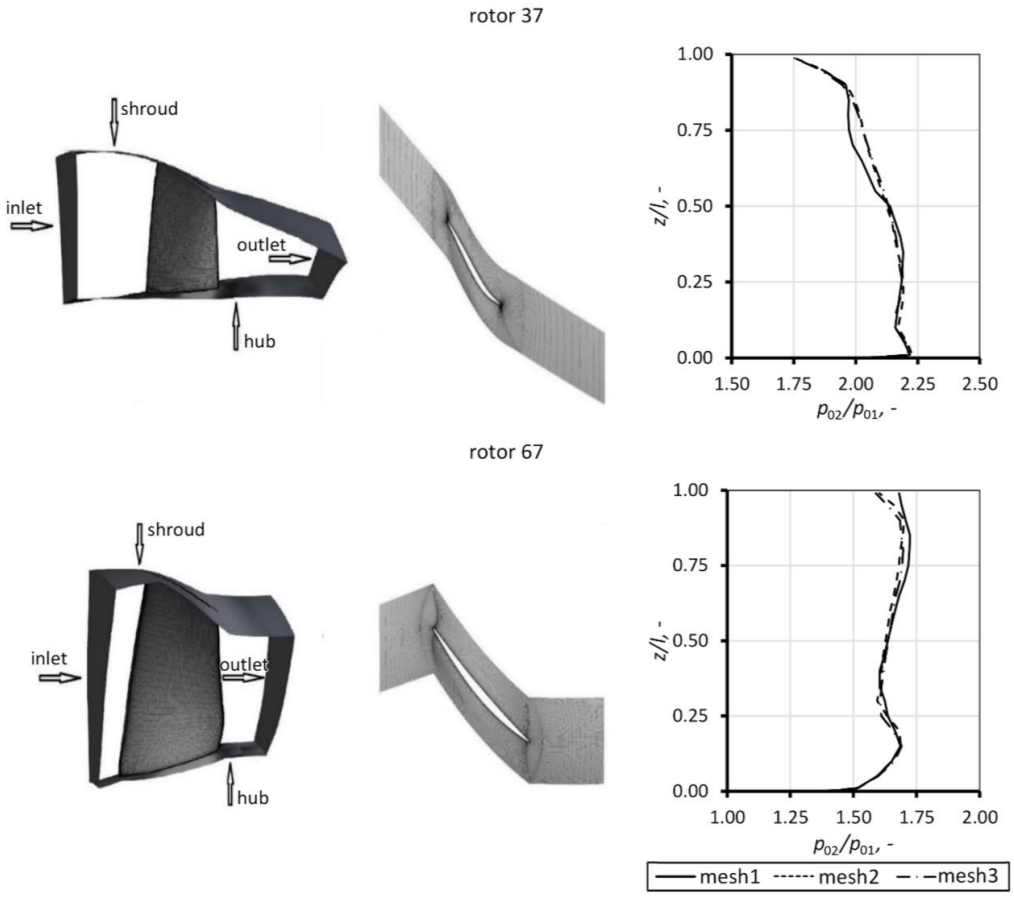

Figure 0.2. Computational domain with numerical mesh at 50% of the blade span and comparison of the spanwise distributions of the total pressure ratio for different meshes for rotors 37 and 67

1.13.2 Steam flow

The Moses and Stein nozzle is relatively small – it is only 115 mm long. It has a large inlet but a small outlet, and its expansion rate is ~9000s^{-1}. To ensure a mesh-independent CFD solution, the mesh-independence study was conducted. The CFD calculations were performed for three mesh resolutions using the steam condensing flow with the YO droplet growth model. The

numerical mesh was refined in the flow direction only (Table 0-2). The number of elements in the Y direction was set to ensure the y^+ value of ~1 while keeping the growth rate of about 1.1.

Table 0-2. Moses-Stein nozzle numerical mesh resolutions

Mesh statistics		
Case	X number of elements	Y number of elements
mesh1	150	90
mesh2	300	90
mesh3	600	90

Figure 5.3 presents the numerical schlieren photos and the static pressure distributions along the nozzle centre line. The comparison of the results for the condensation flow model with a normal condensation wave and a supersonic outlet indicates that the influence of the number of the mesh elements on the pressure distribution is negligible. On the other hand, with an increase in the mesh resolution, the schlieren results reveal structures of condensation and pressure waves which could be significant. However, as there is no visual experimental data and the main focus is on the pressure distribution as well as on the droplet radius, mesh2 was selected for further simulations.

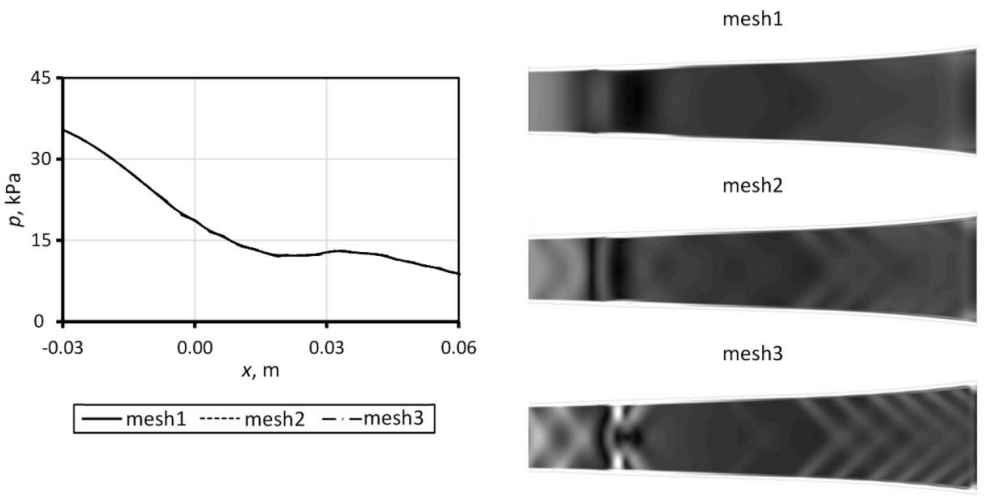

Figure 0.3. Mesh-independence study for the Moses-Stein nozzle

The same procedure was adopted for the IWSMP nozzle, which is much bigger. However, its expansion rate, ~3000s^{-1}, is lower compared to the Moses and Stein nozzle. The mesh-independence study was performed for 3 meshes refined in the flow direction only. The number of elements in the Y direction was set to ensure the y^+ value of ~1 and the growth rate of about 1.1. Table 0-3 shows the number of the mesh elements in direction X and Y. The steam condensing flow with the Young droplet growth model was applied.

Table 0-3. IWSMP nozzle numerical mesh resolutions

Mesh statistics		
Case	X number of elements	Y number of elements
mesh1	100	130
mesh2	200	130
mesh3	400	130

Figure 5.4 presents the numerical schlieren photos and the static pressure distributions along the nozzle centre line. The comparison of the results for the condensing flow model with a normal condensation wave and a supersonic outlet indicates that an increment in the number of elements along the nozzle involves an increase in the resolution of the results. For this reason, mesh3 was used for further simulations.

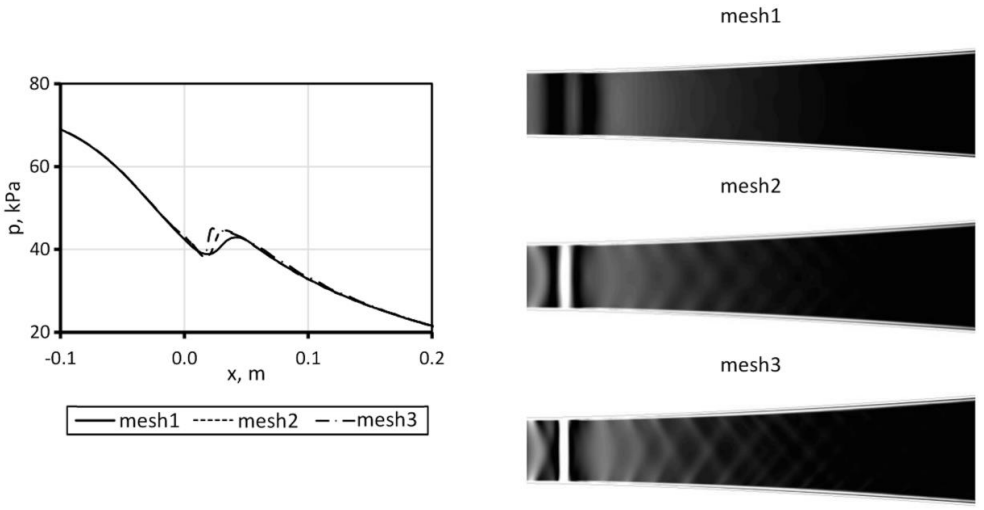

Figure 0.4. Mesh-independence study for the IWSEP nozzle

1.13.3 Humid air flow

The mesh analysis for the moist air flow was conducted for 2 nozzles differing in the expansion rate. This quantity has a substantial impact on the condensation process. At low expansion rates, characteristic X-shaped condensation and aerodynamic waves are created, whereas in nozzles with a high expansion rate the condensation wave is straight. The analysis made it possible to determine the effect of the number of the mesh elements on the position of condensation and aerodynamic waves.

1.13.3.1 Low-expansion rate nozzle

To ensure a mesh-independent CFD solution, the mesh-independence study was conducted using the adiabatic (dry air) and the diabatic (condensing) model. Three meshes differing in the number of elements were analysed. The numerical mesh was refined in the flow direction only (Table 0-4). The number of elements in the Y direction was set to ensure the y^+ value of ~1 while keeping the growth rate of about 1.1.

Table 0-4. Low-expansion rate nozzle numerical mesh resolutions

Mesh statistics		
Case	X number of elements	Y number of elements
mesh1	300	160

mesh2	600	160
mesh3	1200	160

Figures 5.5 and 5.6 show the numerical schlieren photos and the static pressure distributions along the nozzle centre line for the adiabatic flow. It can be seen that increasing the number of the mesh elements above 600 in the X direction has no effect on the pressure distribution along the nozzle centre line or the nozzle wall. Despite a slight increment in the schlieren photography resolution for mesh3 compared to mesh2, mesh2 is sufficient to map the phenomena appearing in the flow.

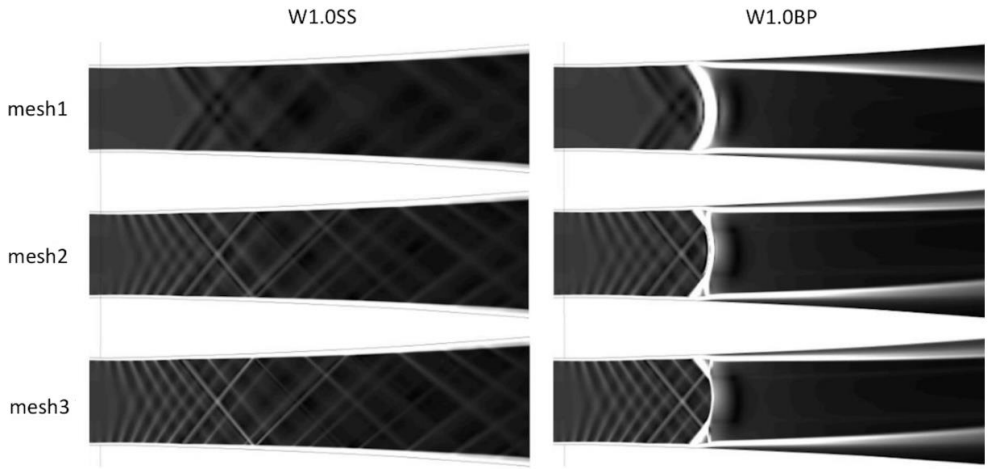

Figure 0.5. Resolution test of numerical schlieren photography for the test case with a supersonic outlet (left) and with elevated back pressure (right) for the dry air flow

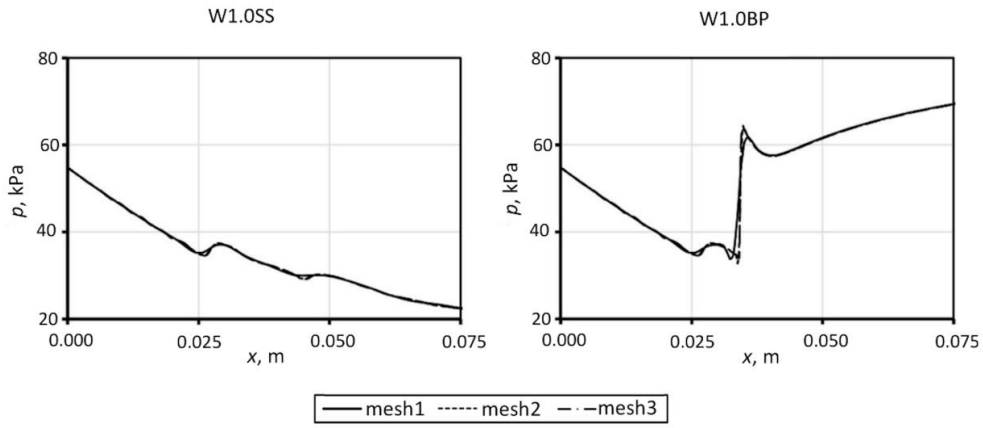

Figure 0.6. Static pressure distribution along the nozzle centre line

Figure 5.7 shows the influence of the mesh resolution on the diabatic flow. Like in the adiabatic simulation, mesh2 gives reliable results while maintaining a low computational cost. The pressure distribution along the nozzle wall is computed correctly with mesh2, but an increase in the number of the mesh elements involves a slight increase in the schlieren image resolution. The important thing is that if the mesh provides a reliable solution for the adiabatic flow, it is also appropriate for the diabatic case analysis.

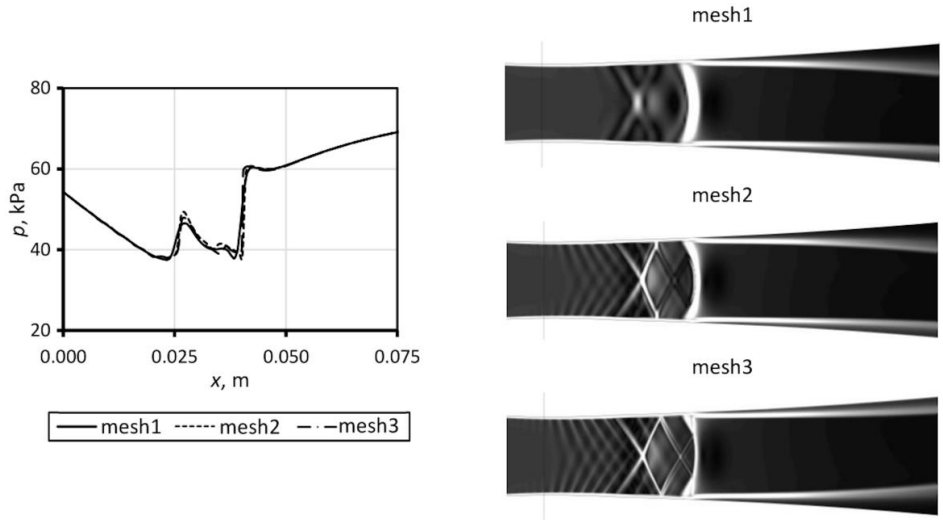

Figure 0.7. Mesh-independence study for the diabatic low-expansion rate nozzle

1.13.3.2 High-expansion rate nozzle

The geometry of the circular nozzle presented below (Figure 5.8) was applied to investigate the moist air condensing flow. A mesh-independence study was performed for three meshes (mesh1, mesh2 and mesh3) generated with 90x100, 115x125 and 140x150 2D elements along the X and the Y axis. In all the meshes a boundary layer was introduced to obtain $y^+ = 1$. The results of the mesh-independence study are presented in Figure 5.8, which shows the effect of the number of the mesh elements on the position of the condensation shock. It can be concluded that both the coarse and the fine mesh predict the condensation location and intensity similarly. The coarse mesh could thus have been a reasonable choice for this analysis. However, because the mesh was meant to be used further for investigations of flows with a shock wave, the finest mesh (mesh3) was selected to ensure reliable reference.

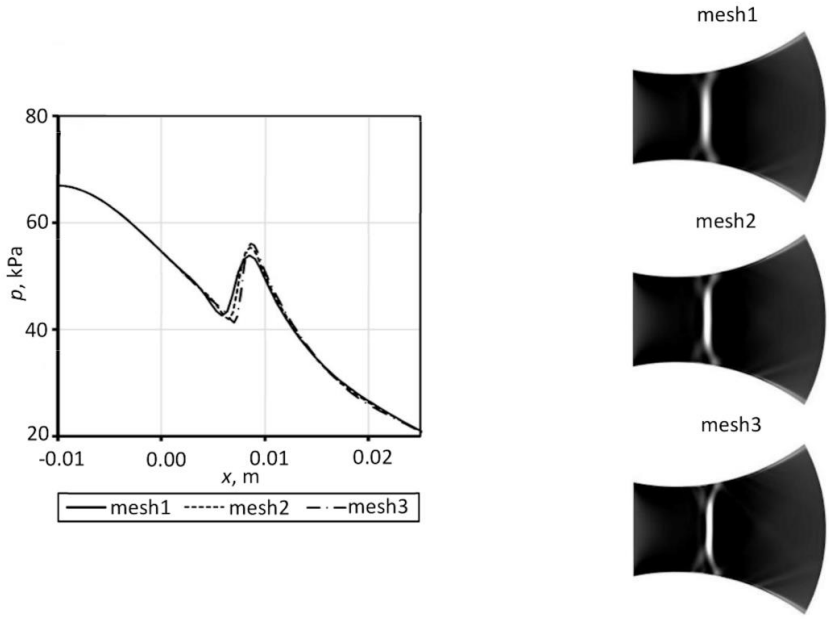

Figure 0.8. Influence of the number of the mesh elements on the condensation wave location

1.14 Numerical model validation

To make sure that the obtained results are reliable, mathematical models require validation. This, however, is difficult considering the scarcity of comparative material and the great number of applied models. One of the basic problems in modelling phase changes in transonic flows is the selection of the condensation model. Generally, two types of the droplet growth model are considered: the continuous and the kinetic one. The two models differ in origin. The

continuous model was constructed to simulate steam condensation in steam flows and works well for large droplets, whereas the kinetic model was created to deal with droplets with very small dimensions. The criterial number that makes it possible to decide whether a droplet is small or large is the Knudsen number. The Knudsen number decides which model should be used (cf. eq. 3.17). Therefore, the steam molecule mean free path l_s should be determined first to find the size of the droplets that should be expected choosing one of the two types of the droplet growth model under consideration (Figure 5.16).

1.14.1 Dry air flow

The dry air flow was validated for the NASA benchmark test regarding a simple 2D converging-diverging nozzle, i.e. the Sajben Transonic Converging-Diverging Diffuser, and against complex 3D geometries of the NASA rotor 37 and the NASA rotor 67. Such validation provides a solid basis for the dry air flow reliability for further studies on the impact of humidity and related phase-change phenomena on the performance of devices and turbomachinery.

1.14.1.1 Sajben diffuser

The dry air flow model was validated against the NASA benchmark test, i.e. the Sajben Transonic Converging-Diverging Diffuser. Therefore the nozzle geometry and boundary conditions were based on the literature data [60]. The data are gathered in Table 0-5. Based on the mesh-independency study, mesh2, which consists of 300x131 elements, was used. The boundary layer was introduced in the mesh to ensure the y^+ function value of ~1 and the element growth ratio of 1.1 (cf. Figure 5.9). The turbulence effects were modelled using the k-ω SST model proposed by Menter [55].

Table 0-5. Boundary conditions for the NASA Sajben Transonic Converging-Diverging Diffuser [60]

	p_0, kPa	T_0, K	φ, %	p_b, kPa
		Normal Shock Wave		
Sajben	135	278.00	0	97

In this experimental study, static pressure was measured on the top and the bottom wall. The velocity profile is given and available in the literature. The testing was carried out for the SF model with relative humidity of 0% and the air was assumed not to contain any pollutants. The

results were confronted with experimental data (cf. Figures 5.10 and 5.11 (*x/h* is the position of the profile in relation to the nozzle throat height, and *y/H* is the position in relation to the nozzle local height)). The model gives a precise estimation of the shock wave position and of the velocity profile. The validation results prove the model reliability for internal flow simulations and provide a basis for further studies.

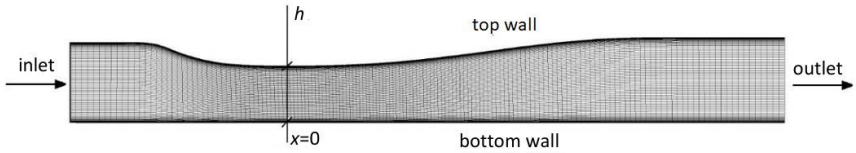

Figure 0.9. Computational grid of the Sajben diffuser

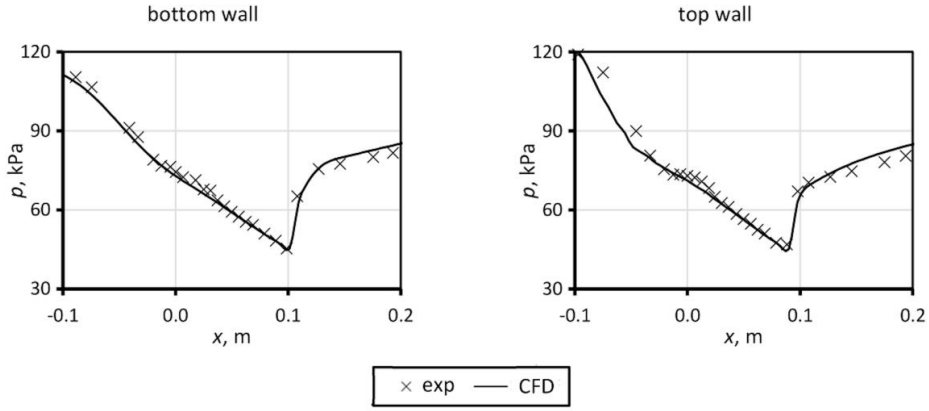

Figure 0.10. Static-to-total pressure ratio along the bottom (left) and the top (right) wall of the nozzle for dry air

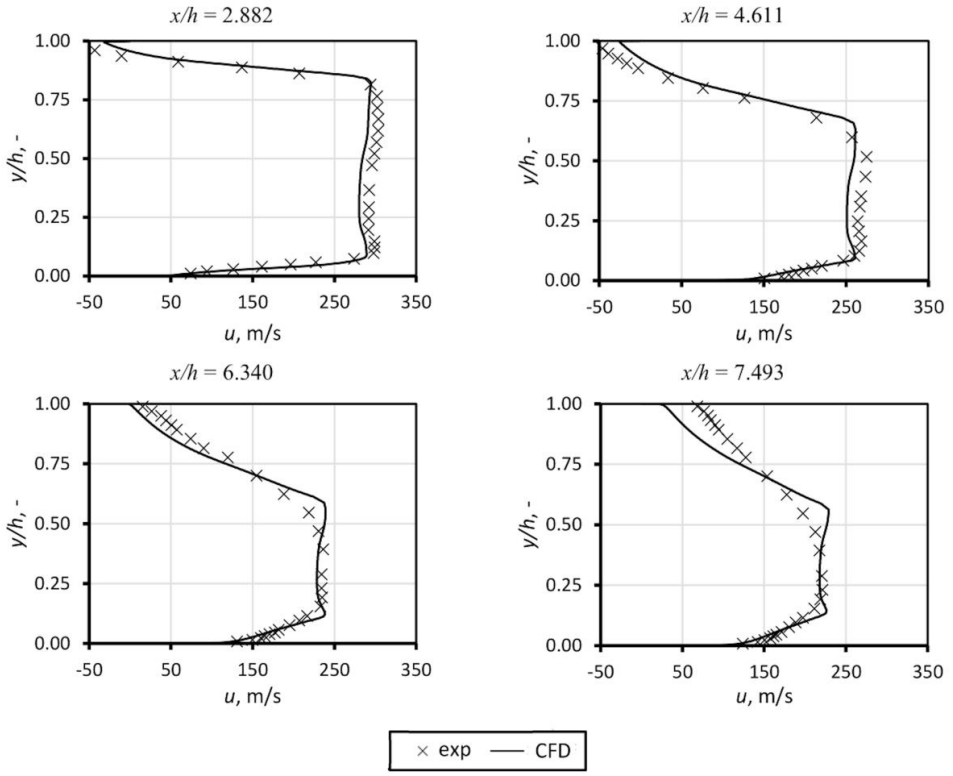

Figure 0.11. Comparison between the numerical and the experimental velocity profile along the nozzle

1.14.1.2 Compressor rotor

The NASA rotor 37 and the NASA rotor 67 were considered. Table 0-6 presents the overall mass flow rate, the total temperature and the total pressure ratios determined from the CFD simulations and from the experiments. The <1.5% discrepancy between the numerical and the experimental results may be attributed to the omission of the tip clearance in the numerical analysis. The good agreement between the numerical and the experimental results lays a solid foundation for further studies. Figure 5.12 shows the numerically and experimentally obtained spanwise total pressure distribution. These results show good convergence of the numerical model with the experimental data. It is thus proved that, like in the case of the Sajben diffuser, the model is reliable for the analysis of the dry air flow in 2D and 3D geometries.

Table 0-6. Experimental (EXP) and numerical (CFD) mass flow rate, total pressure and total temperature ratio.

	Rotor 37				Rotor 67			
	$\dot{m}$, kg/s	$\frac{p_{02}}{p_{01}}$, -	$\frac{T_{02}}{T_{01}}$, -	η,-	$\dot{m}$, kg/s	$\frac{p_{02}}{p_{01}}$, -	$\frac{T_{02}}{T_{01}}$, -	η,-
EXP	20.19	2.11	1.27	0.88	32.31	1.73	1.19	0.89
CFD	20.41	2.09	1.27	0.87	31.84	1.71	1.19	0.87
Error, %	1.09	0.95	0	1.14	1.45	1.16	0	2.25

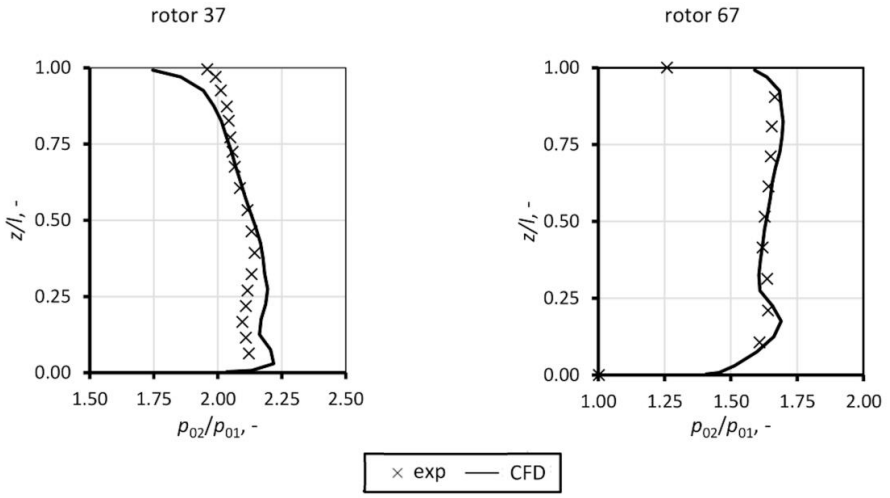

Figure 0.12. Comparison between numerical and experimental results of the spanwise distributions of the total pressure ratio for rotors 37 and 67

1.14.1.3 External flow

Condensation occurs not only in internal but also in external flows, around a wing of a flying aircraft for example. To investigate the impact of condensation, the dry air model was validated against the external flow over the RAE 2822 airfoil. External flow considerations raise another issue, i.e. the domain size. To find a valid size, 4 domains were considered differing in the length of the airfoil chord. The domain and its dimensions affect the pressure coefficient ($C_\mathrm{p} = \frac{p_\infty - p}{p_0 - p_\infty}$, where p_∞ is free stream pressure, p_0 is total pressure and p is static pressure). The results of the testing are shown in Figure 5.13. The domain with the length of 20 chord lengths and the width of 25 chord lengths was considered to give results unaffected by the boundary conditions.

As a result, the domain with 123,065 elements was considered in further studies. It has to be mentioned that the number of the mesh elements along the airfoil is 500. The boundary layer was introduced to ensure the $y+$ value of ~1 and the growth ratio of 1.1.

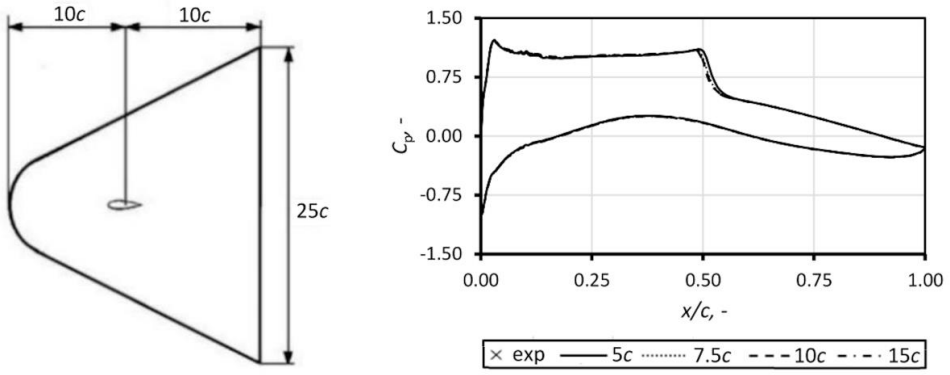

Figure 0.13. Domain size and its influence on the pressure coefficient distribution on the airfoil surface

In the next step, the results were confronted with the experimental data (cf. Figure 5.14). The results obtained numerically show good agreement with the experimental results.

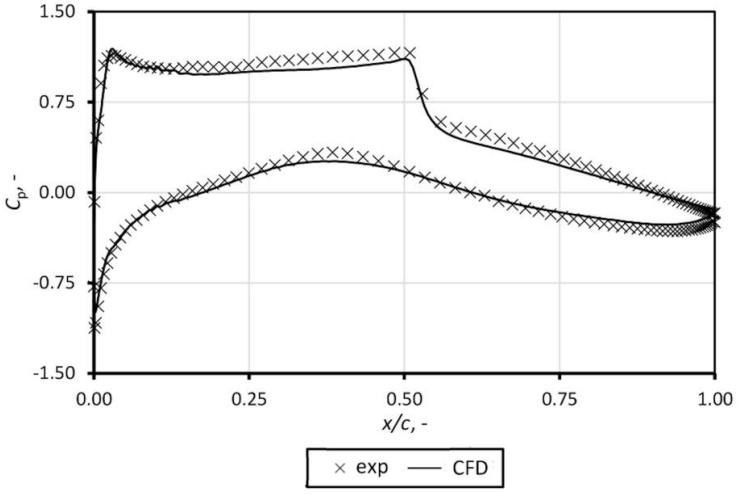

Figure 0.14. Comparison between numerical and experimental results of the pressure coefficient distribution along the blade

1.14.2 Steam flow

The state of the art in steam condensing flows is presented in the paper written to sum up the International Wet Steam Modelling Project (IWSMP). It includes the results produced by numerous wet steam methods. They are compared with each other and with the experimental data obtained for several cases of nozzle testing. Among others, the project resulted in the creation of a base of experimental data enabling validation of mathematical condensation models. The paper presents the results obtained using different codes developed by renowned research units and is focused on the impact of the applied condensation models on the convergence with experimental results obtained for the Moses nozzle in test cases 252 and 257. Although a detailed analysis was conducted, the authors concluded among others that due to numerous factors, such as the uncertainty of nucleation or condensation models, it was difficult to draw unequivocal conclusions. Still, their work points to the droplet growth model proposed by Young as the most appropriate for steam calculations after its calibration at the time. Figure 5.15 presents the impact of the adopted condensation model on the modelling of the steam condensing flow in the Moses and Stein nozzle for test cases 252 and 257. Figure 5.16 presents a comparison of the same analysis for case 5 in the IWSEP nozzle.

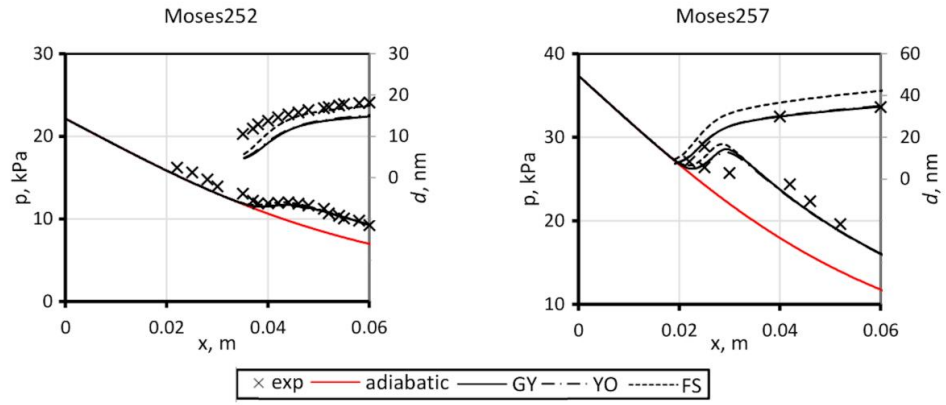

Figure 0.15. Impact of the condensation model on total pressure along the nozzle axis and the size od droplets arising due to condensation

The kinetic model of condensation overestimates the droplet growth rate and for this reason it was not included in Figures 5.15 and 5.16. The GY, the FS and the YO model give very similar results. This is due to the fact that they are based on the continuous model extended with additional correction factors, and in the presented work it is assumed that the factors are equal to 1. The models overestimate condensation for all analysed cases, which is due to the

assumption that steam satisfies the ideal gas equation of state. This simplification is acceptable in considerations of a steam-air mixture where the steam content is relatively small. The results obtained using the model proposed in this work agree with the predictions of the obtained values based on Starzman's paper [1].

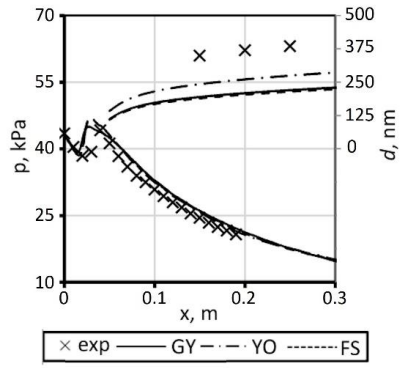

Figure 0.16. Impact of the condensation model on total pressure along the nozzle axis

1.14.3 Humid air flow

The validation of mathematical models of moist air flows involving a phase change is extremely challenging due to the limited experimental database. In order to build a model ensuring solid results, the model was validated using the data from the experiments carried out by Dykas et al. in the DPET of the SUT and from the experiment performed by Wiśniewski. The data make it possible to analyse the impact of the adopted condensation model on the expansion process in nozzles with different expansion rates and for various atmospheric conditions.

Analysing the values of the mean free path of the steam molecule (Figure 5.17) in a high-expansion rate steam nozzle, it can be noticed that for the continuous droplet growth model the droplet expected size is bigger than $1 \cdot 10^{-5}$m, which is much bigger than the size of droplets which are usually formed due to the nucleation process. In the case of moist air condensing flows, the so-called coarse droplets arise only when heterogeneous condensation takes place on the water droplets or solid particles already existing in the flow.

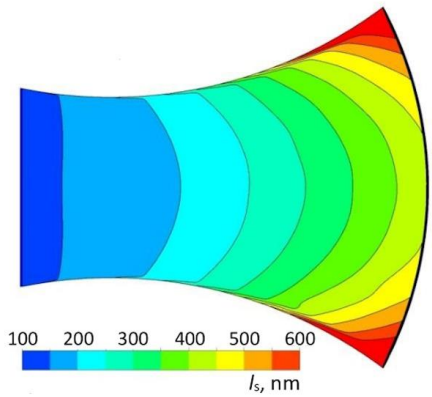

Figure 0.17. Distribution of the mean free path of steam molecules

1.14.3.1 Comparison of droplet growth models based on the continuous model

Due to the fact that in transonic condensing flows the range of the Knudsen number values can be wide, the use of the kinetic Hertz-Knudsen (HK) droplet growth model seems to be a simplification. However, the majority of continuous droplet growth models already include a correction concerning the Knudsen number, such as the Gyarmathy (GY), the Fuchs-Sutugin (FS) or the Young (YO) correction. Nevertheless, these corrections are rarely used in moist air condensing flow modelling. Figure 5.18 presents a comparison of the moist air condensing flow modelling in a circular nozzle by means of four different droplet growth models. The simulation results were compared with the experimentally obtained static pressure distribution along the nozzle centre line. The calculation results obtained from simulations using the Hertz-Knudsen (HK) model, with condensation coefficient $\alpha_c = 1$, and the continuous model with the Fuchs-Sutugin (FS) correction are similar and close to the experimental data. On the other hand, the continuous models with the Gyarmathy (GY) and the Young (YO) correction in both cases differ from the experiment significantly. For D1.1SS, with the lower relative humidity value, the HK and the FS droplet growth models are very close to each other, even in terms of the droplet size.

Using the continuous droplet growth model, information is obtained about the temperature difference between the droplet and steam $\Delta T = T_l - T_v$. In the case of the kinetic model it is assumed that this difference is zero. Figure 5.19 presents the distribution of the rise in the

droplet temperature due to condensation. The highest value of this temperature difference is observed for the model with the Fuchs-Suttugin correction.

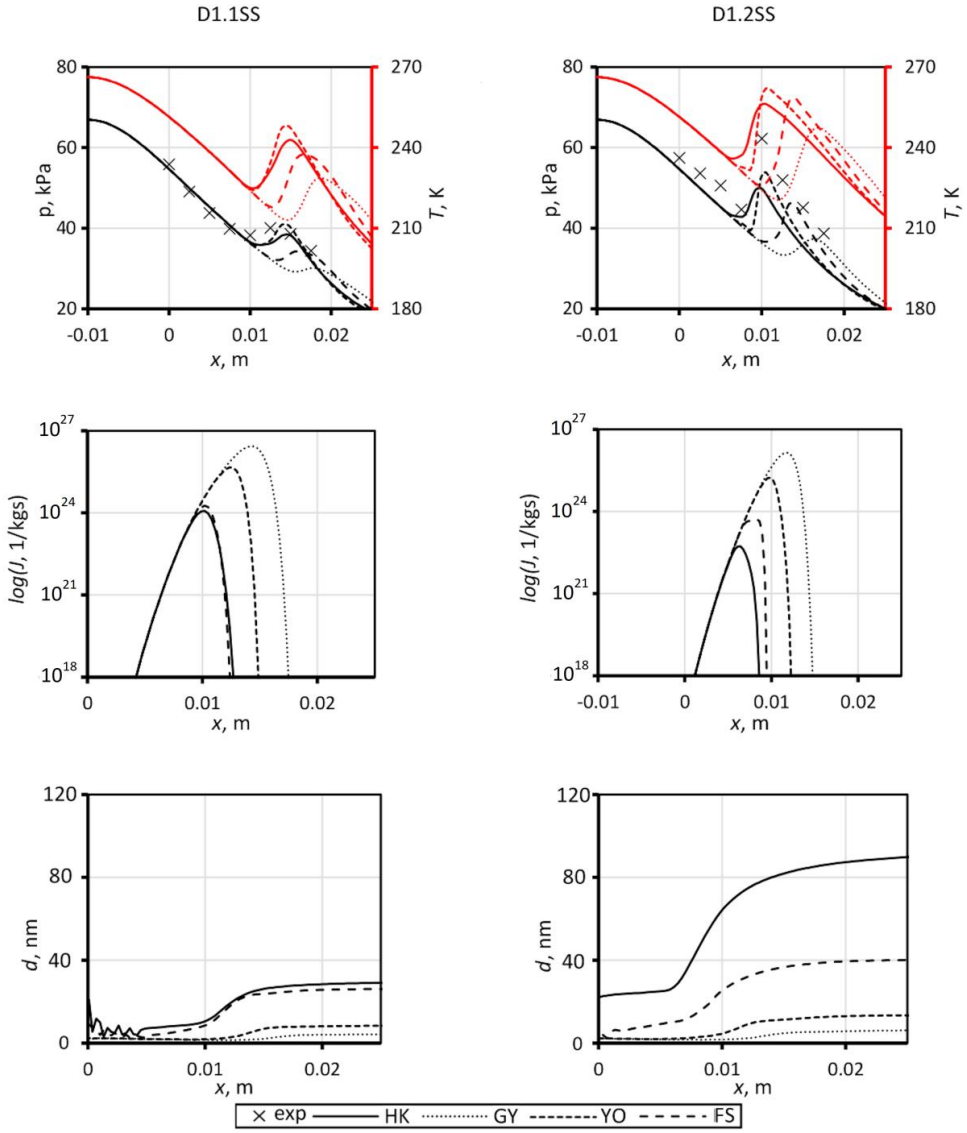

Figure 0.18. Comparison of numerical results with different droplet growth models against experimental testing [24]: static pressure and static temperature; nucleation rate and droplet size distributions along the nozzle axis

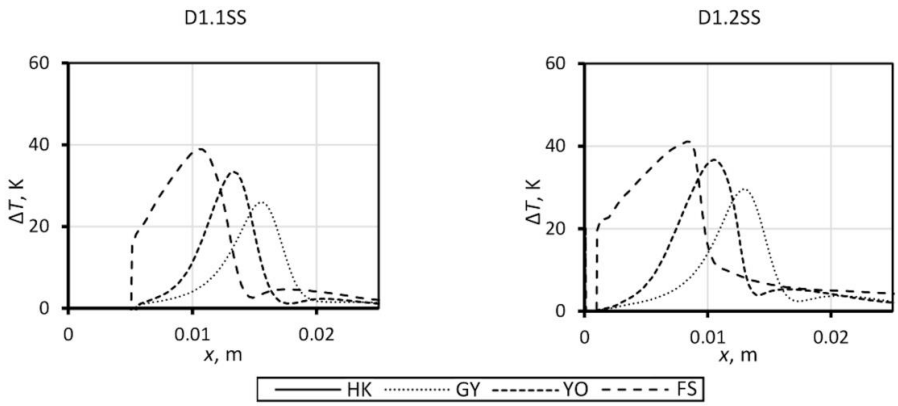

Figure 0.19. Comparison of temperature difference $\Delta T = T_l - T_v$; distributions along the nozzle centre line calculated using different continuous droplet growth models

1.14.3.2 Evaluation of the Hertz-Knudsen droplet growth model with different condensation coefficients

In the Hertz-Knudsen droplet growth model, the condensation coefficient plays an important role. Most researchers set it at 1, assuming thereby that all steam molecules are captured by the growing water droplet. In reality however, some molecules can be deflected from the water droplet surface.

Figure 5.20 presents the computational results of the moist air condensing flow through a circular nozzle obtained for the Hertz-Knudsen droplet growth model with different condensation coefficients. It can be noticed that a decrease in the condensation coefficient value involves weakening of the condensation process, moving the condensation wave downstream and – thereby – decreasing the droplet size.

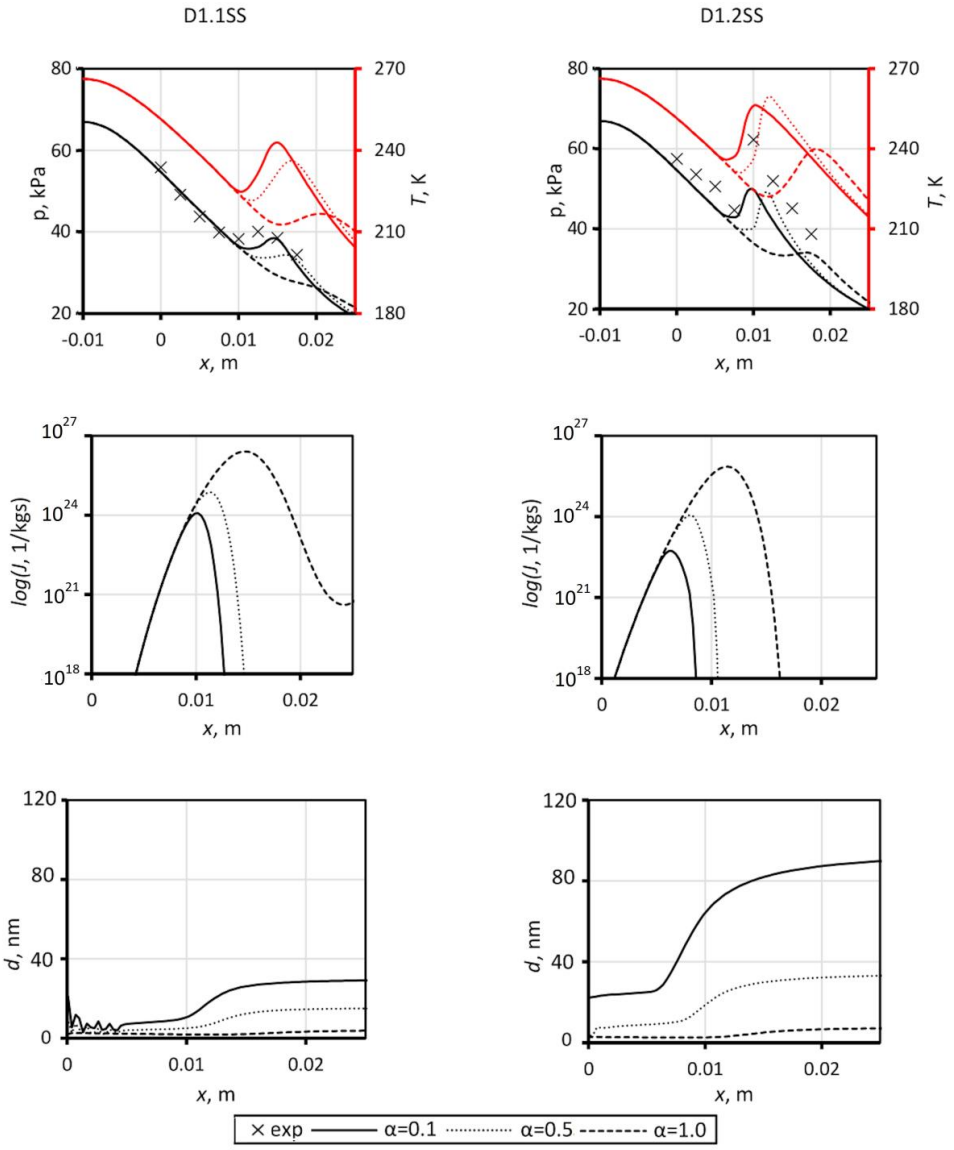

Figure 0.20. Comparison of numerical results against experimental data [24] for the kinetic Hertz-Knudsen droplet growth model with different condensation coefficient values

1.14.3.3 Hybrid droplet growth model proposal and evaluation

As discussed above, the Knudsen number, i.e. the mean free path of the steam molecule over the droplet diameter, decides the type of the droplet growth process. Therefore it seems rational to employ the Blend model described in section 1.8.3, which blends the Continuous and Kinetic models based on the Knudsen number. Figure 5.21 presents the distribution of the blending

factor for the droplet diameter equal to 10^{-6}m. It can be seen that the blending function is applicable over the entire flow domain. Therefore for the process of heterogeneous condensation in moist air, it seems necessary to use eq. 3.25 for the droplet growth model. At first, from the inlet, the kinetic character of the droplet growth is noticeable. However, due to the change in the fluid parameters farther downstream, the importance of the continuous droplet growth model increases.

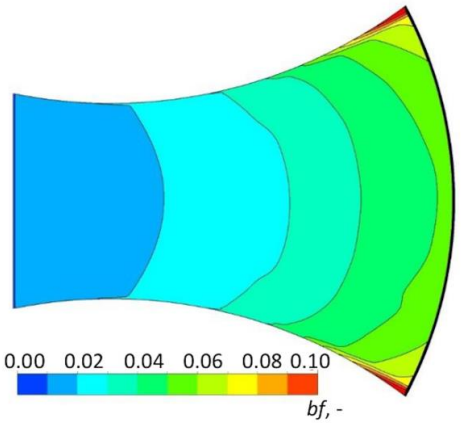

Figure 0.21. Distribution of blending factor *bf* for the condensing flow in a circular nozzle with droplets at the inlet

The proposed model was tested against the Hertz-Knudsen and the Fuchs-Sutugin models. It has to be mentioned that the evaporation coefficient was set to 1 and a continuous model without the FS correction was used. Figure 5.22 presents the impact of the considered Blend model on the condensation process. Due to the character of homogeneous condensation, i.e. the nucleation and growth of very small droplets resulting in large Knudsen numbers, the blending function promotes the Hertz-Knudsen model – the results obtained with the Blend model converge with it. However, if the droplet size is larger, the continuous model starts playing a significant role, which is of great importance for heterogeneous condensation. The proposed Blend model allows omitting the relevance of the droplet size, which is used in the estimation of the Knudsen number and exerts a significant effect on the prediction of the condensation models. It has to be mentioned that the continuous model is derived for the droplet growth in the macroscopic and free molecular region, and the GY, FS and YO correlations were created to meet the predictions of the droplet growth rate in steam. For this reason, their applicability in the analysis of condensation in humid air cannot be assumed arbitrarily. It is therefore

reasonable to perform a comprehensive analysis of the Blend model, as it combines the advantages of the HK model for small droplets and the Continuous model for large droplets.

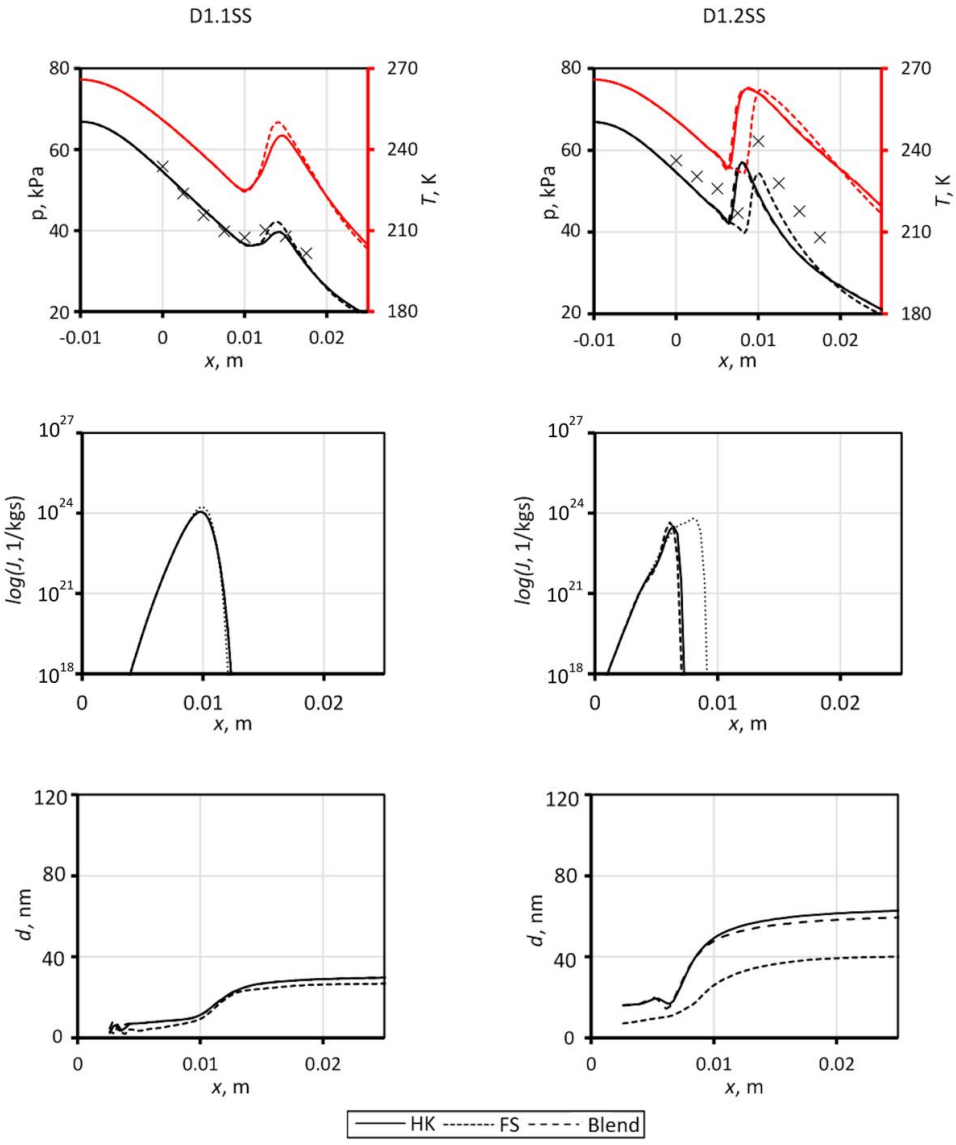

Figure 0.22. Comparison of the Blend, the Hertz-Knudsen and the Fuchs-Suttugin models against experimental data [24]

1.14.3.4 Pressure and condensation wave interaction

This subsection provides a short insight into the condensing flow oscillation due to mutual interaction between the pressure and condensation waves. As this aspect of the research is not

the main focus of this dissertation and because it is presented only to draw attention to the importance of turbulence modelling in the condensing flow analysis, the reader is referred to Wiśniewski's previous work for details regarding the mesh study and the adopted numerical approaches [26].

The nozzle with parallel outlet walls creates the possibility of perceiving high instabilities of the condensation phenomenon yielding to symmetric or non-symmetric oscillations depending on humidity. Therefore the numerical studies were conducted based on Adam's data [4]. The calculations were made for inviscid and viscid flow models, where the *k*-ω SST model was used to describe shear stresses.

The impact of turbulence modelling on the condensing flow was investigated for atmospheric air with the stagnation temperature of 292.8K and the stagnation pressure of 98.8kPa. Three cases with humidity values of 0%, 51.6% and 82% were considered. Figure 5.23 shows the numerical schlieren images for the dry and the humid air flow. In the case of the dry air flow, a characteristic pattern of so-called shock diamonds or Mach disks can be observed (cf. Figure 5.23 A).

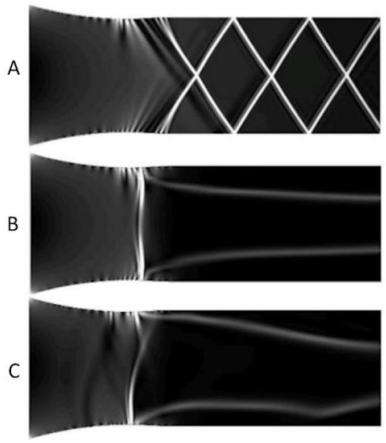

Figure 0.23. Numerical schlieren images for the inviscid flow in a parallel nozzle with the humidity values of A – 0%, B – 51.6% and C – 82%

The Mach discs are consecutive expansion and compression waves. This phenomenon occurs when the flow is underexpanded, i.e. its pressure is lower than ambient, so the supersonic expansion process occurs to reach the ambient pressure value. The flow has to be parallel to the nozzle centre line. Then, if the expansion shock is strong enough to reach the centre line, another

expansion wave occurs and a region where the pressure drops below the ambient pressure value is created. As pressure drops below ambient, a compression shock occurs. For the viscid flow, the distance between consecutive shocks decreases significantly, which is due to viscous losses. Figure 5.24 shows one full oscillation cycle (from top to bottom), the oscillation period for the low-humidity case is 1/195s and for the high-humidity case it totals 1/984s. It shows the influence of the air humidity on the character of the arising condensation waves. Non-symmetric oscillations appear for the high-humidity case. Based on the obtained results, the Fast Fourier Transform was performed to distinguish the major oscillation frequency. The transform was performed on 1024 data points covering 0.04s of the flow. This time is considered to give a reliable description, as it covers at least 10 full oscillation cycles. Figure 5.25 shows the pressure amplitude as a function of frequency for the nozzle with the relative humidity value of 51.6%. The results distinguish two major frequencies for the inviscid method and one for the *k*-ω SST turbulence model. The discrepancy between the numerical simulation and the experimental testing is significant. Additionally, the influence of the turbulence description is not negligible. However, such discrepancy was not observed in the simulation of higher relative humidity values. The frequencies in both the inviscid and the *k*-ω SST models are consistent and show better agreement with the experimental results. The frequency of oscillations computed numerically and the experimental results for the flow with relative humidity φ equal to 51.6% and 82% are shown in Table 0-7. Experimental and numerical frequency of oscillations for the flow with relative humidity φ equal to 51.6% and 82%. Theoretically, the shape of the nozzle contributes to the minimization of viscous effects, due to the very thin wall boundary layer. However, the interaction of the pressure waves with the wall boundary layer, for the viscous flow modelling, has a visible effect on the flow field. The significant influence of turbulence modelling is driven by viscous forces. The experimental data and the numerical results indicate that there is a need for further studies. A comprehensive analysis is planned of the impact of turbulence models on oscillation phenomena.

Table 0-7. Experimental and numerical frequency of oscillations for the flow with relative humidity φ equal to 51.6% and 82%

T_{01}, K	p_{01}, Pa	φ, %	f_{exp}, Hz	f_{invis}, Hz	$f_{k\omega SST}$, Hz
292.8	99800	51.6	225	195 1661	1610

288.2	100000	82.0	905	984	984

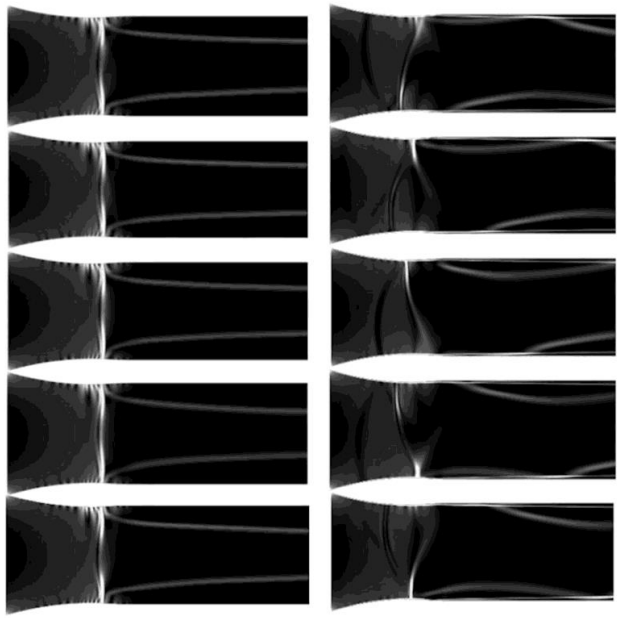

Figure 0.24. One oscillation cycle in a parallel nozzle for the inviscid flow model with the air relative humidity of 51.6% (left, ~Δt=10^{-3}s) and 82% (right, ~Δt=20^{-4}s)

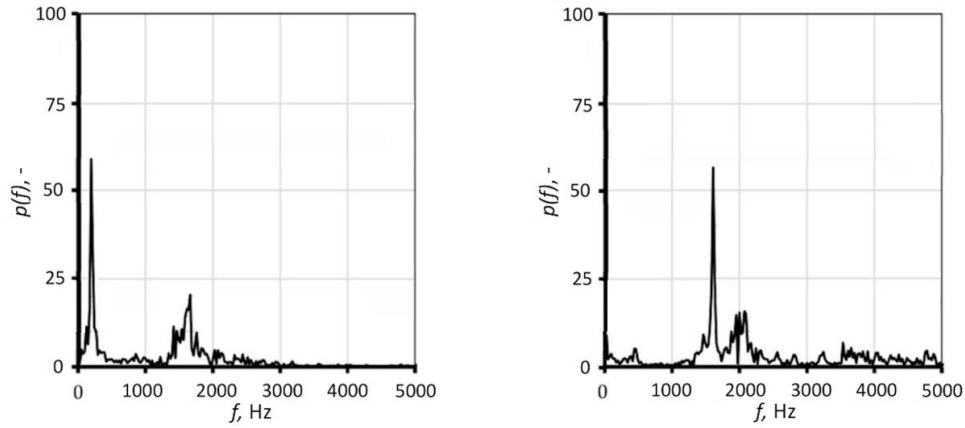

Figure 0.25. Oscillation frequency for the parallel nozzle with the air relative humidity of 51.6%; inviscid (left) and kω-SST(right) modelling

Phase change analysis

The previous chapter concentrated on the validation of the mathematical model of water vapour condensation in air, starting from the testing of the model used to simulate the adiabatic flow for 2D and 3D geometries, through the validation of steam condensation in steam, and ending with the evaluation of the model of steam condensation in the mixture of steam and air, i.e. in humid air. A model validated in this way becomes a powerful tool that makes it possible to investigate the physics of the phenomena occurring in transonic flows of mixtures with a phase change, especially in view of the fact that the mathematical model produces results for quantities that cannot be measured experimentally, such as enthalpy, entropy etc. In this chapter, the focus is on the identification of the condensation phenomenon and determination of the losses arising due to the phase change, i.e. on the condensation impact on the efficiency of machines and equipment.

1.15 Identification of condensation in nozzle flows

As known from the theory of gas dynamics, when the CD nozzle back pressure is elevated above its design value, oblique and then normal shock waves are created in the nozzle diverging part. When the flow conditions are stable, i.e. the back pressure value is constant, the position of the normal shock wave is usually stable, too. In the present analysis, the experimental and numerical CFD results are discussed for the design back pressure corresponding to the supersonic outlet and for the back pressure value raised to 78 kPa.

The subject of the investigations presented herein is the moist air condensing flow through the de Laval nozzle with a low expansion rate $\dot{P} \approx 1000 s^{-1}$. Two main types of flow conditions are considered here. One is the flow through the converging-diverging nozzle with elevated back pressure causing a normal shock wave in the supersonic (divergent) part of the nozzle, while the other is the flow through a nozzle with a supersonic outlet. In each type of flow conditions four cases are analysed, which differ in the air relative humidity at the inlet. In total, this gives eight flow cases that are presented and compared. For all of them a CFD analysis is carried out, but the in-house experimental data are available for some of them only. The research presented herein is a follow-up to earlier works performed by the author in collaboration with other researchers on the moist air transonic flow. It supplements the author's previous studies with a flow case not considered in the literature yet. The moist air condensing flow through a nozzle with a low expansion rate was previously analysed, e.g. by Adam [19],

but his works dealt with the CFD analysis focused on the unsteady effects of the condensation shock in the vicinity of the nozzle throat. The presented results thus have a cognitive value, providing at the same time a very good source for the validation of condensation models.

1.15.1 Identification of flow phenomena

The adiabatic expansion process in the presented nozzle is characterized by the occurrence of aerodynamic waves. The distributions of pressure along the nozzle axis and wall suggest the occurrence of compression waves. However, if the diabatic flow is considered, the waves induced by the phase change impose on the aerodynamic waves, leading to a complex structure of waves interacting with one another. In addition, this varies with an increment in relative humidity. Figure 6.1 confronts the schlieren images, the contours of the Mach number and the source terms with the distribution of pressure, temperature, the mass fraction and the number of droplets along the nozzle axis. This comparison gives an insight into the flow phenomena occurring in the nozzle. As it can be observed, nucleation zones appear downstream of the nozzle throat. Nucleation triggers condensation phenomena causing a condensation wave (marked in yellow). The condensation wave is visible in the form of a bright line in the schlieren photograph and as a jump in temperature and pressure due to a release of latent heat. Further on, the shock wave (marked in red) is visible, causing a sudden increment in pressure and temperature. The shock wave is related to local evaporation, which is represented as a slight decrease in the mass fraction of liquid water. A question arises about the character of the aerodynamic wave present in between the condensation and the compression wave (marked in green). Is it a shifted compression wave present in the adiabatic flow or is it an expansion wave triggered due to condensation? Unfortunately, considering the limited comparative material, it is difficult to answer this question unequivocally.

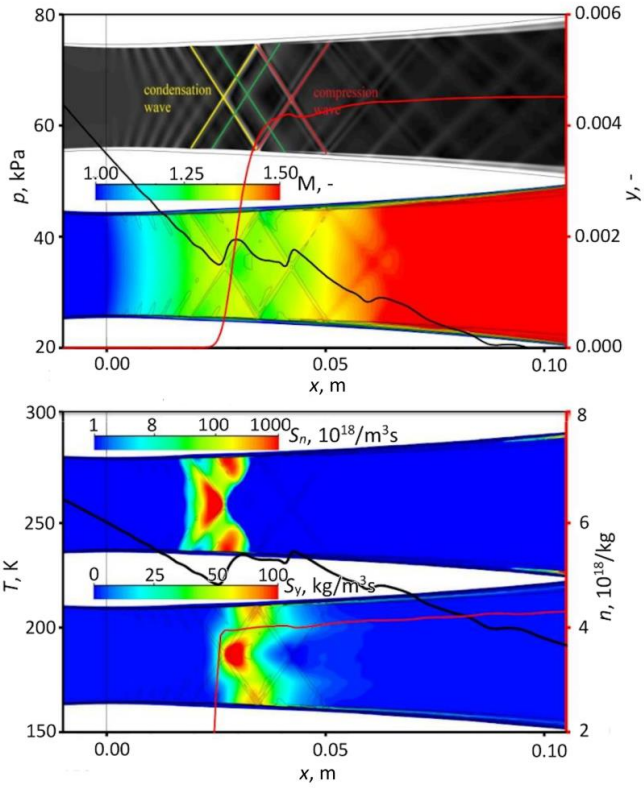

Figure 0.1. Confrontation of contour maps (schlieren image, Mach number, source of mass and droplets) with flow parameters (temperature, pressure, liquid water mass fraction and number of droplets) along the nozzle centre line

1.15.2 Condensation in a nozzle with a supersonic outlet

Because the nozzle in question has a very low expansion rate, the outlet pressure corresponding to the supersonic outlet flow condition is a little higher than 20 kPa. Also, for such a nozzle there is no separation close to the bottom and top walls in the supersonic region (divergent part). The boundary layers do not affect the flow field in a visibly significant way here. Figures 6.2 to 6.5 present the results obtained for the flow test cases with a supersonic outlet. Using experimental and numerical schlieren photography, it is easy to identify the pressure wave structures. Due to the lack of drying of atmospheric air ahead of the nozzle inlet, the experiment was impossible to perform for adiabatic flow conditions. The oblique shock wave structure is visible in the numerical schlieren image for the adiabatic flow case. The X-shaped shock can be easily confused with a condensation shock. A proper condensation wave appears with an increase in the air relative humidity (cf. Figure 6.1). At first, and at a low humidity value, a

clear X-shaped condensation wave appears in the vicinity of the compression wave position for the adiabatic case, whereas the compression wave appears downstream of the condensation wave. With an increment in the air humidity, the amount of latent heat released on the condensation wave increases. For this reason, the condensation wave becomes stronger and moves upstream to form a normal wave. It is worth mentioning that as the condensation wave is shifted and strengthened, the compression wave also moves upstream, but weakens and – in the extreme case – combines with the condensation wave.

Figure 6.3 shows the Mach number and the liquid mass fraction formed due to homogeneous condensation for all the flow cases with a supersonic outlet. The rise in the air relative humidity affects the mass fraction value of the liquid phase at the nozzle outlet. The impact of the latent heat released during condensation on the Mach number corresponds to the phenomena observed using visual quantification. The latent heat released due to condensation leads to a local drop in the flow velocity. As the air humidity increases, this effect strengthens, leading to a significant drop in the Mach number for high humidity values.

The static pressure distributions on the nozzle bottom wall and along the nozzle centre line are presented in Figure 6.4. It can be noticed here that the condensation wave for low values of humidity appears in the vicinity of the compression wave in the adiabatic case. With an increment in humidity, the condensation set-off moves upstream the nozzle in the wall region as well as along the nozzle centre line. It can be seen here that the increase in local pressure is strictly related to the air humidity, i.e. its value grows as the air humidity rises. The pressure peaks correspond to the positions of the pressure waves observed in the schlieren images.

Figure 6.5 gathers the static pressure distributions along the bottom wall and the centre line of the nozzle. It can be concluded that the higher the air relative humidity, the earlier the occurrence of condensation. Moreover, it can be seen that the compression wave weakens with the increasing impact of condensation.

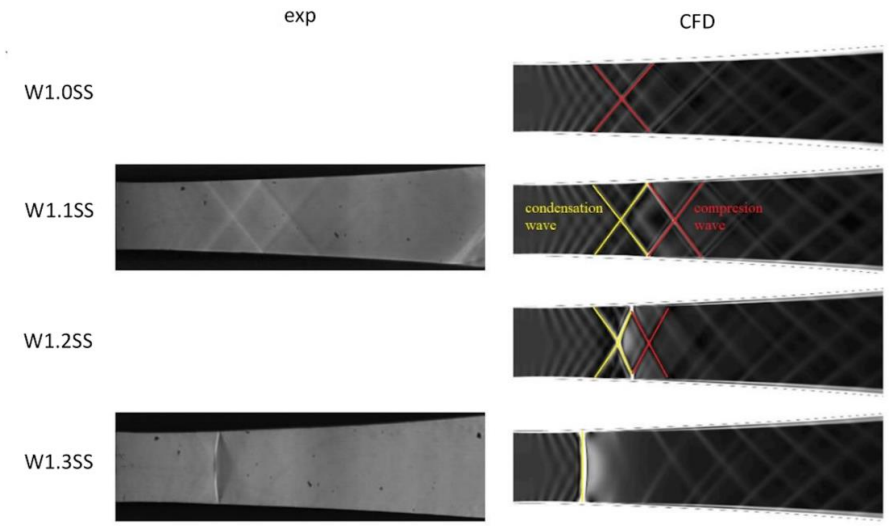

Figure 0.2. Experimental (left) and numerical (right) schlieren photographs for the test cases with a supersonic outlet

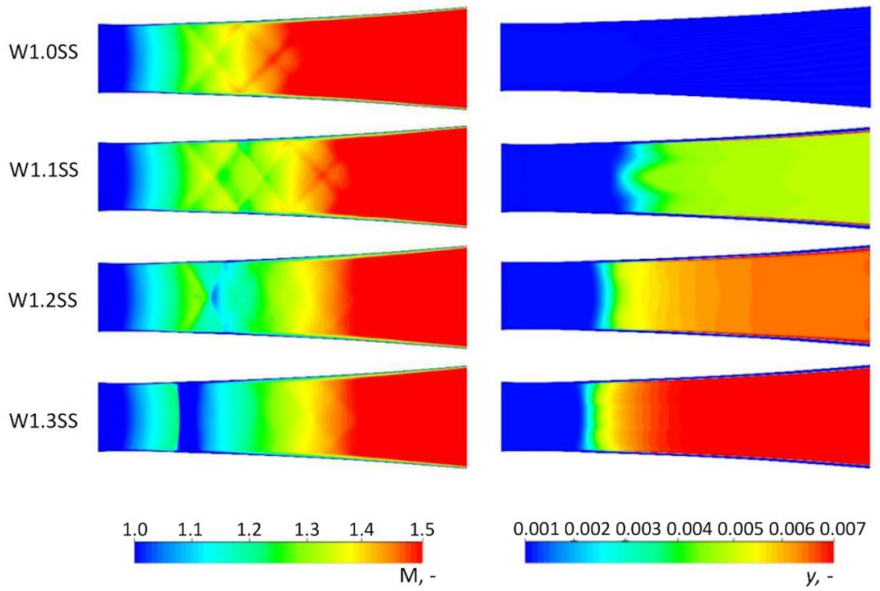

Figure 0.3. Contours of the Mach number (left) and the liquid water mass fraction (right) for the test cases with a supersonic outlet

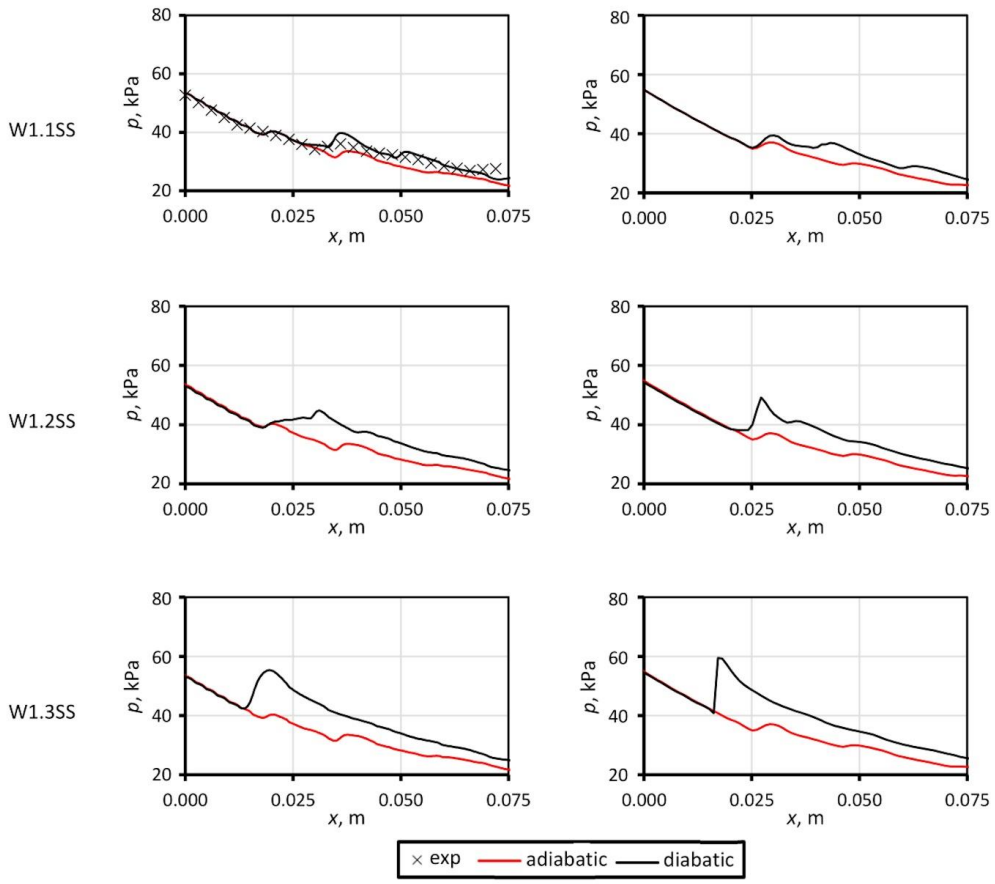

Figure 0.4. Pressure distribution on the nozzle wall (left) and along the nozzle centre line (right) in comparison with experimental results for the cases with a supersonic outlet

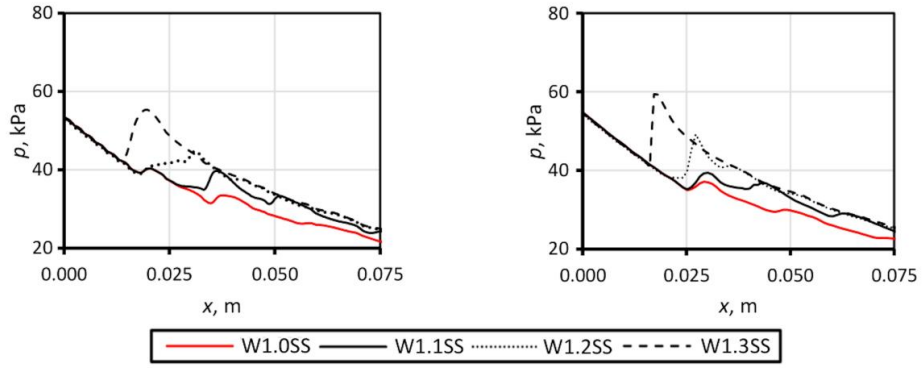

Figure 0.5. Impact of humidity on the shock wave position on the nozzle wall (left) and along the nozzle centre line (right) for different cases with a supersonic outlet

1.15.3 Condensation in a nozzle with elevated back pressure

The other group of flow test cases corresponds to the same relative humidity of air at the inlet as for the cases with a supersonic outlet. The only difference is in the back pressure value, which is raised here to 78 kPa. Due to the raised value of back pressure, a normal shock wave appeared in the nozzle supersonic part. The adiabatic case (dry air) was studied only numerically because it was impossible to dry air at the nozzle inlet. Like for the cases with a supersonic outlet, experimental and numerical schlieren imaging makes it possible to identify condensation and pressure wave structures. In Figure 6.6 it can be observed that the shock wave, which is a strong compression wave, is preceded by a compression wave in the adiabatic case. However, if air humidity is considered, the condensation wave appears downstream of the nozzle throat in the vicinity of the compression wave position based on the adiabatic flow, which leads to a shift of the shock wave downstream the diverging part of the nozzle. Like in the supersonic cases, the condensation wave is followed by a compression wave, which weakens with a rise in humidity to finally combine with the condensation wave. Additionally, it can be seen that with an increment in the air humidity, the shock wave moves downstream the flow and weakens. This can be explained by the constant pressure at the nozzle outlet in both experimental and numerical testing. Due to the release of latent heat, the fluid static pressure downstream of the condensation wave increases. Therefore, the pressure ratio before and after the shock decreases, leading to a weaker shock.

Figure 6.7 shows the Mach number contours and the liquid mass fraction for the considered flows with elevated back pressure. The flow field ahead of the normal shock wave is identical to the cases with a supersonic outlet. The Mach number contours show that with the increasing importance of condensation, the lower maximum velocity is reached before the shock wave. Figure 6.7 also illustrates partial evaporation of the liquid phase on the normal shock wave. The strength of the normal shock wave is not high enough for complete evaporation. A question arises about the state of the droplets after the shock wave. Did rapid freezing occur due to the collision with the flow discontinuity, or did the droplet splash into smaller ones? These phenomena need to be investigated further, as they might be crucial while studying the condensation impact on the reliability and wear of turbomachinery.

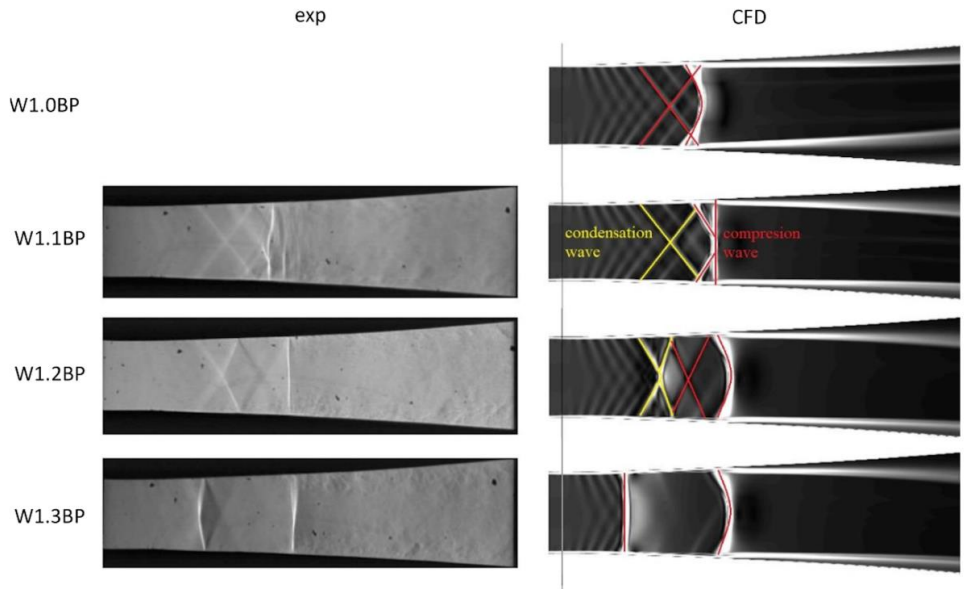

Figure 0.6. Experimental (left) and numerical (right) schlieren images for the test cases with elevated back pressure

The static pressure distributions along the nozzle bottom wall and the nozzle centre line are shown in Figure 6.8. The results on the bottom wall for the diabatic cases were compared with experimental data, and very good agreement was found between the numerical model and the experiments. The charts show how big a difference there is between static pressure distributions for adiabatic and diabatic flows. If condensation is taken into consideration, the pressure increment, the velocity drop, and other phenomena due to the release of latent heat, affect the position of the shock wave – it is shifted downstream the flow. It is especially visible in Figure 6.9, which gathers the static pressure distributions for all the cases with a normal shock wave. It proves that the condensation process must be taken into consideration in the analysis of the flow of atmospheric air.

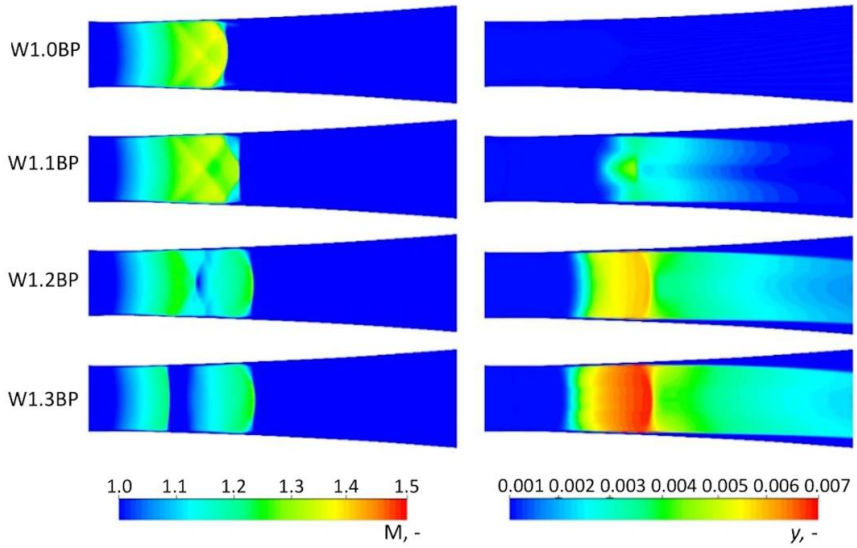

Figure 0.7. Contours of the Mach number (left) and the liquid water mass fraction (right) for the test case with elevated back pressure

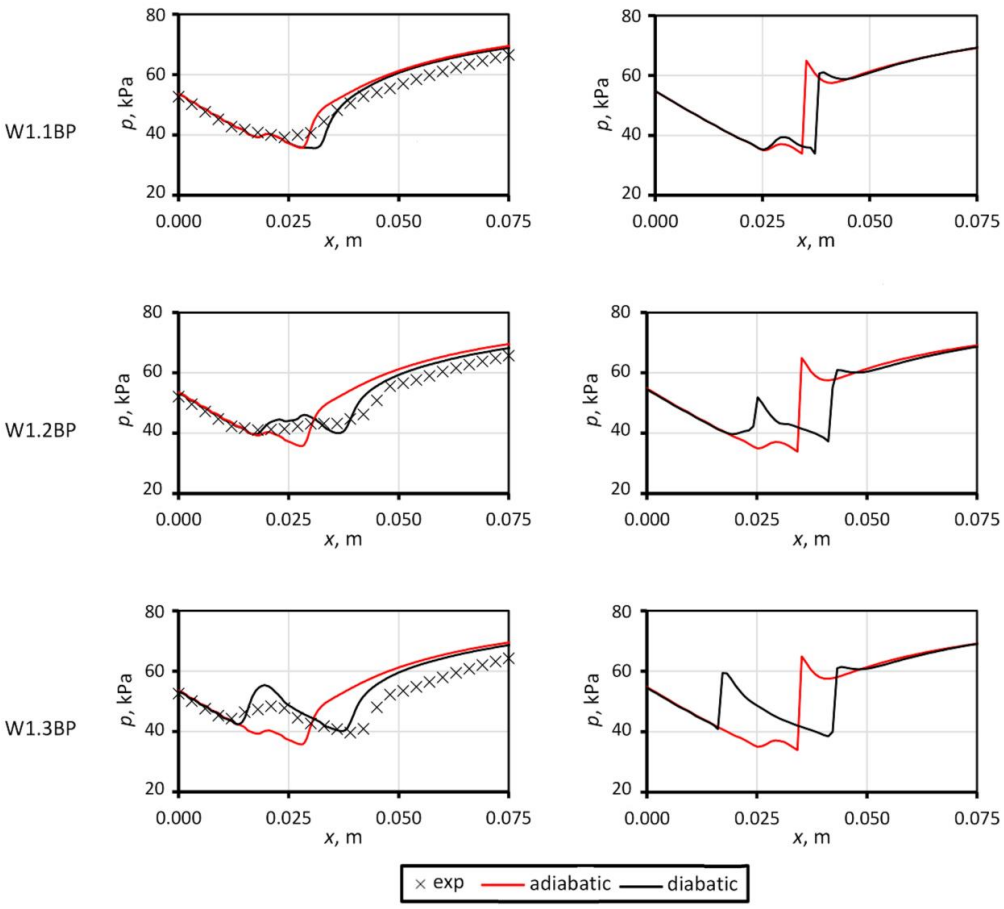

Figure 0.8. Pressure distribution on the nozzle wall (left) and along the nozzle centre line (right) in comparison with the experimental results for the cases with elevated back pressure

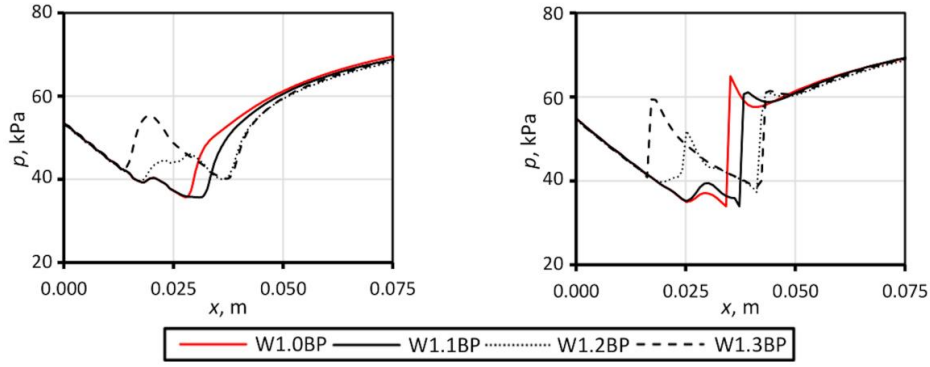

Figure 0.9. The impact of humidity on the shock wave position on the nozzle wall (left) and along the nozzle centre line (right) for the cases with elevated back pressure

1.15.4 Assessment of aerodynamic and thermodynamic losses

The design of high-efficiency machinery is the focus of interest in many technical applications. For this reason, the assessment of aerodynamic and thermodynamic losses is very important. The losses can easily be understood as a drop in total flow parameters. Figure 6.10 shows the distribution of static and total parameters along the nozzle, as well as the impact of condensation and shock on them. For the adiabatic flow, the losses are related to viscous effects and the shock wave. In the case of an adiabatic flow with a supersonic outlet, viscous losses are present only. For a geometry as simple as the nozzle, they are negligible and do not affect total parameters. However, if back pressure is elevated, the shock wave is present, causing a decrease in the fluid total pressure. In the case of a diabatic flow with a supersonic outlet, both the decrease and the increase in total pressure are caused by condensation. It should be noted that if a shock wave appears in the flow, the condensate evaporates on it, which leads to partial recovery of total pressure and a drop in total temperature to the initial value.

The efficiency of a nozzle is usually computed based on the increment in entropy [67]. For the adiabatic flow, the entropy increase can be calculated based on the change in total pressure (eq. 6.1). However, if a diabatic case is considered, the calculations should be extended to include the change in the fluid total temperature (eq. 6.2).

$$ds = -Rln\left(\frac{p_{02}}{p_{01}}\right) \tag{6.1}$$

$$ds = c_p \ln\left(\frac{T_{02}}{T_{01}}\right) - Rln\left(\frac{p_{02}}{p_{01}}\right) \tag{6.2}$$

The entropy loss coefficient can be defined as follows:

$$\zeta = \frac{T_2\left(c_p \ln\left(\frac{T_{02}}{T_{01}}\right) - Rln\left(\frac{p_{02}}{p_{01}}\right)\right)}{\frac{v_2^2}{2}} \tag{6.3}$$

whereas the relation between efficiency and entropy can be seen on the entropy diagram (cf. Figure 6.11). Assuming no difference between static temperature in real and ideal processes, efficiency can be defined as follows:

$$\eta = \frac{h_1 - h_2}{h_1 - h_2 + T_2 ds} \tag{6.4}$$

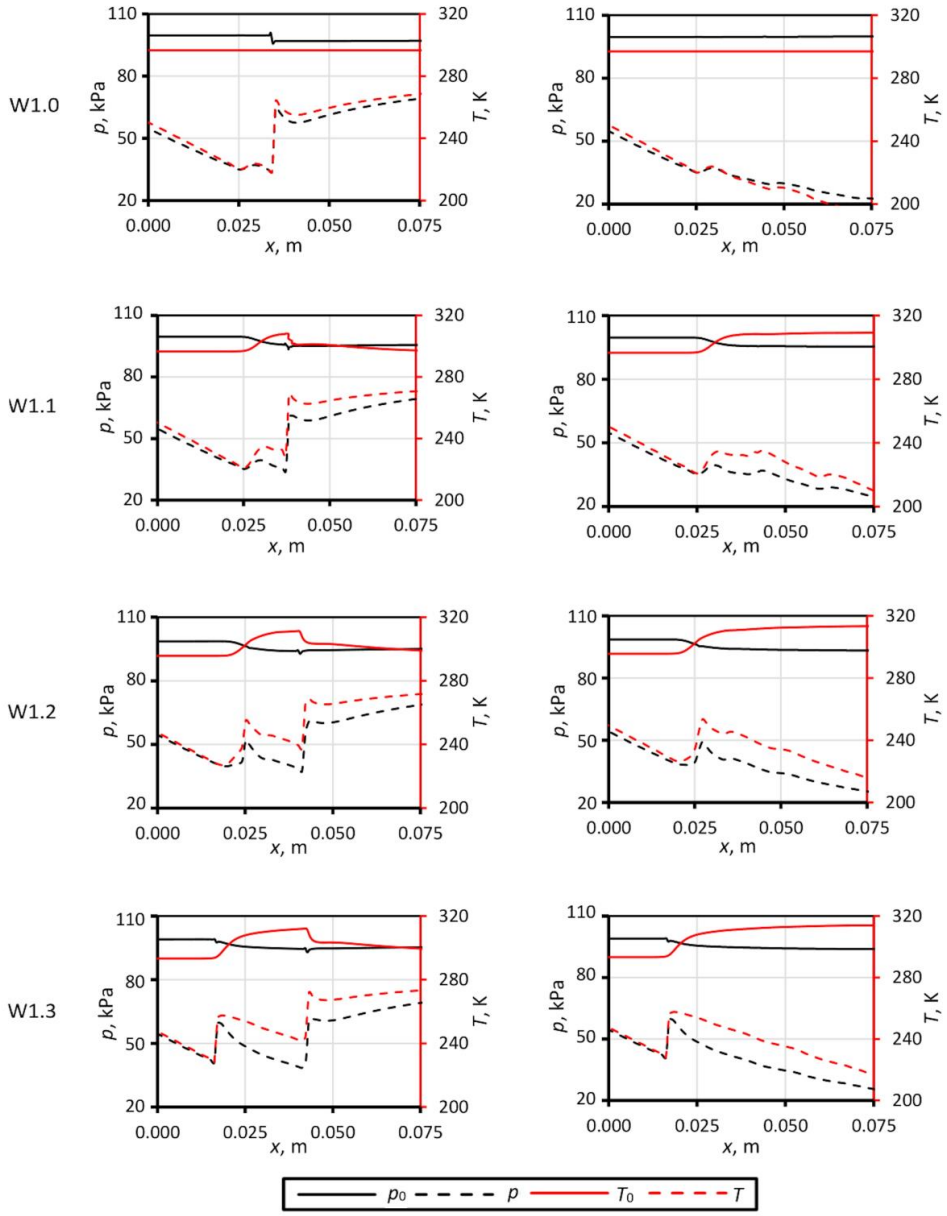

Figure 0.10. Static and total parameters along the nozzle centre line for different humidity for cases with elevated back pressure (left) and a supersonic outlet (right)

Table 0-1 presents the efficiency value for a nozzle with a supersonic outlet determined along the nozzle centre line, i.e. along the streamline. The values of efficiency based on the calculations performed for adiabatic and diabatic flows are shown to present the importance of phase-change considerations. As it can be seen, if the phase change is omitted, the nozzle efficiency calculated along the nozzle centre line is 100%. This means that the boundary layer has no effect on the nozzle efficiency. Efficiencies η_1 and η_2 differ from each other by the definition of the entropy increase, they use eq. 6.1 and eq. 6.2, respectively. The results listed below confirm the need to take account of the total temperature change in diabatic flows by evaluating losses. It should be noted that with an increase in humidity, condensation-related thermodynamic losses become more important and rise with the humidity of air.

Table 0-1. Value of isentropic efficiency for the W1 nozzle with a supersonic outlet

Test case	η_1	η_2
W1.0SS	1	1
W1.1SS	0.9844	0.9421
W1.2SS	0.9823	0.9360
W1.3SS	0.9818	0.9274

The expansion line is a representation of expansion in the enthalpy-entropy chart. It represents the expansion phenomena along the nozzle centre line and gives a valuable insight into the impact of condensation on the increase in entropy in the humid air flow through a nozzle with a supersonic outlet. The expansion line presented in Figure 6.11 for the adiabatic case is almost straight. However, a sudden increment in enthalpy and entropy is observed on the lines representing the expansion of humid air. This peak is due to condensation, which leads to a sudden release of latent heat, causing a local increment in the fluid static enthalpy. The increase in entropy is of the same origin. It can be noticed that with a rise in humidity, the entropy increase due to condensation is bigger, which decreases the nozzle efficiency.

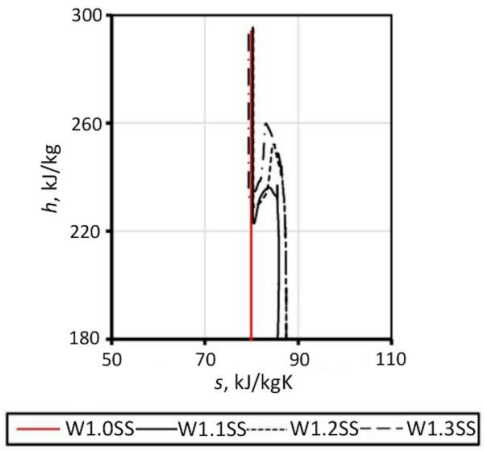

Figure 0.11. Influence of air relative pressure on the expansion curve in the nozzle with a supersonic outlet

1.15.5 Condensation in an asymmetric nozzle

Most of the flows occurring in nature and engineering are asymmetric. The blade channel of a turbine, compressor or fan is curved no matter whether it is axial or radial. Due to that, the flow becomes asymmetric, which may give rise to additional physical phenomena, such as swirls or reverse flows. A numerical analysis of condensation in this type of flow reveals some interesting phenomena. This work presents experimental and numerical testing of flows through asymmetric nozzles with a low expansion rate for different atmospheric conditions where the outlet is supersonic and the inlet is characterized by elevated pressure.

The flow asymmetry results in an asymmetric character of condensation and pressure waves. Figure 6.12 shows the numerical schlieren image for the W2.0SS nozzle and the pressure distribution along the nozzle bottom and top walls. As it can be seen in the W2.0SS case, pressure waves with an asymmetric nature (marked in red) appear in the flow instead of X-shaped waves observed in the symmetric nozzle.

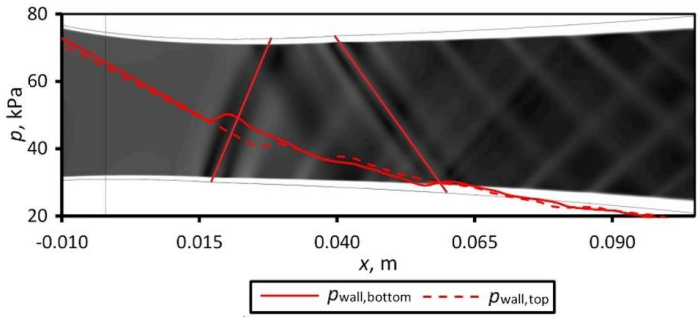

Figure 0.12. Schlieren photography and static pressure along the top and bottom walls of the asymmetric nozzle for the adiabatic flow

1.15.5.1 Condensation in an asymmetric nozzle with a supersonic outlet

If the humid flow is considered, compression waves interact with condensation waves and can be easily confused with them, especially for low-humidity flows. If the static pressure distributions on the nozzle bottom wall are obtained experimentally and numerically (cf. Figure 6.13), good agreement can be seen between them. The static pressure values along the nozzle wall and centre line for the adiabatic and the diabatic flow (red and black line, respectively) suggest that the condensation wave position on the bottom as well as on the top wall is similar.

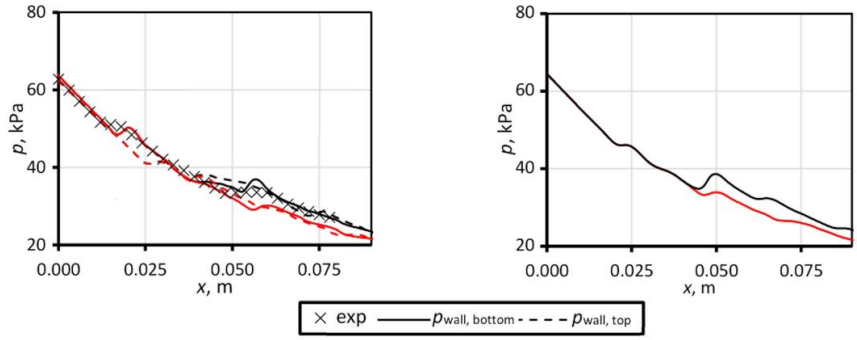

Figure 0.13. Static pressure distribution along the nozzle walls obtained experimentally and numerically (left) and static pressure along the nozzle centre line (right) for the adiabatic and diabatic asymmetric nozzle with a supersonic outlet

However, if schlieren photography is considered, numerical studies indicate a strengthening of the second expansion wave (cf. Figure 6.14), which suggests that the condensation wave

appears in the vicinity of the compression wave position for the adiabatic case, whereas the compression wave appears downstream of the condensation wave as a reflected wave. Similar conclusions can be drawn considering the experimental schlieren photographs below, where the oblique wave might be considered as a condensation wave.

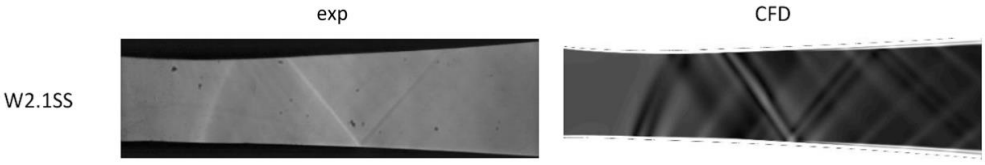

Figure 0.14. Experimental and numerical schlieren photographs for the asymmetric nozzle with a supersonic outlet

Confronting the pressure distribution along the nozzle walls with the Mach number and the condensate mass, it is found that the waves obtained from visual measurements can be misleading. It can be seen in Figure 6.15 that condensation occurs ~0.04m downstream of the nozzle throat and it is almost normal to the flow direction. This phenomenon is not visible using the schlieren technique and the observed waves are compression waves. This indicates that there is a need for further experimental and numerical research in a wide range of ambient conditions to achieve a better understanding of condensation-related phenomena in asymmetric flows.

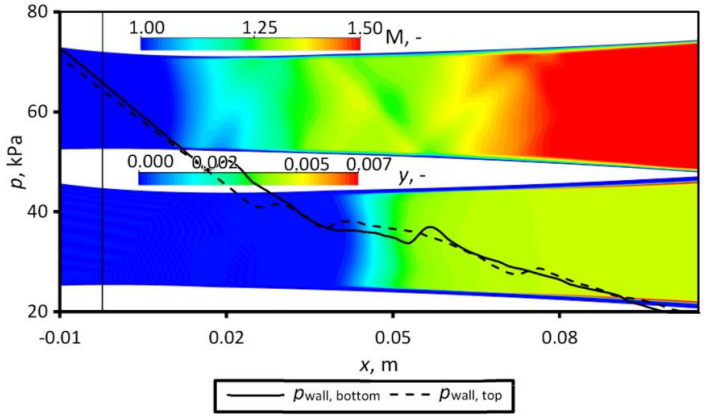

Figure 0.15. Confrontation of contour maps (Mach number, condensate mass) with the pressure distribution along the nozzle top and bottom walls

1.15.5.2 Condensation in an asymmetric nozzle with elevated back pressure

The condensing flow with a shock wave was tested for two back pressure values. The back pressures were selected to obtain shock waves slightly upstream and downstream of the position of the condensation wave obtained in the numerical study of a case with a supersonic outlet. Figure 6.16 shows that for the case with lower back pressure (PB1), i.e. the case with a shock wave downstream of the condensation zone, the shock wave is shifted downstream in comparison to the adiabatic case. In the case of higher back pressure (PB2), the shock wave is also shifted downstream, but only a little, which indicates that the effect of condensation is smaller.

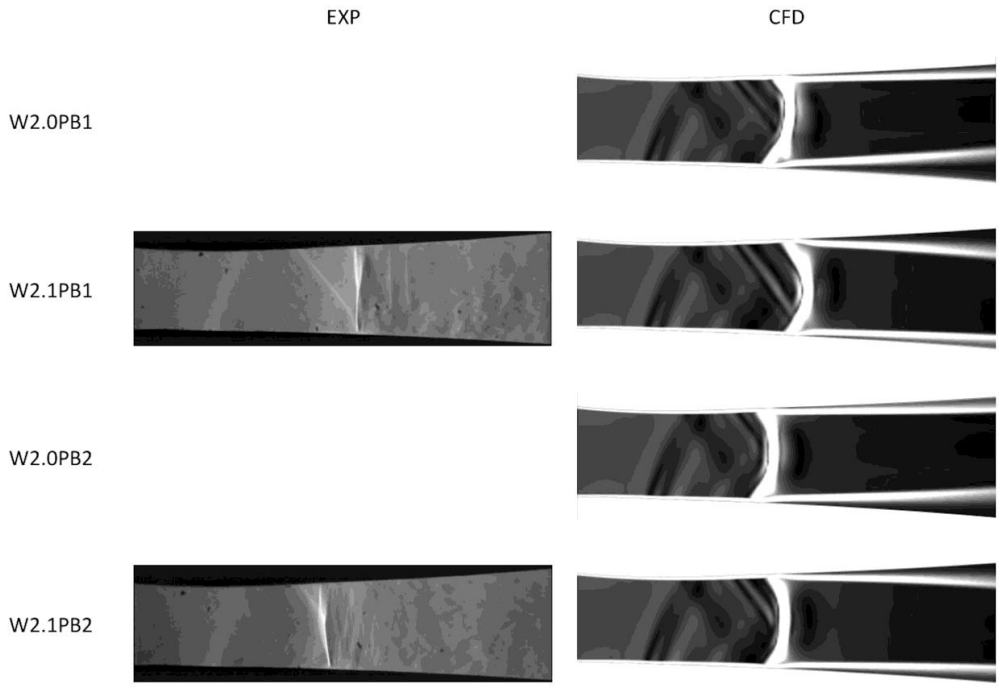

Figure 0.16. Experimental and numerical schlieren photographs for the asymmetric nozzle with an elevated back pressure

Figure 6.17 shows the static pressure distribution obtained numerically and experimentally along the nozzle wall for the adiabatic and the diabatic case (red and black line, respectively). It also shows the static pressure values along the nozzle centre line. It can be seen that in the PB1 case, the numerical model predicts the position of the shock wave correctly, whereas the computed position of the shock wave for PB2 is slightly shifted downstream of the nozzle. This

points to an overestimation of condensation, which causes an increase in the static parameters upwind the shock wave, and thus the wave is shifted downstream.

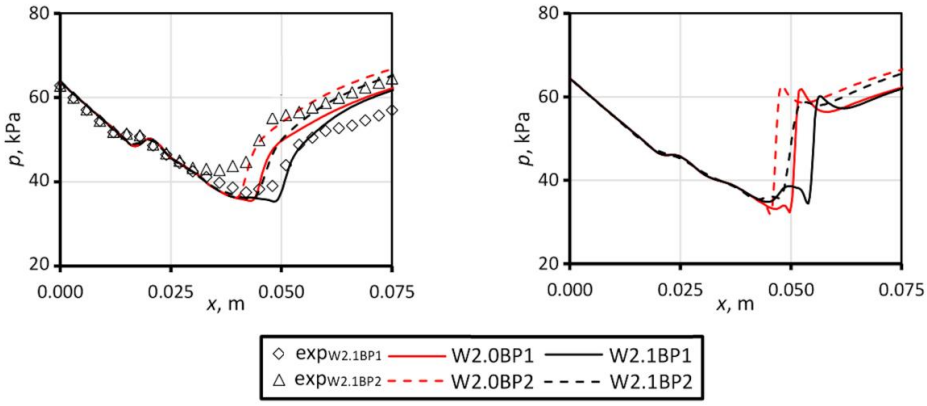

Figure 0.17. Static pressure distribution along the nozzle wall obtained experimentally and numerically (left) and static pressure values along the nozzle centre line (right) for the adiabatic and the diabatic asymmetric nozzle with elevated back pressure

The contours of the Mach number and the condensate mass fraction together with the static pressure and the condensate mass along the nozzle centre line are compared in Figure 6.18 for PB1 and PB2. The contour maps show that the condensation in the PB2 case is lower than in the PB1 case. This is also visible on the pressure curve, as there is a lower increment in static pressure in the condensation region. The condensate evaporation on the shock wave is due to the increment in static parameters. It can be seen that in both cases the mass of liquid water is about 0.02, which is due to the local saturation parameters.

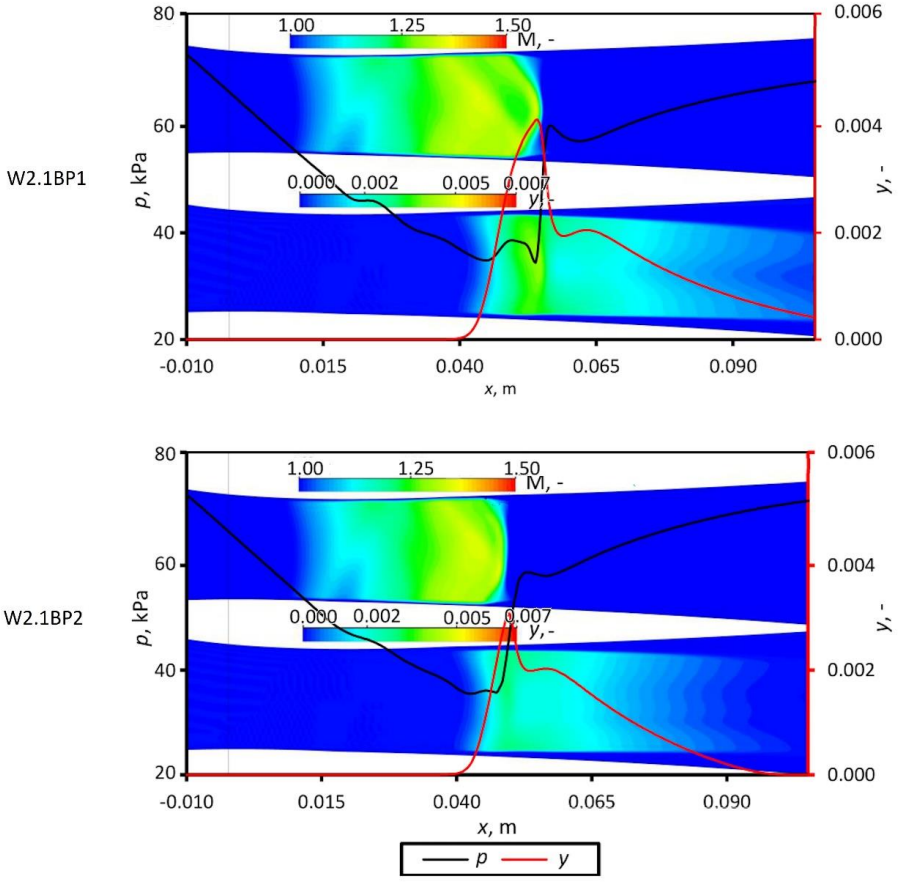

Figure 0.18. Confrontation of contour maps (Mach number, condensate mass fraction) with pressure and the condensate mass fraction along the nozzle centre line

1.15.6 External flow

External flows are of major importance especially in aviation, where the understanding of the flow around the airfoil is crucial during the aircraft design and operation. The impact on the flow around a blade exerted by steam condensation, triggered spontaneously or resulting due to the presence of suspended particles or evaporation of water on the shock wave, affects the pressure distribution along the airfoil. It also affects the airfoil lift and drag forces. This section presents an evaluation of atmospheric air properties (humidity, temperature). Table 0-2 shows the boundary conditions adopted for the computations. The Mach number value corresponds to the RAE 2822 experimental study, but temperature, pressure and velocity were varied to simulate real parameters of an aircraft wing operation in typical take-off and landing conditions.

Table 0-2. Boundary conditions for NASA RAE282

	p_0, kPa	T_0, K	φ, %	$M, -$
RAE1.0	155	335	0	0.73
RAE1.1	155	335	70	0.73
RAE1.2	155	335	90	0.73

At first, computations were performed to determine the impact of the air relative humidity (φ) of 70% and 90%. For a low angle of attack (less than 4º), the local acceleration, and thus the drop in static temperature and pressure, is relatively low and the condensation phenomenon almost does not occur. The importance of condensation increases with the angle of attack. Figure 6.19 presents the static pressure distribution using the pressure coefficient along the airfoil obtained in numerical studies for the angle of attack of 4º and 8º. The condensation process occurs at the suction surface of the airfoil, in the vicinity of the sonic region. This is accompanied by a sudden rise in pressure in this region. The release of latent heat causes an increment in pressure; the pressure coefficient drops and the wing works under a less favourable regime.

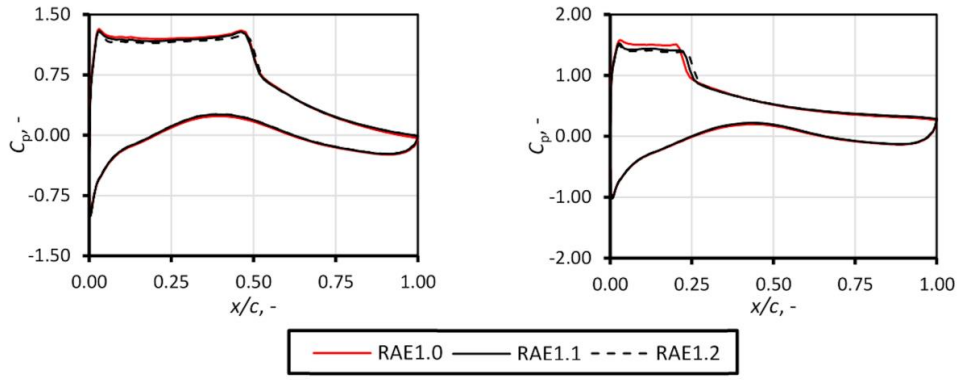

Figure 0.19. Influence of relative humidity on the pressure coefficient distribution along the airfoil for an angle of attack of 4º (left) and 8º (right)

Figure 6.20 shows the impact of relative humidity on the lift and drag coefficients. As it can be seen, for a low angle of attack the impact of condensation is small. With an increment in the angle of attack, the lift generated by the airfoil decreases, whereas the drag increases compared

to the adiabatic case. However, due to the fact that the airfoil efficiency is defined as the ratio between lift and drag coefficients, the relative change in both values is considered. As it can be observed in Figure 6.21, even a slightest change in lift and drag coefficients is significant. Thus the impact of condensation on the airfoil efficiency is crucial at low and moderate angles of attack.

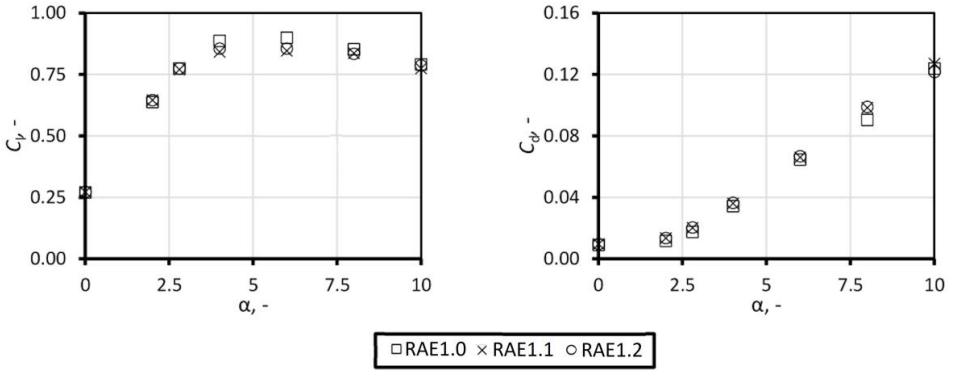

Figure 0.20. Influence of relative humidity on the lift coefficient (left) and the drag coefficient (right) depending on the angle of attack

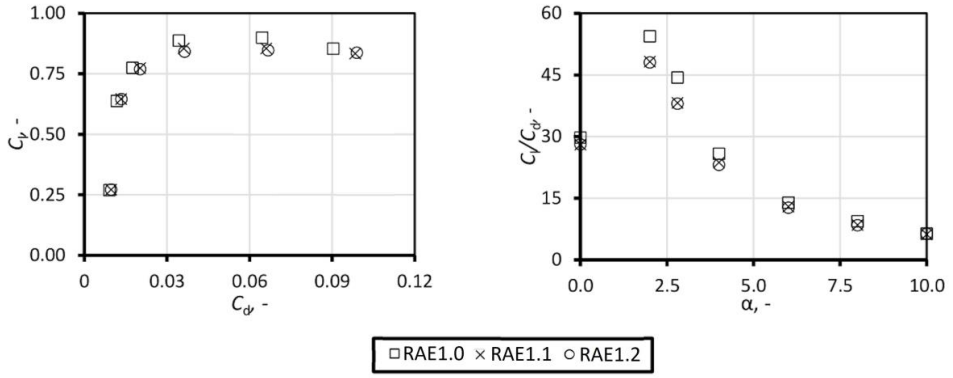

Figure 0.21. Lift-to-drag ratio for different relative humidity values (left) and the impact of relative humidity on the lift-to-drag ratio as a function of the angle of attack

Figure 6.22 shows the contours of condensed water and indicates the sonic region. As the angle of attack increases, up to ~6º the local velocity value increases while maintaining a large sonic region. Further on, the shock wave moves significantly upwind the airfoil. Condensation occurs in the sonic region, where the vapour pressure drops below the saturation pressure value. Then

evaporation is observed on the shock wave. Despite the fact that the shock wave is relatively strong (the drop in the Mach number is from 1.4 to 0.7), only partial evaporation is observed. However, there appears a wake region, where the temperature increase is significant.

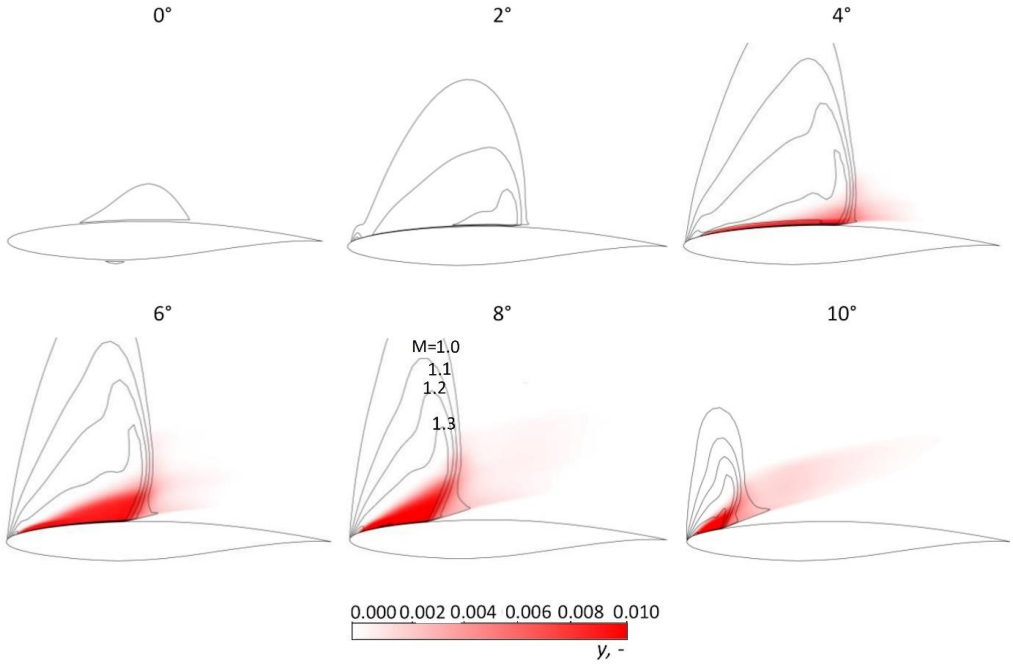

Figure 0.22. Contours of the condensate mass and the indication of the sonic regime for angles of attack in the range from 0º to 10º for RAE1.2

All the observations concerning the impact of condensation on the pressure distribution along the airfoil, the lift and drag coefficients, the mass fraction and velocities for different angles of attack complement one another. In conclusion, condensation is of major importance for low and moderate angles of attack due to a relatively large sonic region, where due to the latent heat release, the pressure coefficient drops (fluid pressure increases) and the airfoil works under a less favourable regime. For large angles of attack the importance of condensation diminishes as the shock wave moves upstream and shrinks the sonic region. It has to be emphasized that during a normal flight, the airfoil usually works in the range of low and moderate angles of attack and therefore the condensation phenomenon should be taken into consideration because it affects the work of the wing and can be crucial from the economic point of view.

1.16 Impact of suspended particles on the condensation process

In many applications it is physically impossible to dry or filter the working fluid. As shown in previous chapters, the phase change affects flow phenomena considerably. To this extent the focus was on homogeneous condensation. However, due to the omnipresent existence of suspended particles in atmospheric air, heterogeneous condensation should not be omitted. This section investigates heterogeneous condensation on solid particles (HS) and liquid droplets (HW). The data regarding the number and the radius of solid particles present in polluted air are based on the literature data, whereas the number and the radius of liquid droplets are based on the literature data for typical rain and fog conditions. Table 0-3 gathers the data for the considered HS and HW cases.

The number of suspended solid particles (n_{het}) adopted for cases HS1, HS2 and HS3 totalling 10^{13}, 10^{14} and 10^{15} per kg of air, respectively, is based on the data of PM10 air pollution available in the literature [57]. Cases HS1, HS2 and HS3 can be considered as air of good, average and bad quality, respectively. It has to be mentioned that the particle diameter is constant and equal to $2 \cdot 10^{-7}$m, which is smaller compared to a standard PM10 particle. However, it is justified considering that PM10 consists of particles with a diameter of up to $2 \cdot 10^{-5}$m. In the HW approach, the number of suspended droplets n_{het} for cases HW1, HW2 and HW3 is adopted as 10^{11}, $2.5 \cdot 10^{11}$ and 10^{12} per kg of air, respectively, which results in standard mass values of water suspended in the air over a range of different weather conditions (e.g., cloud and fog) [72]. The diameter of the droplets at the inlet is $2 \cdot 10^{-6}$ m.

Table 0-3. Details of the number and diameter of heterogeneous droplets

	$n_{\mathrm{het}}, \frac{1}{\mathrm{kg}}$	$d_{\mathrm{het,0}}$, m		$n_{\mathrm{het}}, \frac{1}{\mathrm{kg}}$	$d_{\mathrm{het,0}}$, m
HS1	10^{13}	$2 \cdot 10^{-7}$	HW1	10^{11}	$2 \cdot 10^{-6}$
HS2	10^{14}	$2 \cdot 10^{-7}$	HW2	$2.5 \cdot 10^{11}$	$2 \cdot 10^{-6}$
HS3	10^{15}	$2 \cdot 10^{-7}$	HW3	10^{12}	$2 \cdot 10^{-6}$

1.16.1 Heterogeneous condensation

The particles suspended in the fluid have a significant impact on the condensation phenomena and the fluid properties. The effect of the presence of liquid or solid particles on the flow is

different. The presence of solid particles triggers heterogeneous condensation; a high number of particles decreases the importance of homogeneous condensation as steam condensation occurs gradually upstream of the location of the condensation wave. Moreover, if liquid droplets are present in the fluid, additional latent heat is introduced into the system and absorbed by the fluid due to evaporation of the droplets on the shock wave. In this study, the investigation of the condensation model in terms of the importance of heterogeneous condensation is shown for three cases differing in the number of liquid droplets (cf. Table 0-3). These numbers correspond to standard mass values of water suspended in the air in different weather conditions (e.g. cloud or fog). The presented numerical study investigates the suitability of different droplet growth models for heterogeneous condensation.

Figure 6.23 shows the impact of the presence of liquid droplets at the nozzle inlet. It can be seen that as the number of liquid droplets at the inlet rises, the condensation wave is shifted farther downstream of the nozzle. This is an effect of steam condensation on the suspended particles. The nucleation process, which triggers homogeneous condensation, occurs when the supercooling of steam is significant [43]. By contrast, heterogeneous condensation is a process that does not involve nucleation and occurs gradually in a less supercooled environment. Steam condenses on suspended particles or droplets and latent heat is absorbed by the condensate. Due to that, the flow temperature, pressure, vapour partial pressure, etc., decrease, which leads to lower supercooling of steam and a shift of the nucleation zone downstream the flow. If the number of droplets is large, heterogeneous condensation becomes the major condensation phenomenon.

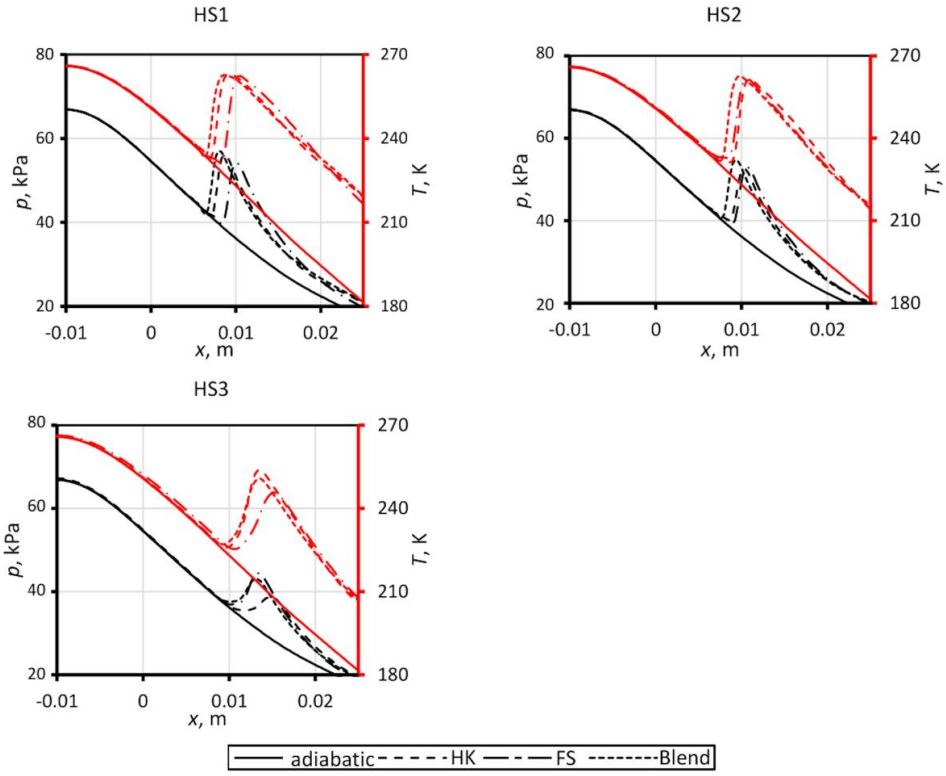

Figure 0.23. Impact of the number of suspended solid particles and the condensation model on the importance of heterogeneous condensation in D1.2SS

Considering the blending function, it is worth mentioning that for a relatively low number of droplets, the blend model gives results similar to the Hertz-Knudsen model. However, with a rise in the number of droplets, the condensation process based on the blending function changes its character. The Knudsen number decreases, favouring the continuous model, and the results become similar to those obtained from the Fuchs-Sutugin model. It has to be mentioned that with an increment in the Knudsen number, the correction factor of the GY, FS and YO models fades away and the continuous model is reached.

1.16.2 Low-expansion rate nozzle with suspended solid particles and liquid droplets

The study regarding the importance of heterogeneous condensation triggered by suspended solid or liquid particles was carried out for the W1.3SS and W1.3BP cases, i.e. a low-expansion rate nozzle with a supersonic outlet, as well as for the case with elevated back pressure and the

relative humidity value of 51.5%. The studies were performed for different numbers of PM particles $n_{het,}$ with a different diameter d_{het}.

Figure 6.24 presents the impact of condensation on the pressure distribution along the axis of a nozzle with a supersonic outlet (W1.3SS). It can be seen that for low levels of pollution (HS1) heterogeneous condensation plays a minor role, and the expansion process in the nozzle is identical to the case with no pollutants. As pollution gets higher, the share of heterogeneous condensation is increased, steam condenses on droplets already at low velocities, which results in a release of evaporation heat and a rise in pressure parameters upstream of the nozzle throat and weakening, or – in the extreme case (HS3) – total decay of the condensation wave.

Figure 6.24 presents the share of homogeneous (black) and heterogeneous (red) condensation. As it can be observed, homogeneous condensation prevails for the HS1 case, but with a rise in the number of pollutants the share of heterogeneous condensation increases, whereas the effect of homogeneous condensation fades away to completely disappear in the end.

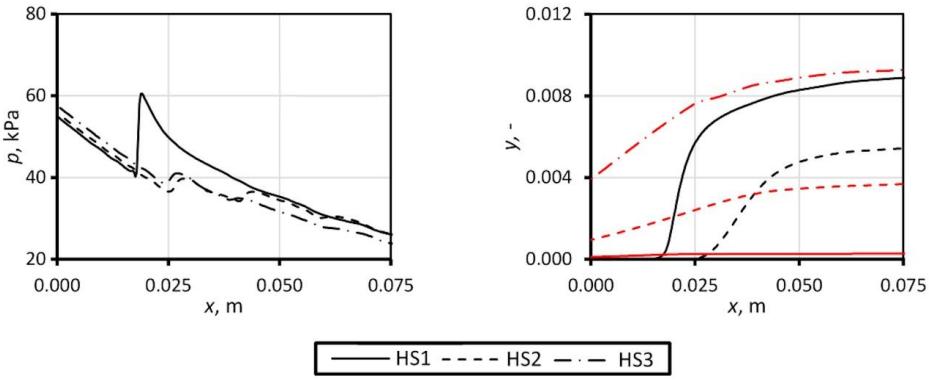

Figure 0.24. Impact of solid particles contained in the air on pressure along the nozzle (left) and the share of homogeneous and heterogeneous condensation (right)

Figure 6.25 presents the size of the droplet created due to homogeneous (black) and heterogeneous (red) condensation. The biggest droplets appear in the case with the intermediate level of pollution – HS2. This is because a condensation wave arises for case HS1, which inhibits the droplet growth. In this situation, abrupt homogenous condensation results in total evaporation of steam, whereas for the HS3 case, despite the fact that the transition occurring in it is mainly heterogeneous, due to the large number of droplets and the limited content of steam in the air, the maximum size of droplets is limited.

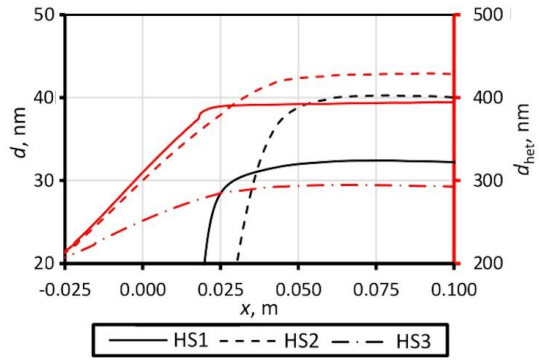

Figure 0.25. Droplet diameter due to homogeneous (black) and heterogeneous (red) condensation; cases HS1, HS2 and HS3 with a supersonic outlet

Similar phenomena can be observed for the flow with a shock wave, i.e. for the W1.3BP variant. As illustrated by Figure 6.26, the condensation wave weakens with the growth of droplets and expansion reaches lower pressure values. The shock wave is thus shifted upstream the flow to meet the boundary condition at the outlet, i.e. back pressure.

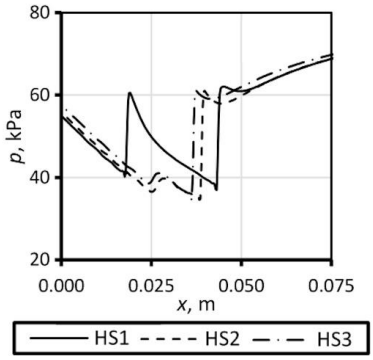

Figure 0.26. Static pressure along the nozzle centre line for cases HS1, HS2 and HS3 for variants with elevated back pressure

Figure 6.27 and Figure 6.28, respectively, present the mass content and the diameter of droplets arising due to homogeneous (black) and heterogeneous (red) condensation. Analysing the figures, a correlation can be noticed between the size of the droplets and the amount of water evaporated on the shock wave.

For the HS1 case, the shock wave results in the evaporation of mainly small droplets formed during the homogeneous transition. Homogeneous condensation involves the creation of droplets with a very small diameter, which results in a high rate of the condensation process,

i.e. a change in diameter *dr*/*dt*. About 50% of the condensate is evaporated on the shock wave: the y_{hom} value drops from 0.008 to 0.004. Because the temperature downstream of the wave totals about 275K, the air capacity for steam is very low. Therefore steam appears at once in the supercooled state, which effectively prevents further vaporization. In the y_{hom} chart this is visible as a flattening following a sudden drop. Next, evaporation occurs due to compression (rise in temperature and pressure).

In the case of the air intermediate level of pollution (HS2), homogeneous condensation and heterogeneous condensation occur in parallel. As the condensation wave is shifted farther compared to case HS1, the droplets due to heterogeneous condensation reach bigger diameters. Due to jump evaporation, the condensate created due to homogenous condensation is partially evaporated on the shock wave, which results in the creation of supercooled steam. Simultaneously, partial evaporation also occurs of the droplets arising due to heterogeneous condensation. Farther downstream the flow, evaporation occurs due to compression.

For a high number of pollutants (HS3), heterogeneous condensation plays the leading role and practically all the steam contained in the mixture is condensed on the foreign particles. As a result, the condensation wave fades away. Because condensation occurs already at the nozzle inlet, droplets grow slowly giving away evaporation heat and raising the fluid pressure and temperature. When the shock wave occurs, the droplets are large. Due to that, jump evaporation is not the case – the process of evaporation on the shock wave is slow, which can be observed on the chart illustrating the droplet mass content and diameter.

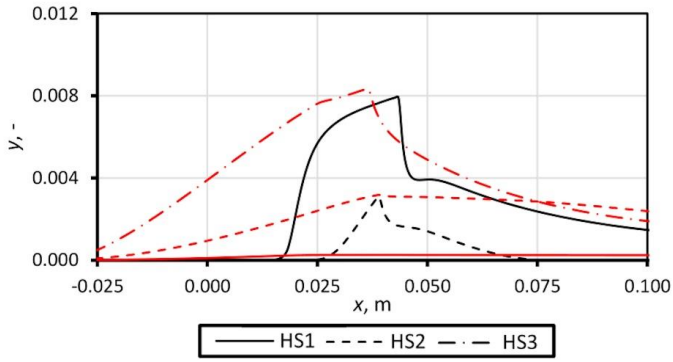

Figure 0.27. Liquid water mass fraction due to homogeneous (black) and heterogeneous (red) condensation for HS1, HS2 and HS3

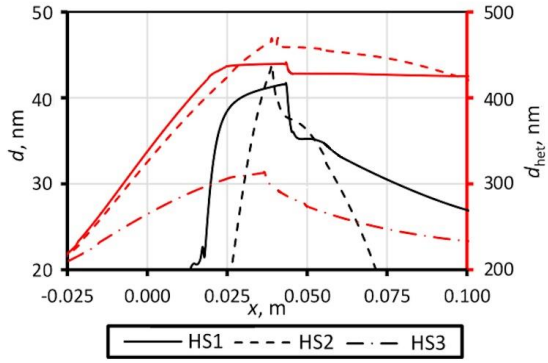

Figure 0.28 Droplet diameter due to homogeneous (black) and heterogeneous (red) condensation for HS1, HS2 and HS3 in the flow with elevated back pressure

In air flows both with and without aerodynamic waves, the diameter and the number of suspended particles define the heat transfer area, which is of key importance in the phase change process. Figure 6.29 presents the impact of the heat transfer area (the number and diameter of particles) per a kg of air on the share of homogeneous and heterogeneous condensation. The broken lines denote the number of droplets per a kg of the mixture as a function of the heat transfer area and the droplet diameter ($n_{\mathrm{het}}(A_{\mathrm{het}}, d_{\mathrm{het0}})$); the black and the red line, respectively, represent the amount of the condensate due to homogeneous and heterogeneous condensation depending on the droplet diameter and the heat transfer area at a constant number of droplets ($y(A_{\mathrm{het}}, d_{\mathrm{het0}})|_{n_{\mathrm{het}}=const}$). Assuming a constant heat transfer area, a rise in the number of particles is accompanied by a drop in their diameter. It can be seen clearly that the share of heterogeneous condensation increases with a rise in the number of pollution particles.

The impact of the number and size of suspended particles at the nozzle inlet on the share of homogeneous and heterogeneous condensation is the same, which is illustrated in Figure 6.30. The broken lines denote the constant mass fraction of water at the inlet per a kg of the mixture ($y_{\mathrm{het0}}(n_{\mathrm{het}}, d_{\mathrm{het0}})$) as a function of the number and diameter of droplets; the black and the red line, respectively, represent the condensate mass due to homogeneous and heterogeneous condensation depending on the diameter and the number of droplets at a constant mass fraction of water at the inlet ($y(n_{\mathrm{het}}, d_{\mathrm{het0}})|_{y_{\mathrm{het0}}=const}$). Assuming a constant mass of water at the inlet, a rise in the number of particles is accompanied by a drop in their diameter. It is easy to notice that due to the rise in the number of droplets, the mass of water condensed due to heterogeneous condensation increases.

The effect of heterogeneous condensation importance rising with a drop in the diameter and a rise in the number of particles or droplets, assuming a constant heat transfer area or mass at the nozzle inlet, can be justified using the physics of condensation. The droplet growth depends on the Knudsen number, and thus also on the droplet diameter. As a drop occurs in the droplet size, the dynamic of the change in the droplet diameter increases. It follows that heterogeneous condensation is favoured, especially if the particles suspended in the fluid are small.

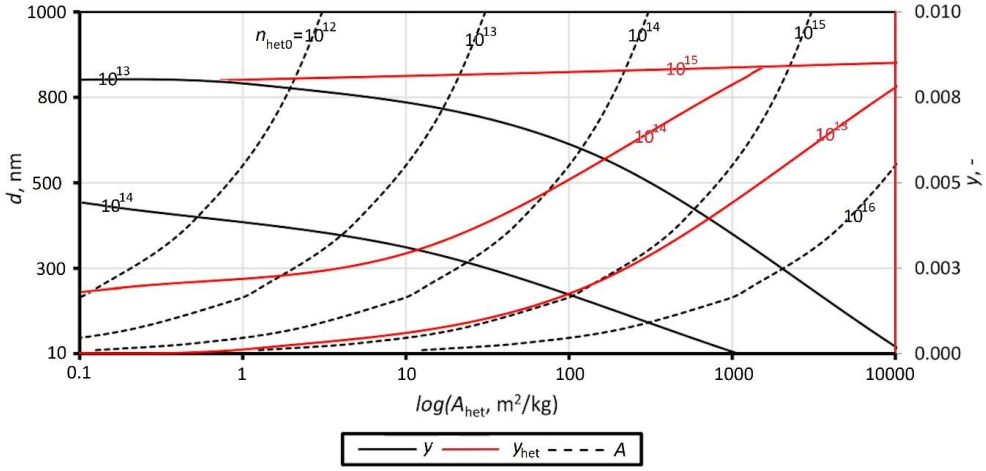

Figure 0.29. Impact of the size and number of solid particles suspended in the air on the share of homogeneous and heterogeneous condensation

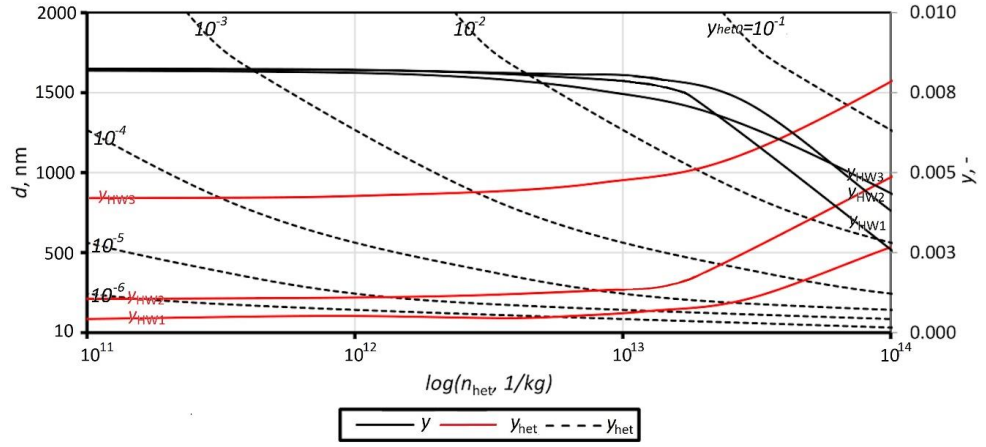

Figure 0.30 Impact of the size and number of droplets suspended in the air on the share of homogeneous and heterogeneous condensation

Table 0-4 presents the impact of the diameter and number of suspended particles on expansion efficiency in the nozzle. The expansion process efficiency drops with a rise in the number of suspended particles at their constant diameter. If the number of the particles is constant, the efficiency value decreases with an increase in their diameter. It can be seen clearly that a rise in the heat transfer area involves a drop in the expansion process efficiency. It may therefore be concluded that heterogeneous condensation has a negative effect on expansion in the nozzle and causes a drop in its efficiency.

Table 0-4. Isentropic efficiency values for the nozzle with a supersonic outlet and suspended solid particles

$n_{\mathrm{het}}, \frac{1}{\mathrm{kg}}$	d_{het}, m		
	$2 \cdot 10^{8}$	$2 \cdot 10^{7}$	$2 \cdot 10^{6}$
10^{13}	0.9160	0.9158	0.9092
10^{14}	0.9081	0.9024	0.8746
10^{15}	0.8914	0.8861	0.8371

1.16.3 External flow with suspended particles

The study of the influence of the water presence on the external flow over an airfoil presented herein regards the impact of the applied condensation model and the water mass fraction on the airfoil performance. The investigation of the condensation model in terms of the importance of heterogeneous condensation is shown for three cases: HW1, HW2, HW3, varying from one another in the number of liquid droplets (cf. Table 0-3). The values correspond to standard mass values of the water content suspended in the air in different weather conditions (e.g. cloud or fog). The flow parameters correspond to the values in the humidity impact study – case RAE1.2. As a result, three typical conditions are obtained of the wing operation in rain or fog during take-off and landing [72].

As it can be seen in Figure 6.31, even for a relatively low water mass fraction, heterogeneous condensation affects the flow considerably. However, as the number of droplets increases, the impact of the heat exchange on the flow becomes significant. Due to the release of latent heat, the fluid pressure and temperature increase, which causes a drop in the Mach number and a

shift of the shock wave downstream of the blade. It is observed that with an increment in the number of droplets, the pressure coefficient drops upstream of the shock wave and increases downstream of the shock. Owing to heterogeneous condensation and evaporation of droplets on the shock wave, the shock waves move downstream the flow. It is especially important for a large angle of attack, where velocities are the highest due to acceleration. For this reason, static parameters drop and condensation is stronger. At the same time, due to the strengthening of the shock wave, more droplets evaporate on it releasing latent heat to the air increasing its temperature. The pressure on the pressure side of the airfoil increases.

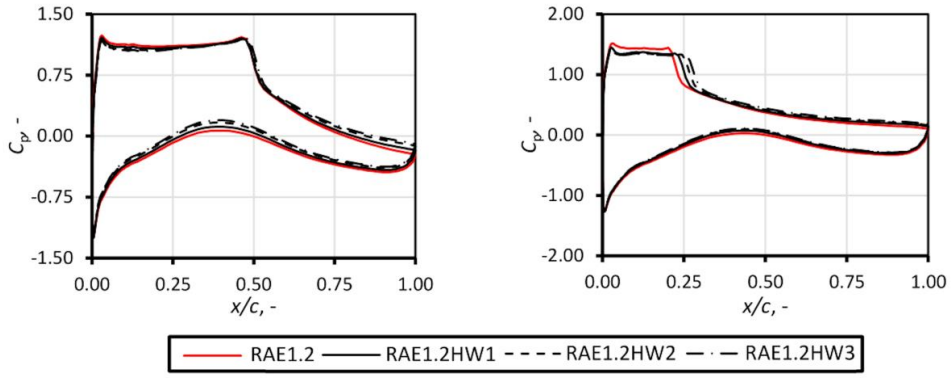

Figure 0.31. Impact of the suspended droplet (case HW1, HW2 and HW3) on the pressure distribution along the airfoil under the angle of attack of 4º and 8º

Figures 6.32 and 6.33 show the impact of the presence of water droplets on the lift and the drag coefficient, as well as the ratio between the lift and the drag coefficient for angles of attack from 0º to 10º. As it can be seen, the lift coefficient decreases for the low angle of attack, but increases for a large angle of attack. The drag coefficient increases. The decrease in the lift force is due to condensation, like in the case of the phenomena occurring with pure homogeneous condensation. The main influence of the droplets suspended in the air is on the drag force. Due to evaporation in the wake region, the pressure drops thus increasing the induced drag. Figure 6.33 shows that for a given drag, the lift is lower, especially for low angles of attack. The impact is significant and the lift-to-drag ratio decreases by up to 40%, for AoA = 2º.

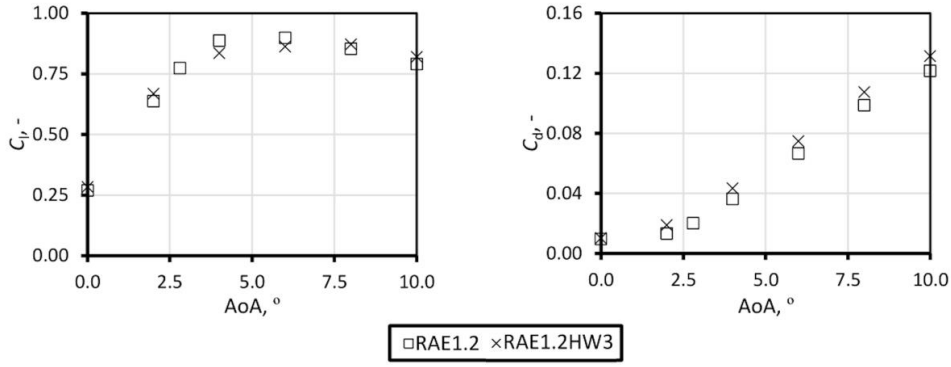

Figure 0.32. Influence of relative humidity on the lift and the drag coefficient (left and right, respectively) as a function of the angle of attack

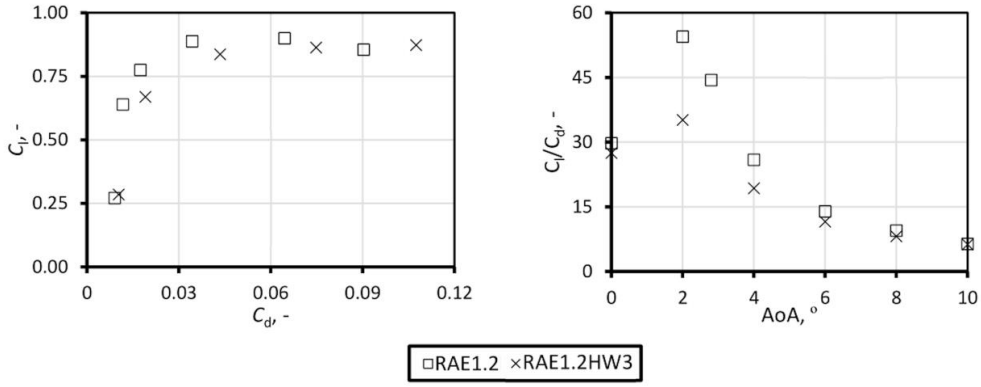

Figure 0.33. Lift and drag coefficients for different relative humidity values (left) and the impact of relative humidity on the lift-to-drag ratio as a function of the angle of attack

1.17 Phase change impact on the performance of modern turbomachinery

The effect of heterogeneous condensation in moist air transonic flows was investigated numerically using the two approaches described in section 6.2. The HS and the HW contamination is assumed to be solid particles and liquid droplets, respectively. The testing was carried out varying the number of droplets with the same size and then varying the mass fractions. Table 0-5 presents summarized boundary conditions for the comparative study.

Table 0-5. NASA rotor 37 and NASA rotor 67 boundary conditions

	$p_{0,in}$,Pa	$T_{0,in}$, K	Φ, %	f, rad/s
R37.0	101325	303.15	0	1800

R37.1	101325	303.15	70	1800
R37.2	101325	303.15	100	1800
R67.0	101325	303.15	0	1680
R67.1	101325	303.15	70	1680
R67.2	101325	303.15	100	1680

1.17.1 Analysis of the impact of suspended particles and droplets on the performance of turbomachinery for constant operating conditions

The influence of different flow conditions on the rotor performance was assessed using specific work. In its definition, specific work includes the information on the thermodynamic state of the compression process. Additionally, the total pressure value at the rotor outlet in the absolute frame was compared for the analysed test cases. Figures 6.34 and 6.35 present the influence of steam condensation on specific work and the distribution of absolute total pressure at the domain outlet. It is observed that the influence of HS and HW on the total pressure profile at the outlet is significant. Total pressure increases in the region close to the hub and decreases in the upper blade component. This is attributed to the higher velocity at the blade tip, which facilitates condensation and a stronger shock wave. Variations can be observed between individual cases of specific work, and the heterogeneous condensation phenomenon resulting from the solid particles contained in the air affects the specific work value along the blade span. Specific work is the difference between total specific enthalpies at the rotor outlet and inlet:

$$l = h_{02} - h_{01} \tag{6.5}$$

and total specific enthalpy is computed as follows:

$$h_0 = h + \frac{1}{2}v^2 \tag{6.6}$$

For low numbers of particles, specific work is higher compared to the adiabatic case. This is attributed to the higher specific heat of humid air. Due to condensation-related losses, the specific work value decreases with an increase in the number of suspended particles in the flow. The influence of fluid droplets at the rotor inlet is even more significant. Specific work is

observed to decline with a rise in the liquid content at the inlet. This is caused by the temperature drop due to latent heat absorption in the evaporation process.

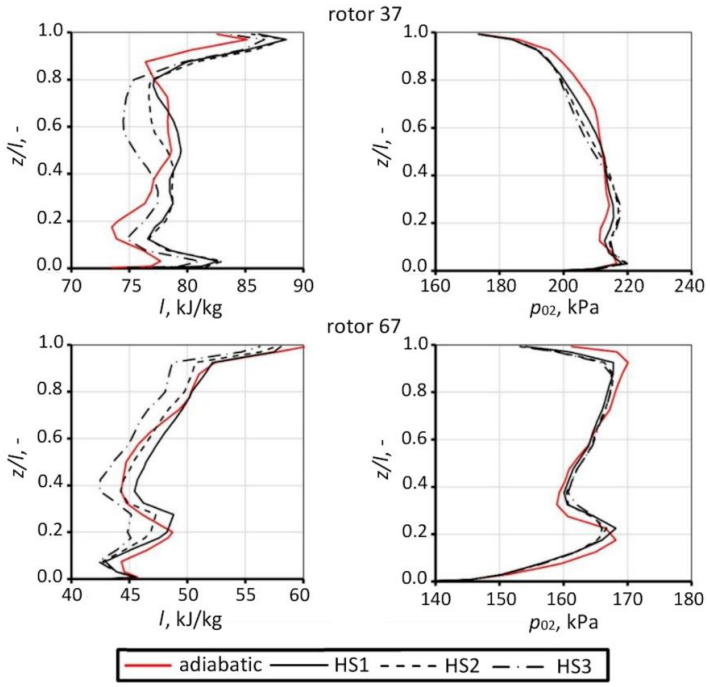

Figure 0.34. Specific work of the rotor and total pressure spanwise distribution at the outlet for R37.1 and R67.1 cases for HS1, HS2 and HS3

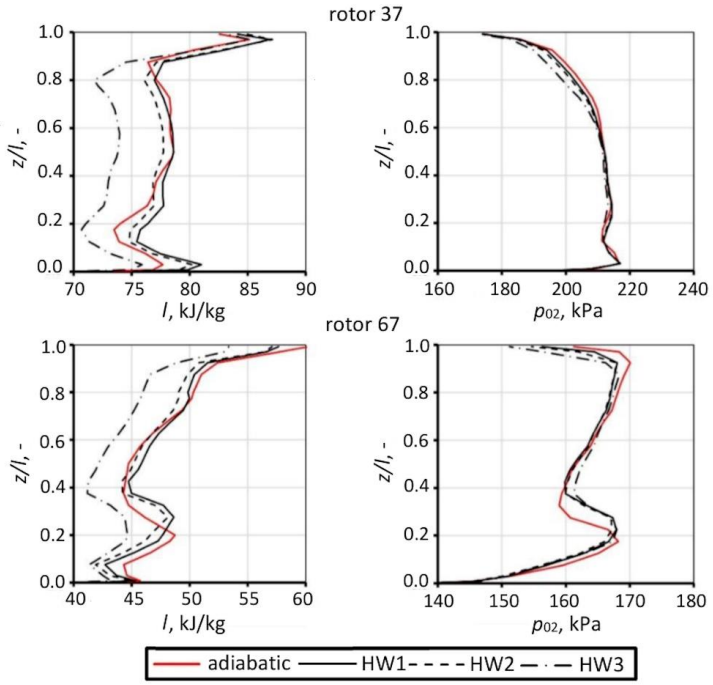

Figure 0.35. Specific work of the rotor and total pressure spanwise distribution at the outlet for R37.1 and R67.1 cases for HW1, HW2 and HW3

Figure 6.36 presents the mass-averaged values of specific work (l) and the outlet-to-inlet relative total pressure ratio. The enhanced specific work in the flow with suspended solid particles is attributed to the flowing air humidity and, thereby, the air increased specific heat. The reduced specific work for the liquid droplets at the inlet is caused by the absorption of latent heat released due to evaporation on the shock wave.

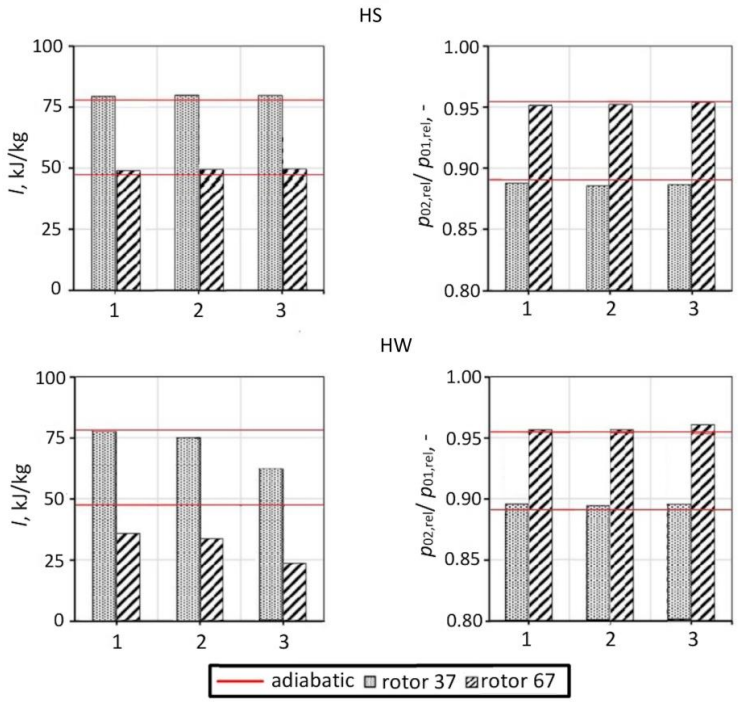

Figure 0.36. Mass flow rate-averaged values of specific work and outlet-to-inlet relative total pressure ratio for rotors 37 and 67 for HS1, HS2, HS3 and HW1, HW2, HW3

1.17.2 Analysis of the impact of suspended particles and droplets on the flow field for constant operating conditions

The steam condensation phenomenon has a substantial effect on the flow field structure. Figure 6.37 shows a 3D quantitative representation of the mass fraction of water in the compressor rotor (condensation case HW3, rotor 67). Because the condensation phenomenon occurs mainly in the middle and tip parts of the rotor, the focus is on these areas for reasons of clarity.

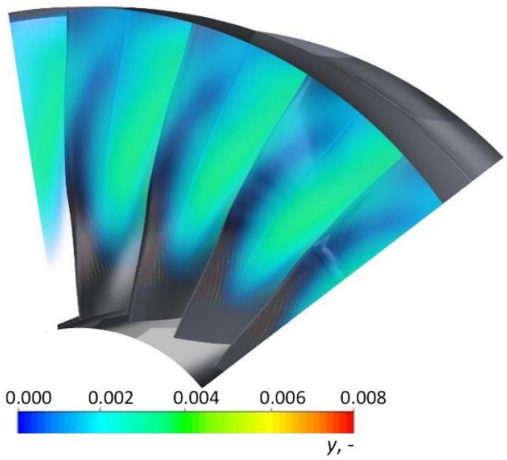

Figure 0.37. Quantitative representation of the condensate mass fraction in the compressor rotor (R67.1 for HW3).

Figures 6.38 and 6.39 present the mass fraction of the liquid phase and the Mach number contours for HS and HW, respectively. The maps of the liquid water mass fraction in Figure 6.38 indicate condensation to occur on the solid particles and evaporation on the shock wave. An increase in the number of solid particles in the air involves an increase in the condensed water content, which subsequently results in a release of latent heat and a reduction in the Mach number. The bigger mass of condensed water produced due to the increasing number of suspended particles is considered to be an effect of more favourable condensation conditions. More specifically, condensation occurs on the solid particles suspended in the air.

Figure 6.39 demonstrates condensation to occur on the suspended droplets entering the computational domain. The water then evaporates on the shock wave. For the flow with liquid droplets at the inlet, a lower number of droplets results in less favourable condensation conditions compared to the flow with suspended solid particles. The condensed water mass upstream of the shock wave is thus lower than in the case with suspended solid particles. The impact of evaporation is principally observed in the shock wave region. The evaporating fluid absorbs latent heat, which reduces the temperature and the shock wave moves downstream the

blade-to-blade channel.

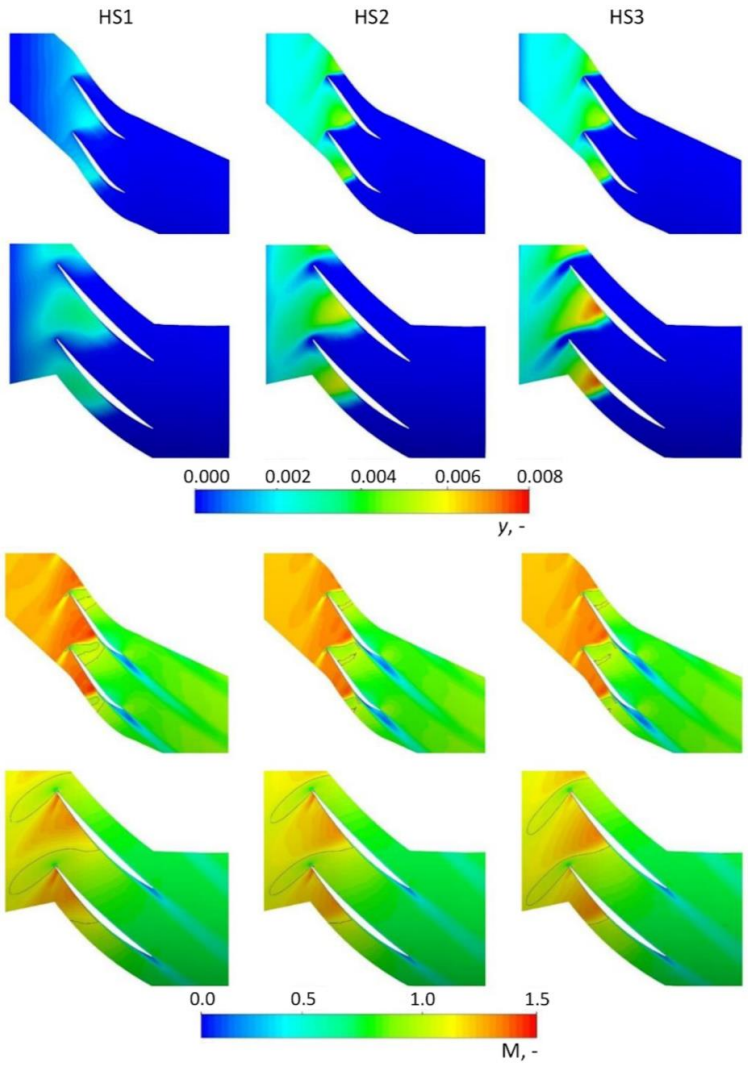

Figure 0.38. Liquid water mass fraction and Mach number contours for HS1, HS2 and HS3 at a 0.5 span for R37.1 (top) and R67.1 (bottom)

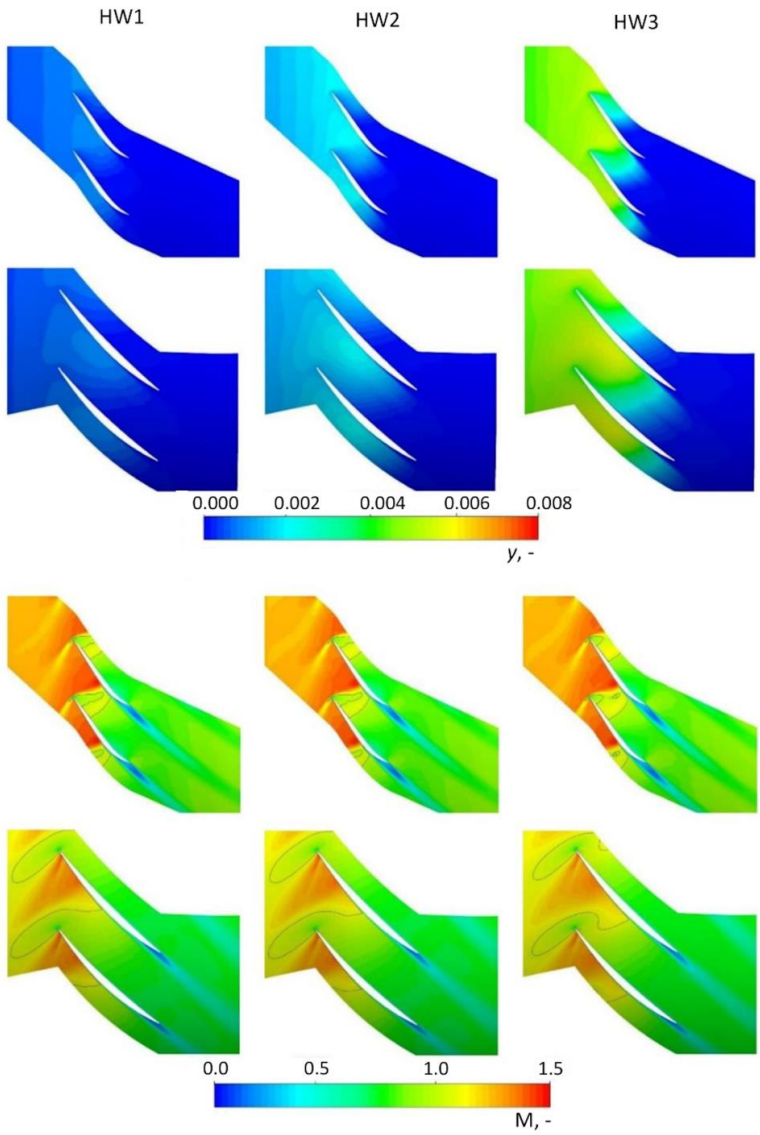

Figure 0.39. Liquid water mass fraction and Mach number contours for HW1, HW2 and HW3 at a 0.5 span for R37.1 (top) and R67.1 (bottom)

Figures 6.40 and 6.41 show a comparison of the pressure distribution along the blade surface at the 10, 50 and 90% span for rotor 37 and rotor 67, respectively, considered as adiabatic, HS and HW cases. The static pressure distribution on the blade surface at the 90% span differs slightly in comparison to the data available in the literature, especially for rotor 67. This is due

to the tip gap omission. Regardless of the discrepancies near the shroud region for the adiabatic case, the impact of heterogeneous condensation is clear, and this aspect is the focus of this study. Figure 6.40 shows the influence of HS and HW condensation on the rotor 37 blade loading. It can be seen that for the HS cases, the shock wave moves upstream on the blade pressure side. If the hub region of the blade suction side is taken into account, the shock wave moves downstream, whereas for the shroud region the shock wave moves upstream. If the liquid droplets are present at the inlet (HW cases), the shock wave on both sides of the blade moves downstream the blade-to-blade channel, which is caused by the latent heat release due to evaporation causing a drop in the fluid temperature.

Figure 6.41 shows the influence of HS and HW condensation on the blade loading for rotor 67. It can be seen that for the HS cases, the shock position on the pressure side is affected only near the shroud region, and it moves downstream. On the suction side, condensation delays the shock wave. The influence of the presence of liquid droplets at the inlet on the blade loading for rotor 67 is the same as in rotor 37. The character of the pressure distribution along the blade at span 0.5 (Figures 6.40 and 6.41) fits the Mach number contours (Figures 6.38 and 6.39).

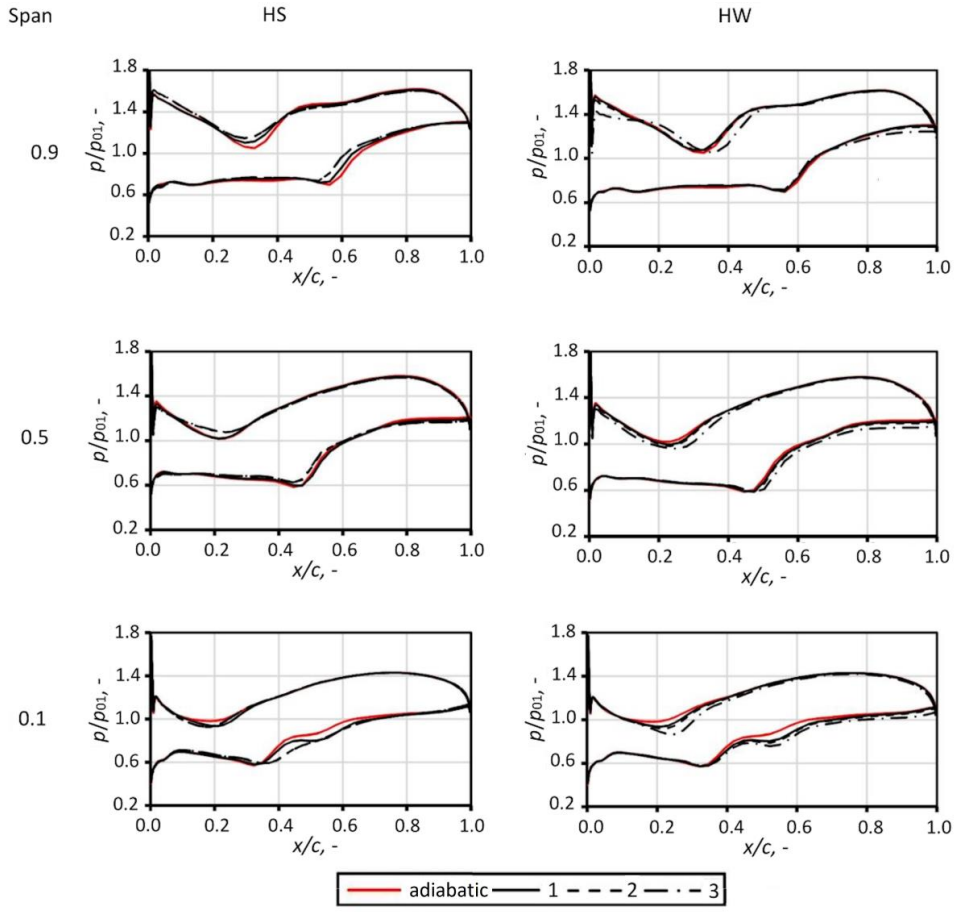

Figure 0.40. Influence of condensation and evaporation on the normalized pressure distribution along the R37.1 blade at span 0.1, 0.5 and 0.9 for the adiabatic case and all the considered HS and HW cases

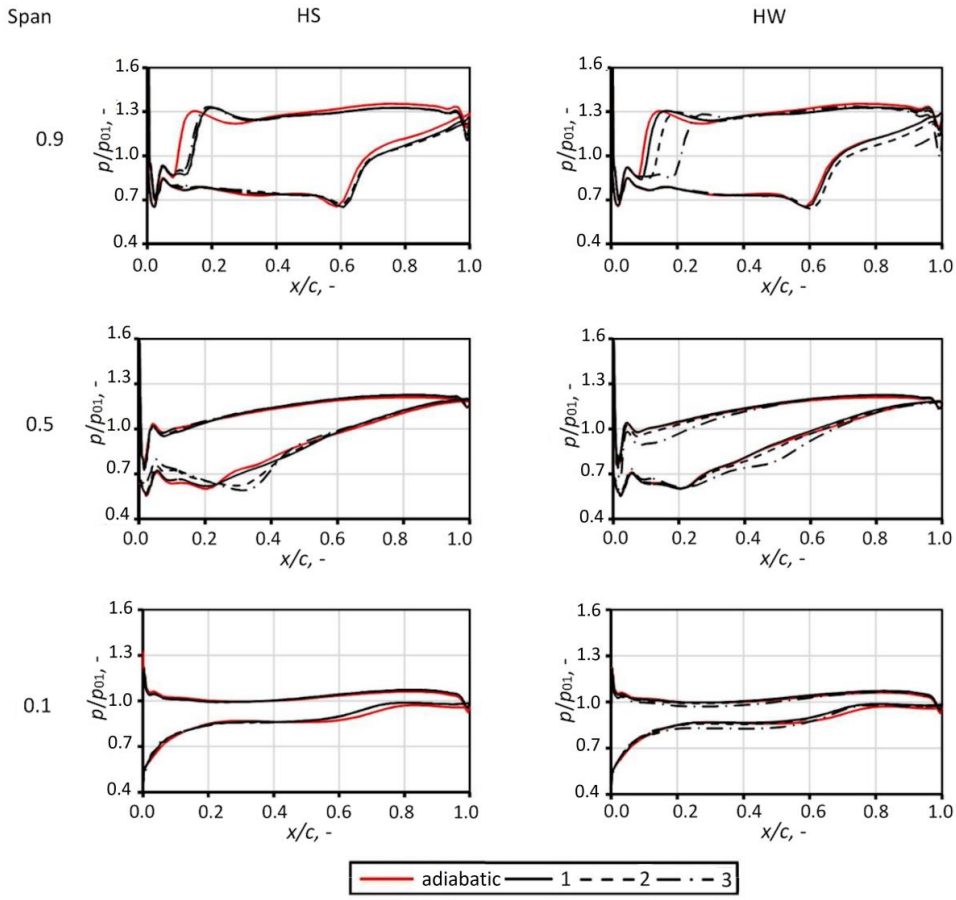

Figure 0.41. Influence of condensation and evaporation on the normalized pressure distribution along the R67.1 blade at span 0.1, 0.5 and 0.9 for the adiabatic case and all the considered HS and HW cases

Figure 6.42 presents the water mass fraction and the Mach number for the HW3 and HS3 condensation cases at the 0.9 span of rotor 37 and rotor 67. As it can be seen, the condensation process near the tip of the rotor is more gradual than at the 0.5 span. Condensation starts farther upwind the rotor, but the droplet growth is slower. For this reason, the total amount of condensed water is lower compared to the mid-span area.

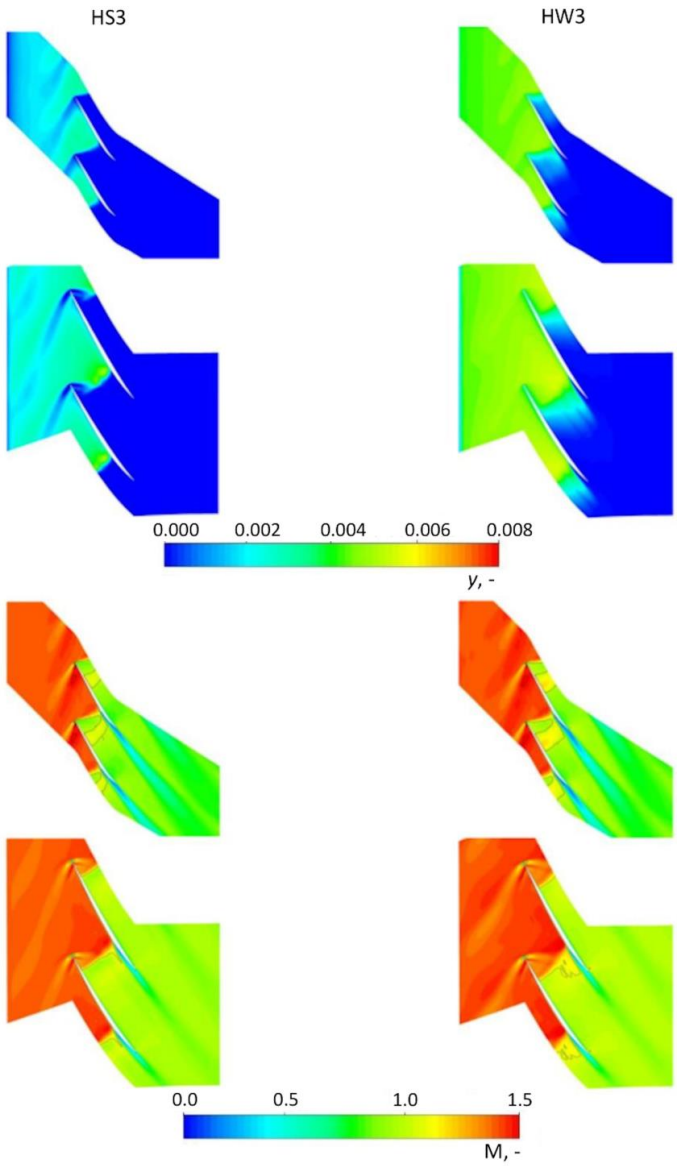

Figure 0.42 Liquid water mass fraction and Mach number contours for HW3 and HS3 at the 0.9 span for R37.1 (top) and R67.1 (bottom)

1.17.3 Assessment of losses due to the phase change in turbomachinery

Condensing flows of moist air involve both aerodynamic and thermodynamic losses. Aerodynamic losses such as those caused by turbulence or shock waves can be intensified or weakened by the presence of the condensation phenomenon. Thermodynamic losses caused by phase-change processes can be dominant and they may have a significant impact on the entropy

change. With an increment in air humidity at the rotor inlet, the efficiency of the compression process in the first stage of the compressor or the fan of a turbofan engine decreases, which is related to the increase in specific entropy of the fluid due to condensation. The homogeneous condensation phenomenon occurring in the region near the blade affects the fluid local properties and causes additional losses. It has to be mentioned that the specific entropy values of steam and water are calculated using the IAPWS formulations. The fluid specific entropy is computed as the sum of dry air, vapour and liquid specific entropies from the following equation:

$$s = s_{\mathrm{a}}(1 - y_{\max}) + s_{\mathrm{v}}(y_{\max} - y) + s_{\mathrm{l}} y \tag{6.7}$$

where s_{a}, s_{v}, s_{l} are specific entropies of dry air, water vapour and condensate, respectively.

Isentropic efficiency is computed as:

$$\eta = \left(\left(\frac{p_{02}}{p_{01}} \right)^{\left(\frac{\gamma - 1}{\gamma} \right)} - 1 \right) / \left(\frac{T_{02}}{T_{01}} - 1 \right) \tag{6.8}$$

where T_{01} and T_{02} are the inlet and outlet total temperature, p_{01} and p_{02} are the inlet and outlet total pressure and γ is the ratio of specific heats.

Figure 6.43 shows the influence of air humidity on the specific entropy increment in the blade-to-blade channel and its efficiency. With an increase in relative humidity, the entropy increment in the blade-to-blade channel is augmented due to condensation losses, which affects the flow parameters, increasing the importance of vapour entropy in the entropy of the mixture. The influence of homogeneous condensation on the efficiency of rotor 37 is negligible, while the efficiency drop in rotor 67, due to the presence of humidity in the working fluid, is significant. The influence of homogeneous condensation on the efficiency of rotor 67 is higher in comparison to the effect of homogeneous condensation on rotor 37 efficiency, as the condensation conditions in rotor 67 are more favourable. Moreover, the compression work realized by rotor 67 is lower compared to rotor 37. For this reason, the effect of the release or absorption of a comparable amount of latent heat, due to condensation and evaporation, has a greater impact on the flow parameters and, thereby, on the efficiency of the machinery.

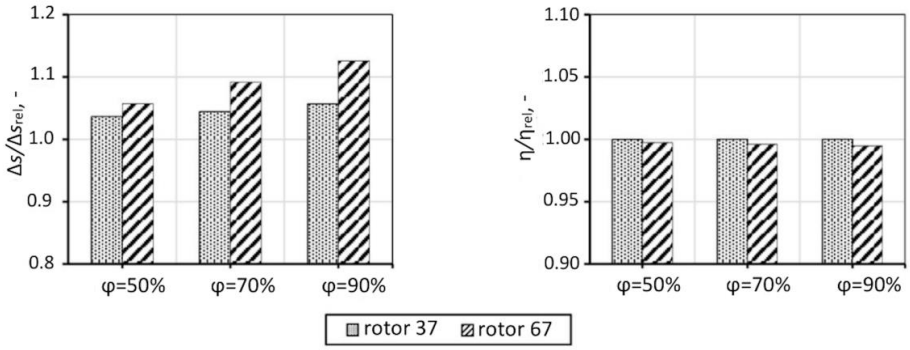

Figure 0.43. Increase in the outlet-to-inlet specific entropy ratio (left) and the ratio of efficiency (right) for different values of inlet humidity compared to the adiabatic case

Figure 6.44 shows the influence of the presence of solid particles and water droplets at the compressor inlet on the specific entropy increment and the rotor efficiency. With the increasing number of suspended solid particles, heterogeneous condensation becomes a major condensation process. The heterogeneous condensation phenomenon triggered by the presence of foreign nuclei in the fluid accelerates condensation upstream of the rotor, which decreases the importance and speed of nucleation and the growth of droplets due to the homogeneous process. The same phenomena occur if the air contains suspended liquid droplets. Moreover, with an increase in the water content at the rotor inlet, more latent heat is absorbed during the liquid fraction evaporation on the shock wave, which leads to a significant drop in the fluid total temperature. The adopted definition of isentropic efficiency (eq. 6.8) may result in values above 1 when dealing with evaporation of a large amount of water. Latent heat evaporation should be taken into account here. The result is a significant increment in efficiency compared to the adiabatic case. This is of major importance, especially in fans, where the total temperature increment is relatively low in comparison to the compressor, and the absorption of latent heat during evaporation exerts a strong effect on the flow structure and the efficiency of turbomachinery.

Figure 6.45 shows the influence of the liquid water content on the performance curve of R37.1. The performance curves for the adiabatic and HW3 cases are confronted with experimental results. The adiabatic simulation overestimates compression in the rotor stage, which is due to the omission of tip losses. If tip losses are taken into account, the adiabatic curve moves to a lower pressure ratio, thus fitting the experimental results better. However, in this study the focus is on the shift of the performance curve due to humidity and phase-change phenomena. If liquid

water is present at the compressor inlet, the compression ratio drops due to latent heat absorption on the shock wave, which leads to a decrease in the fluid pressure and temperature. Moreover, it must be remembered that the air humidity and the presence of water at the rotor inlet mean a change in the fluid density, which must affect the mass flow rate as well. In the considered HW3 case, the drop in the fluid density due to the presence of steam is much higher than the fluid density rise due to the presence of water droplets at the inlet. It leads to a decrease in the fluid density and finally to a drop in the mass flow rate. The choking mass flow rate $\dot{m}^*$ based on the experimental study totals 20.93 kg/s; $\dot{m}^*$ obtained numerically for the adiabatic flow equals 20.83 kg/s and $\dot{m}^*$ for the HW3 case is 19.87 kg/s.

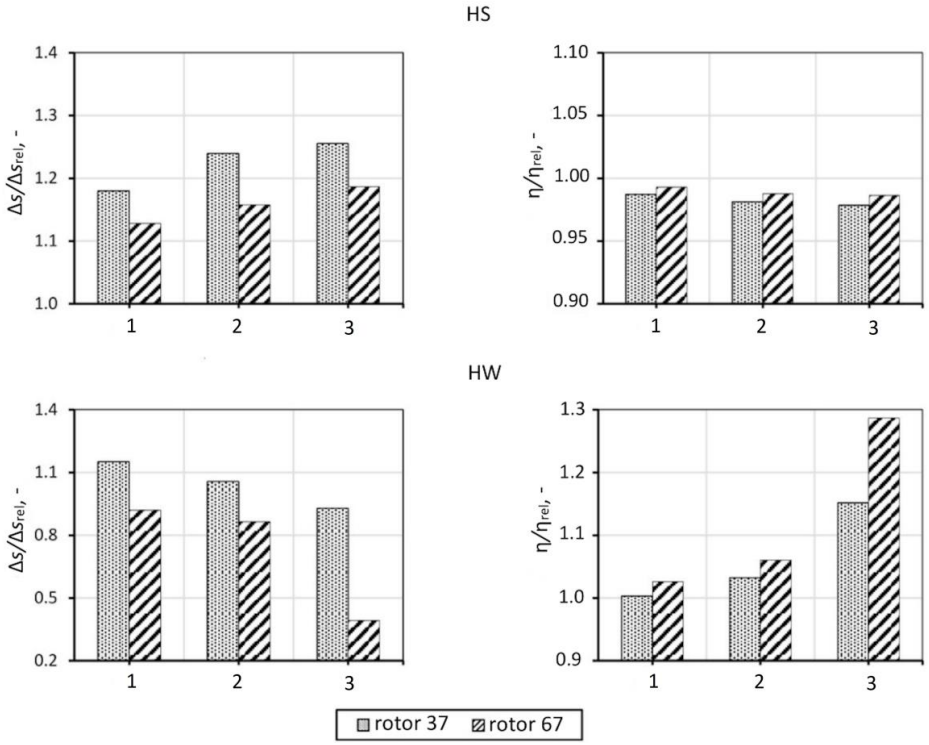

Figure 0.44. Increase in the outlet-to-inlet specific entropy ratio (left) and the ratio of efficiency (right) for HS1, HS2, HS3 and HW1, HW2, HW3 compared to the adiabatic case

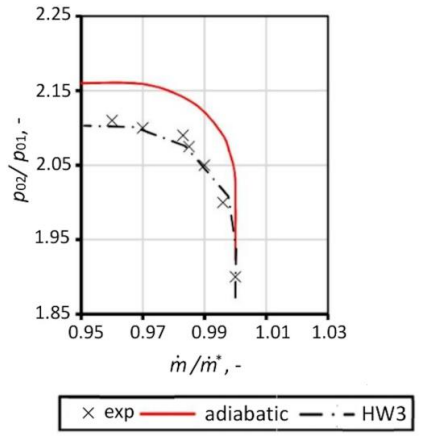

Figure 0.45. Influence of the liquid water content (HW3) at the inlet on the performance curve of R37.1

1.18 Superposition of the Single-Fluid and the DPM model

This section discusses the discrepancies between the SF and the DPM model. It has to be mentioned that all physical properties in both models are unified. Therefore the differences in the results are only due to the Euler and Lagrange-based approaches.

Figure 6.46 shows a comparison of static pressure and temperature for the D1.1SS and D1.2SS cases using the HK and the GY growth rate model obtained with the SF and the DPM model. Also, the adiabatic D1.0SS case is demonstrated to show that both models give the same solution for flows without a phase change. According to the figure, the DPM model indicated stronger and earlier condensation, especially for the GY model. This is due to the fact that nucleation takes place on a certain length. The SF model averages the droplet size, and therefore the droplets that appear in the nucleation zone have a mean diameter based on the mass of the condensate and the number of droplets, whereas the DPM computes the droplet size individually based on the individual source of mass. The appearing small droplets provoke considerably high rates of the droplet growth. For this reason, the local mass and energy sources for the DPM are higher than for the SF model. The above explains the difference in the condensation strength and position.

The proposed superposition of the SF and the DPM model is based on the post-processing of the Euler model using the Lagrange approach. This makes it possible to obtain information regarding the entire droplet spectrum, individual droplet trajectories, as well as interphase slip

velocities, i.e. information that can be obtained only from the DPM model while maintaining the SF model robustness.

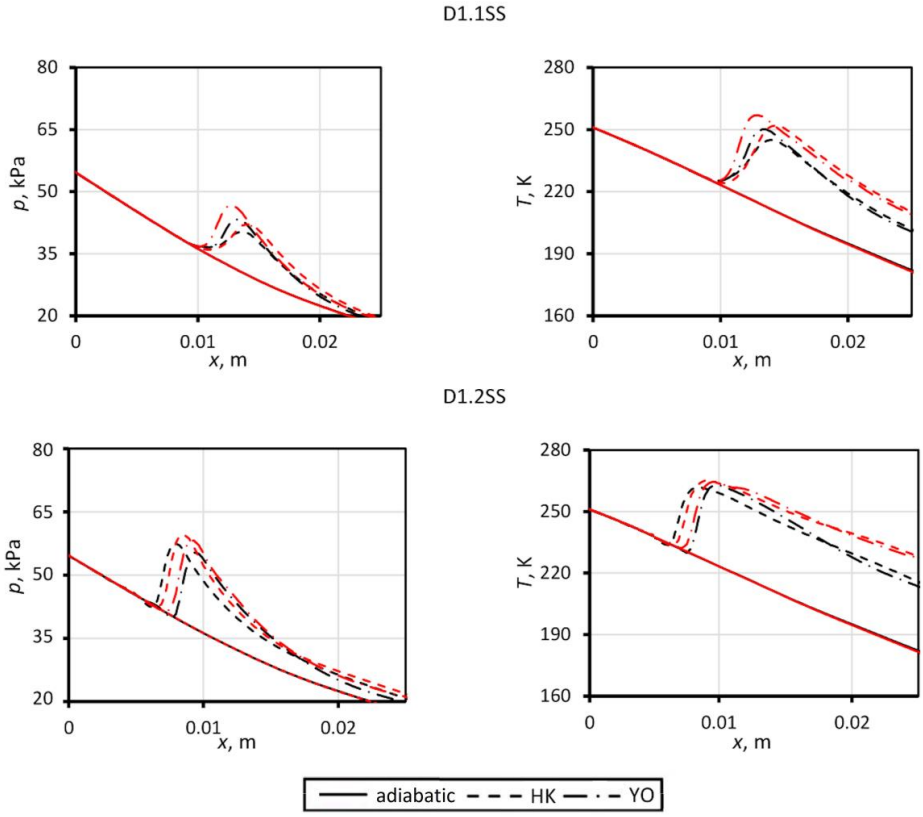

Figure 0.46. Static pressure and temperature along the nozzle centre line obtained from the SF (black) and the DPM (red) model

Figure 6.47 shows the spectrum of droplet diameters at the D1.1SS and the D1.2SS outlets; the results obtained using the superposition approach are confronted with the DPM results and the YO droplet growth model is applied. The prediction of the droplet diameter spectrum by the Superposition model is very similar to the DPM model results. The Superposition model suggests slightly larger droplets for cases with lower humidity, which is due to the fact that in cases with lower humidity condensation proceeds more gradually than in high-humidity cases. As a result, the nucleation zone is larger, which – combined with slower droplet growth – results in a slight overestimation of the droplet size by the superposition approach.

Considering the results obtained using the superposition approach, i.e. employing the Lagrange post-processing of data obtained from the single-fluid model, the potential of this idea is apparent. The proposed technique ensures highly reliable results while maintaining a low computational cost, which is going to be a great benefit in studies on complex 3D flows. However, it has to be mentioned that it needs parallel development, adjustment and validation of two complex codes.

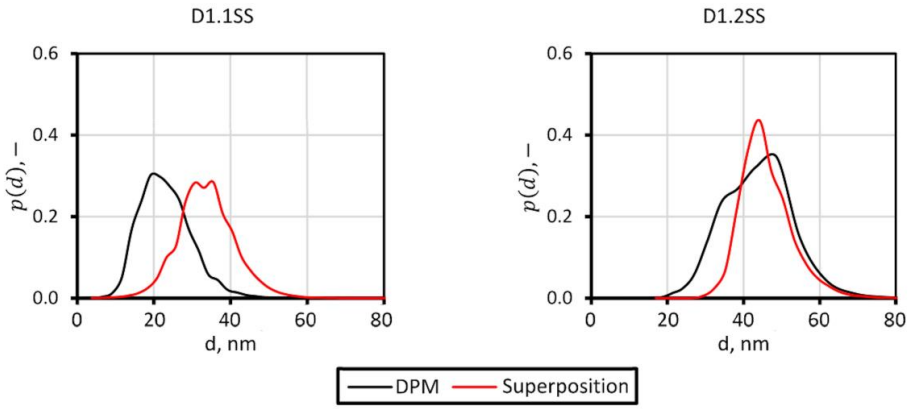

Figure 47. Droplet diameter spectrum at the nozzle outlet obtained using the DPM model and superposition approach

Summary and conclusions

The thorough analysis of the research results presented herein leads to several conclusions concerning the importance of the phase change in flow modelling. The first stage of this work is the model validation against several benchmarks. The dry air model validation shows the applicability of the utilized numerical tools for consideration of transonic flows, both internal and external. Then the modelling of steam condensation is validated. The results of the studies on the condensation phenomenon arising in nozzles in different conditions are confronted with experimental and numerical data. The conclusions that can be drawn based on the presented analysis coincide with the findings of other research works. The performed studies demonstrate that the kinetic model overestimates the condensation rate, whereas the Gyarmathy and the Young models give very similar results. The results of the analysis of condensation in steam indicate that the model proposed by Young is the most appropriate for steam calculations after its calibration at the time.

The next step, which is the first goal of this work, was therefore to conduct a detailed analysis of the application of the models of steam condensation in moist air flows. A number of simulations were performed for this purpose using different droplet growth models. The obtained results were then validated against experimental results from the literature and against experiments serving the needs of this dissertation. The condensation model was compared with the literature data for the flow through a nozzle with a high expansion rate and a nozzle with parallel walls. The results were used for the mathematical model calibration, and a *blend* model of the droplet growth was proposed. Based on the Knudsen number, the blend model uses the continuous model and/or the kinetic model. It is shown in this work that the model gives the best solution for the moist air flow, especially if the air is polluted. Additionally, an analysis was conducted of the impact of the turbulence model on the interaction between the pressure wave and the condensation wave. It is demonstrated that the fluid viscosity is not negligible, and the *k*-ω SST turbulence model is recommended to take account of viscous stresses in the boundary layer area.

The next goal of this work is to fill the essential gap of the lack of experimental studies of the flow through nozzles with a low expansion rate. The experiments were carried out in the DPET of the SUT using the existing vacuum system to investigate condensation in symmetric and asymmetric nozzles. The nozzles were characterized by the expansion rate of $\dot{P} \approx 1000\mathrm{s}^{-1}$, which distinguishes them from the nozzles analysed in the literature so far. The results of the

testing of the de Laval nozzle with a low expansion rate make it possible to draw the following conclusions::

– For the adiabatic (dry air) flow, the visible X-shaped waves have a purely aerodynamic character.

– If humidity is considered, it is set off in the vicinity of the pressure waves in the adiabatic flow.

– For low humidity values, the co-occurrence of a few X-shaped waves is observed. Only one of them is a condensation shock wave, whereas the others are compression or expansion waves. However, due to the limited comparative material, it is difficult to define their character unequivocally.

– As humidity increases, the condensation wave changes its shape from X to a normal wave and moves upstream the flow.

– The condensation wave is followed by the pressure wave. The latter weakens with a rise in humidity and moves upstream with the condensation wave. Finally, for high humidity values, the pressure wave combines with the condensation shock.

– For high air relative humidity values (above 50%), the condensation shock is ahead of the aerodynamically induced X-shock and is very close to the nozzle throat.

– If the shock wave is present in the flow, its position depends on the fluid relative humidity, i.e. the higher the relative humidity value, the farther downstream the shock wave occurs.

– An increment in the air relative humidity involves an increase in the pressure value before the shock wave and a decrease in the Mach number, which weakens the shock wave.

– The observed partial evaporation of the liquid phase on the normal shock wave is caused by its low strength.

– The total temperature change needs to be taken into account to evaluate the condensation loss.

Taking all the above into consideration, it can be concluded that humidity has a significant impact on the flow structure in the converging-diverging nozzle with a low expansion rate. The interaction between the aerodynamic and thermodynamic waves (pressure and condensation waves) is not trivial. However, it is very difficult to distinguish the character of the occurring phenomena unequivocally because the range of the flow properties which can be measured in experiments is rather limited. The combination of experimental and numerical studies gives a

deep insight into the flow structure, but due to the limited amount of measured data, there is a need for more experimental research to obtain reliable validation data for numerical models.

The next stage of the work was the modelling of the effect of humidity on the external flow over an airfoil. The condensation phenomenon influences the pressure distribution along the profile and moves the shock wave position. In the case of homogeneous condensation, steam condenses ahead of the normal shock wave, and then the condensed water partially evaporates on it. Due to the latent heat release, the fluid properties increase, but the ambient conditions are constant. For this reason, the ratios of pressure and velocity are decreased and, as a result, the shock wave must be shifted upstream. The heterogeneous condensation analysis is more complex. If water droplets are present in the fluid due to evaporation on the shock wave, additional latent heat is absorbed by the fluid. If the amount of evaporated water is bigger than that of condensed steam, this causes a rise in the pressure ratio, increases the strength of the shock wave and moves the wave downstream. The condensation phenomenon exerts a significant influence on the lift and drag coefficients, decreasing the airfoil performance. The influence of condensation is strictly related to total temperature and relative humidity. With an increase in total temperature, the water content increases and the amount of heat released during the condensation process gets higher.

The next step was to use the developed model to investigate the impact of condensation on the performance of turbomachines, in particular – on the work of the first stage of the compressor of a turbine and the fan of a turbofan engine. The results demonstrate the significance of humidity, condensation and evaporation on the flow in turbomachinery. If humidity is taken into account, the fluid properties are changed and the air specific heat increases. This enhances specific work in the rotor. The presence of solid particles triggers the condensation process, which consequently affects the pitch-wise-averaged total pressure profile and total temperature. This has a negative impact on the rotor specific work. The liquid water content at the inlet proves to be problematic as the liquid tends to evaporate on the shock wave in the blade-to-blade channel. During evaporation, the released latent heat is absorbed by the fluid and the temperature of the air decreases, which is linked to the reduced total temperature and entropy at the rotor outlet. The presented results are of major importance for cases with a high number of solid particles or a relatively large liquid water content. Suspended solid particles or liquid droplets contained in the air exert a strong impact on the flow field structure and the performance of turbo engines. The condensation phenomenon triggered by solid particles

decreases the Mach number in the flow, while the presence of liquid droplets in the air shifts the shock wave downstream the blade-to-blade channel. Moreover, it has to be mentioned that the condensation phenomenon, both for the HS and the HW case, affects the blade loading. Finally, if humidity and suspended particles in the air are taken into consideration, the rotor performance curve is affected. This is an effect of the change in the flow rate due to the influence of humidity on the fluid density. Additionally, the phase change affects the compression process and the compression ratio decreases.

The last stage of the work was a comparative analysis confronting the single-fluid model with the multi-fluid model, where the condensate is calculated using the Lagrangian approach. As mentioned in this dissertation, the advantages of the SF and the DPM model supplement each other. The SF model is stable and its demand for computational power is low. Moreover, it represents the condensation process adequately. The DPM model, on the other hand, is based on realizing the conservation computations for single droplets, which creates the possibility of modelling the interphase slip or the collisions of droplets with walls limiting the flow or with one another. The results of the testing indicate that already for flows through relatively simple geometries a difference can be noticed in the predicted position and strength of the condensation wave. Because in the DPM model each growth of each droplet arising due to condensation is modelled separately, and the droplet size is not averaged, the model predicts faster condensation and formation of a bigger number of small droplets compared to the SF model. The differences presented in this dissertation and the proposed superposition model point to the need for further development of numerical methods to get efficient tools for the modelling of phase changes in flows through complex geometries or in flows with discontinuities in the form of aerodynamic waves. Further research, both experimental and numerical, is necessary to achieve this goal, which will ensure a better understanding of the physical foundations of the now-used flow models.

Summing up, both homogeneous and heterogeneous condensation has an impact on the transonic flow of gas-steam mixtures. The phase-change phenomenon has a substantial effect on the flow structure through relatively simple geometries such as nozzles, which directly translates into flows through complex geometries - it thus has a significant impact on the work of the first stage of the compressor of a turbine or the fan of a turbofan engine. Moreover, the expansion process is essentially affected by the pollutants suspended in the air in the form of solid particles or water droplets. The presence of the particles suspended in the air affects the

position and strength of the condensation wave and the position of the shock wave in transonic flows, which in the case of turbomachines has an impact on specific work of the rotor, the overall distribution of parameters and the flow field. Considering the importance of the problems discussed above, it is recommended that the air humidity and pollution should be taken into account in numerical studies of transonic air flows.

References

1. Starzman J, Hughes FR, White AJ, Halama J, Hric V, Kolovratnik M, et al. Results of the International Wet Steam Modelling Project. In Wet Steam Conference; 2016; Prague.
2. Chuang W, Yang Y, Ding H, Sun C, Yan Y. Wet steam flow and condensation loss in turbine blade cascades. Applied Thermal Engineering. 2021.
3. Rhee J, Im J, Kim J, Song SJ. Humidity effects on the aerodynamic performance of a transonic compressor cascade. International Journal of Heat and Mass Transfer. 2019: p. 743-751.
4. Gyarmathy G. Grundlagen einer Theorie der Nassdamfturbine Juris-Verlag; 1962.
5. Young JB. Spontaneous Condensation of Steam in Supersonic Nozzles: N81-13307. , Whittle Laboratory, University of Cambridge; 1980.
6. Young JB. Two-dimensional, nonequilibrium, wet-steam calculations for nozzles and turbine cascades. Journal of Turbomachinery. 1992: p. 569-579.
7. Fuchs N, Sutugin A. Topics in Current Aerosol Research New York; 1971.
8. Doerffer P, Dykas S. Numerical analysis of shock induced separation delay by air humidity. Journal of Thermal Science. 2005: p. 120-125.
9. Dykas S, Majkut M, Smołka K, Strozik M. An attempt to make a reliable assessment of the wet steam flow field in the de Laval nozzle. Heat and Mass Transfer. 2018: p. 2675-2681.
10. Dykas S, Majkut M, Smołka K, Strozik M. Analysis of steam condensing flow in a linear blade cascade. Preceedings of the Institution of Mechanical Engineers, POart A: Journal of Power and Energy. 2018: p. 501-514.
11. Dykas S, Wróblewski W. Numerical modelling of steam condensing flow in low and high-pressure nozzles. International Journal of Heat and Mass Transfer. 2012: p. 6191-6199.

12. Zhang G, Dykas S, Majkut M, Smołka K, Cai X. Experimental and numerical research on the effect of the inlet steam superheat degree on the spontaneous condensation in the IWSEP nozzle. International Journal of Heat and Mass Transfer. 2021.

13. Schneer GH, Mundinger G. Similarity, drag, and lift in transonic flow with given internal heat addition. European Journal of Mechanics - B/Fluids. 1993: p. 597-611.

14. Schneer GH, Dohrmann U. Drag and lift in non-adiabatic transonic flow. AIAA Journal. 1994: p. 101-107.

15. Schnerr GH. Homogene Kondensation in stationaeren transsonischen Stroemungen durch Lavalduesen und um Profile. Habilitationsschrift. Karlsruhe; 1986.

16. Goodheart KA, Dykas S, Schnerr GH. Numerical modelling of heterogeneous/homogeneous condensation on the ONERA M6 wing. In Proceedings of the 12th International Conference on Fluid Flow Technologies; 2003; Budapest. p. 335-342.

17. Goodheart KA. 3-D Transonic Flow Dynamics with Nonequilibrium Condensation Munich; 2004.

18. Schneer GH, Dohrmann U. Transonic flow around airfoils with relaxation and energy supply by homogeneous condensation. AIAA Journal. 1990: p. 1187-1193.

19. Adam S. In Adam S. Numerische und experimentelle Untersuchung instationarer Dusenstromungen mit Energiezufuhr durch homogene Kondensation. Karlsruhe; 1996.

20. Dykas S. Badania przepływów transonicznych z kondensacją pary wodnej Gliwice: Wydawnictwo Politechniki Śląskiej; 2006.

21. Wen C, Ding H, Yang Y. Optimisation study of a supersonic separator considering nonequilibrium condensation behaviour. Energy Conversion and Management. 2020.

22. Dykas S, Majkut M, Smołka K, Strozik M. Numerical analysis of the impact of pollutants on water vapour condensation in atmospheric air transonic flows. Applied Mathematics and Computation. 2018: p. 451-465.

23. Dykas S, Majkut M, Smołka K, Strozik M. Study of the wet steam flow in the blade tip rotor linear blade cascade. International Journal of Heat and Mass Transfer. 2018: p. 9-17.

24. Dykas S, Majkut M, Smołka K, Strozik M. Comprehensive investigations into thermal and flow phenomena occurring in the atmospheric air two-phase flow through nozzles. International Journal of Heat and Mass Transfer. 2017 November: p. 1072-1085.

25. Dykas S, Majkut M, Smołka K. Influence of Air Humidity on Transonic Flows with Weak Shock Waves. Journal of Thermal Science. 2019.

26. Wiśniewski P, Dykas S, Yamamoto S. Importance of Air Humidity and Contaminations in the Internal and External Transonic Flows. Energies. 2020 June.

27. Wiśniewski P, Dykas S, Yamamoto S, Pritz B. Numerical approaches for moist air condensing flows modelling in the transonic regime. International Journal of Heat and Mass Transfer. 2020;(162).

28. Wiśniewski P, Majkut M, Dykas S, Smołka K, Zhang G, Pritz B. Selection of a steam condensation model for atmospheric air transonic flow prediction. Applied Thermal Engineering. 2022.

29. Wiśniewski P, Dykas S, Pritz B. Numerical Studies of the Air Humidity and Pollution Importance in the Flow through the Gas Turbine's Rotor Compressor. In Proceedings of 14th European Turbomachinery Conference, Turbomachinery, Fluid Dynamics & Thermodynamics; 2021; Gdańsk.

30. Wen C, Ding H, Yang Y. Numerical simulation of nanodroplet generation of water vapour in high-pressure supersonic flows for the potential of clean natural gas dehydration. Energy Conversion and Management. 2021.

31. Dykas S, Wróblewski W. Two-fluid model for prediction of wet steam transonic flow. International Journal of Heat and Mass Transfer. 2013: p. 88-94.

32. Yamamoto S. Computation of practical flow problems with release of latent heat. Energy. 2005: p. 197-208.

33. Yamamoto S, Hagari H, Murayama M. Numerical simulation of condensation around the 3-D wing. Transactions of the Japan Society for Aeronautical and Space Sciences. 2000: p. 182-189.

34. Yamamoto S. Preconditioning method for condensate fluid and solid coupling problems in general curvilinear coordinates. Journal of Computational Physics. 2005: p. 240-260.

35. Yamamoto S, Moriguchi S, Miyazawa H, Furusawa T. Effect of inlet wetness on transonic wet-. International Journal of Heat and Mass Transfer. 2018: p. 720-732.

36. Moriguchi S, Endo T, Miyazawa H, Furusawa T, Yamamoto S. Numerical Simulation of Unsteady Moist-air Flows through Whole-annulus Rotor Blade Rows in Transonic Compressor. In Proceedings of the ASME-JSME-KSME 2019 8th Joint Fluids Engineering Conference AJKFluids2019 ; 2019; San Francisco.

37. Wiśniewski P, Zhang G, Dykas S. Numerical Investigation of the Influence of Air Contaminants on the Interfacial Heat Transfer in Transonic Flow in a Compressor Rotor. Energies. 2022.

38. Wiśniewski P, Dykas S, Majkut M, Smołka K, Nocoń M, Wittmann T, et al. A comprehensive analysis of the moist air transonic flow in a nozzle with a very low expansion rate. Applied Thermal Engineering. 2022.

39. Wiśniewski P, Dykas S, Yamamoto S, Pritz B. Numerical approaches for moist air condensing flows modelling in the. International Journal of Heat and Mass Transfer. 2020;(162).

40. Zhang G, Zhang X, Wang F, Wang D, Jin Z, Zhou Z. Numerical investigation of novel dehumidification strategies in nuclear plant steam turbine based on the modified nucleation model. International Journal of Multiphase Flow. 2019 November.

41. Zhang G, Zhang X, Wang F, Dingbiao W, Zunlong J. The relationship between the nucleation process and boundary conditions on non-equilibrium condensing flow

based on the modified model. International Journal of Multiphase Flow. 2019 May: p. 180-191.

42. Wittmann T, Bode C, Friedrichs J. The Feasibility of an Euler–Lagrange Approach for the Modeling of Wet Steam. J. Eng. Gas Turbines Power. 2021.

43. Wittmann T, Lück S, Bode C, Friedrich J. Modelling the Condensation Phenomena within the Radial Turbine of a Fuel Cell Turbocharger. Int. J. Turbomach. Propuls. Power. 2021.

44. Wittmann T, Lück S, Hertwig T, Bode C, Friedrichs J. The Influence of Condensation on the Performance Map of a Fuel Cell Turbocharger Turbine. In Conference: ASME Turbo Expo 2021: Turbomachinery Technical Conference and Exposition; 2021.

45. Zhang G, Zhang X, Wang F, Wang D, Jin Z, Zhou Z. Design and optimization of novel dehumidification strategies based on modified nucleation model in three-dimensional cascade. Energy. 2019 November.

46. Wen C, Karvounis N, Walther JH, Yan Y, Feng Y, Yang Y. An efficient approach to separate CO2 using supersonic flows for carbon capture and storage. Applied Energy. 2019.

47. Sun W, Cao X, Yang W, Jin X. Numerical simulation of CO2 condensation process from CH4-CO2 binary gas mixture in supersonic nozzles. Separation and Purification Technology. 2017: p. 238-249.

48. Wen C, Ding H, Yang Y. Performance of steam ejector with nonequilibrium condensation for multi-effect distillation with thermal vapour compression (MED-TVC) seawater desalination system. Desalination. 2020.

49. Wen C, Gong L, Ding H, Yang Y. Steam ejector performance considering phase transition for multi-effect distillation with thermal vapour compression (MED-TVC) desalination system. Applied Energy. 2020.

50. Pruppacher HR, Klett JD. Microphysics of clouds and precipitation: D. Reidel Publishing Company; 1980.

51. Dohrmann U. Ein numerisches Verfahren zur Berechnung stationärer transsonischer Strömungen mit Energiezufuhr durch homogene Kondensation. Dissertation. Karlsruhe; 1989.

52. Sonntag D, Heinze D. Sättigungsdampfdruck- und Sättigungsdampfdichtetafeln für Wasser und Eis Lepizig: VEB Deutscher Verlag für Grundstoffindustrie; 1982.

53. Baek SC, Kwon SB, Kim HD, Setoguchi T, Matsuo S. Study of the Unsteady Condensation of Moist Air in Shock Tube. Journal of Thermal Science. 2004: p. 235-244.

54. ANSYS Fluent Theory Guide, 2021R1. [Online]. [cited 2021 July 1. Available from: https://www.ansys.com/.

55. Menter FR. Two-equation Eddy-Viscosity Turbulence Models for Engineering Applications. AIAA Journal. 1994: p. 1598-1605.

56. Wiśniewski P, Dykas S, Yamamoto S. Importance of Air Humidity and Contaminations in the Internal and External Transonic Flows. Energies. 2020 June.

57. Ferro A, Kopperud R, Hildemann L. Elevated personal exposure to particulate matter from human activities. Journal of Exposure Analysis and Environmental Epidemiology. 2004: p. 34-40.

58. Kantrowitz A. Nucleation in very rapid vapor expansions. J. Chem. Phys.`. 1951: p. 1097-1100.

59. Hill PG. Condensation of water vapour during supersonic expansion in nozzle. Journal of Fluid Mechanic. 1966.

60. Chris N, Julianne D. NPARC Alliance Validation Archive. [Online].; 2008 [cited 2020 April 23. Available from: https://www.grc.nasa.gov/WWW/wind/valid/raetaf/raetaf05/raetaf05.html.

61. Moses CA, Stein GD. On the growth of steam droplets formed in a Laval nozzle using both static pressure and light scattering measurements. NASA STI/Recon, Tech. Rep. N. 77 (3). 1978: p. 311-322.

62. Dykas S, Majkut M, Smołka K, Strozik M. Condensation wave identification in moist air transonic flow through nozzles. Transactions of the Institute of Fluid-Flow Machinery. 2016: p. 67-77.

63. Dykas S, Majkut M, Smołka K, Strozik M. Experimental research on wet steam flow with shock wave. Experimental heat transfer. 2015: p. 417-429.

64. Dykas S, Majkut M, Strozik M, Smołka K. Experimental study of condensing steam flow in nozzles and linear blade cascade. Internationa Journal of Heat and Mass Transfer. : p. 50-57.

65. Witoszyński E. Über Strahlerweiterung und Strahlablenkung Berlin: Springer; 1924.

66. Wiśniewski P, Dykas S, Zhang G. Numerical studies of air humidity importance in the first stage rotor of turbine compressor. Archives of thermodynamics. 2020: p. 223-234.

67. Denton JD. Loss Mechanisms in Turbomachines. Transactions of the ASME. 1993.

68. Stazisar A, Wood J, Hathaway M, Suder K. Laser Anemometer Measurements in a Transonic Axial-Flow Fan Rotor. NASA Technical Paper 2879. 1989.

69. Suder KL. Experimental Investigation of the Flow Field in a Transonic, an Axial Flow Compressor With Respect to the Development of Blockage and Los. NASA/CR—2010-216235. Cleveland: National Aeronautic and Space Administration; 1996.

70. Reid L, Moore RD. Design and Overall Performance of Four Highly Loaded, High-Speed Inlet Stages for an Advanced High-Pressure-Ratio Core Compressor. Technical Paper. Cleveland: National Aeronautics and Space Administration, Lewis Research Center; 1978.

71. Denton JD. Lessons from Rotor 37. Journal of Thermal Science. 1996.

72. Muhammad S, Flecker B, Leitgeb E, Gebhart M. Characterization of fog attenuation in terrestrial free space links. Optical Engineering. 2007.

List of Figures

List of Tables

Abstract

Multiphase flows with a phase transition are ubiquitous both in the environment and in engineering. The phase transition from steam to liquid water is the best-known case of condensation. It occurs when a decrease in pressure or temperature causes steam to cross the saturation line. Condensation is important for efficient design of machinery and equipment in many industries. Traditionally, research on condensation has focused on pure steam flows. Recently, however, there has been a significant increase in interest in the condensation of air-steam mixtures. The existing numerical methods are only reliable for pure steam flows. They require further development to account for condensation in air-steam mixtures. In nature, expansion and condensation occur slowly. In expanding flows in engineering, the drop in pressure or temperature is much faster, and a thermodynamic non-equilibrium is often established. When the supercooling is strong enough, homogeneous nucleation occurs. In this case, nuclei form directly from steam. Once these nuclei reach the critical radius, they grow rapidly as the surrounding supercooled steam condenses onto the droplets. Therefore models typically rely on calibration with validation cases such as supersonic nozzle flows. Such cases of profound validation have been published for several pure steam flows, but only a few air nozzles with high expansion rates have so far been investigated.

The first goal of this work was to fill this gap. An experimental study of the humid air flow in a nozzle with a low expansion rate was carried out. It was performed for different ambient conditions for the supersonic flow and for the transonic flow, i.e. the flow in which a shock wave appears due to the flow supersonic-to-subsonic transition. The experiments were carried out using the existing low-pressure test rig at the Department of Power Engineering and Turbomachinery of the Silesian University of Technology. The stand was extended with a new test section. The experimental results provided a validation case for the considered condensation model. Moreover, the nozzle geometry with all the data is available as a benchmark test for expanding condensing flows.

The second goal of this work was a thorough analysis of the reliability of available condensation models for the humid air flow. In the past, condensation models were developed for pure steam and were not applied for studies of humid air. Nevertheless, with the increasing interest in condensation in humid air, the accuracy of the existing models was investigated. This resulted in an overview of common approaches and proved that the condensation model must not be chosen arbitrarily. It should be selected based on the considered problem. A *blend* model, based

on the kinetic molecular model and the continuous model, was distinguished because it favours the physical correctness for small droplets, while maintaining the condensation prediction for large ones.

The next goal was to study the influence of condensation on the performance of modern turbomachinery. After a reliable tool was obtained for the investigation of condensation in internal and external flows, a comprehensive study was conducted with a focus on the work of the first stage of the compressor of a turbine and the fan of a turbofan engine. It includes a numerical analysis of condensation, as well as evaporation occurring in rotating machines working on atmospheric air that contains solid and liquid suspended particles. It is shown that the phase change significantly affects the flow in the blade-to-blade channel. Condensation decreases the local velocity, whereas evaporation on the shock wave triggers opposite phenomena, leading to a shift of the shock wave downstream the flow. Together with the drop in the fluid density due to the presence of steam, which is often neglected in the numerical study of turbomachinery, this leads to significant changes in the fluid parameters at the outlet of the rotor stage. As a result, it affects the performance and efficiency of the machinery under consideration.

Finally, the Euler- and the Lagrange-based approach were compared and a superposition of both models was proposed. This demonstrates the significant impact of the numerical approach on the investigated phenomena. The pros and cons of both models are discussed and a superposition model combining the advantages of the two approaches is proposed. This shows a scientific gap which has a great potential for the development of condensing models and indicates the need for further studies.

Summing up, the results of the presented experimental and numerical analysis of condensation in expanding flows show a significant impact of the phenomenon. The phase-change phenomena lead to a local change in the flow structure, which affects the entire flow system. Both homogeneous and heterogeneous condensation might lead to a decrease in the efficiency of rotating machines and devices, which is a solid basis for the statement that phase-change phenomena have to be taken into consideration in the study and design of transonic flow systems.

Streszczenie

Przepływy wielofazowe z przemianą fazową są wszechobecne zarówno w środowisku, jak i w inżynierii. Najbardziej znanym przypadkiem kondensacji jest przejście fazowe wody z pary do cieczy, które występuje gdy ciśnienie i temperatura spadają poniżej parametrów nasycenia. Kondensacja jest istotna przy projektowaniu wysoko sprawnych maszyn i urządzeń w wielu gałęziach przemysłu. Tradycyjnie badania nad kondensacją koncentrowały się na przepływach czystej pary. W ostatnim czasie obserwuje się jednak znaczny wzrost zainteresowania kondensacją mieszanin powietrzno-parowych. Istniejące metody numeryczne są niezawodne tylko dla przepływów czystej pary i wymagają dalszego rozwoju w celu badania kondensacji w mieszaninach powietrzno-parowych. W naturze parowanie i kondensacja zachodzą powoli. Przy okołodźwiękowych przepływach w aplikacjach technicznych spadek ciśnienia i temperatury jest znacznie szybszy i często dochodzi do powstania nierównowagi termodynamicznej. Gdy przechłodzenie jest wystarczająco silne, następuje proces nukleacji, t.j. zarodki powstają bezpośrednio z pary. Gdy jądra te osiągną wielkość krytyczną, otaczająca je przechłodzona para skrapla się na ich powierzchni co skutukuje ich szybkim wzrostem. Przemianom fazowych towarzyszy uwalnianie bądź absorpcja ciepła utajonego, zjawiska te wywierają znaczący wpływ na charakter przepływu. Wykorzystywane modele kondensacji opierają się na kalibracji z danymi eksperymentalnymi, takimi jak na przykład przepływy okołodźwiękowe w dyszach. Takie przypadki dogłębnej walidacji zostały opublikowane dla kilku przepływów czystej pary, ale do tej pory zbadano tylko kilka dysz powietrznych o dużej szybkości rozprężania.

Pierwszym celem tej pracy było wypełnienie luki w badaniach eksperymentalnych dlatego wykonano pomiary przepływu wilgotnego powietrza w dyszy o małej szybkości rozprężania. Badania zostały przeprowadzone dla różnych warunków otoczenia dla przepływu naddźwiękowego i transsonicznego, czyli przepływu, w którym pojawia się fala uderzeniowa w wyniku przejścia naddźwiękowo-poddźwiękowego. Eksperymenty przeprowadzono z wykorzystaniem istniejącego stanowiska niskociśnieniowego w Katedrze Maszyn i Urządzeń Energrtycznych Politechniki Śląskiej rozbudowanego o nową sekcję testową. Wyniki eksperymentalne stanowiły podstawę do walidacji rozważanego modelu. Ponadto geometria dyszy ze wszystkimi danymi została udostępniona jako test wzorcowy dla przepływów kondensacyjnych.

Silesian University of Technology
Department of Power Engineering and Turbomachinery
44 -100 Gliwice, ul. Konarskiego 18

Drugim celem pracy była analiza dokładności dostępnych modeli kondensacji dla przepływu wilgotnego powietrza. W przeszłości modele kondensacji były opracowywane dla pary czystej i nie były stosowane do badań wilgotnego powietrza. Niemniej jednak, obserwowany jest wzrost zainteresowania kondensacją w mieszaninach powietrzno-parowcyh. Dlatego przeprowadzono przegląd powszechnie stosowanych modeli i wykazano, iż model kondensacji nie może być wybierany arbitralnie. Dobór modelu przemian fazowych powinien być dobrany do badanego zagadnienia. W tej pracy wyróżniono model mieszany, oparty na modelu kinetycznym i modelu ciągłym, który faworyzuje poprawność fizyczną dla małych kropel jednocześnie zachowując dokładność dla kropel dużych.

Kolejnym celem było zbadanie wpływu przemian fazowcyh na pracę nowoczesnych maszyn wirnikowych. Po uzyskaniu wiarygodnego narzędzia do badania kondensacji w przepływach wewnętrznych i zewnętrznych przeprowadzono kompleksowe badania, skupiające się na wpływie kondensacji oraz parowania na pracę pierwszego stopnia sprężarki turbiny i wentylatora silnika turbowentylatorowego. Przeprowadzono analizę numeryczną zjawisk zachodzących w maszynach wirnikowych, których płynem roboczym jest powietrze atmosferyczne zawierające cząstki stałe i ciekłe. Wykazano, że zjawiska fizyczne towarzyszące przemianie fazowej istotnie wpływają na przepływ w kanale międzyłopatkowym. Uwalnianie ciepła utajonego na skutek kondensacja powoduje wzrost temperatury oraz ciśnienia, co skutkuje spadkiem lokalnej prędkości. Z drugiej strony absorpcja ciepła utajongo, która towarzyszy parowaniu kropel występującemu na fali uderzeniowej wyzwala zjawiska przeciwne, prowadzące do przesunięcia fali uderzeniowej w dół przepływu. Dodatkowo, wykazano iż spadek gęstości płynu na skutek obecności pary wodnej, często pomijany w badaniach numerycznych, implikuje znaczną zmianę parametrów płynu co wpływa to na process ekspansji a w w rezultacie także na sprawność rozważanych maszyn.

Na koniec porównano podejście Eulera i Lagrange'a i zaproponowano superpozycję obu modeli. Zaprezentowane wyniki świadczą o istotnym wpływie podejścia numerycznego na otrzymywanie wyniki wykorzsystujac ten sam modelu fizyczny danego zjawiska. Omówiono zalety i wady obydwu modeli oraz zaproponowano model superpozycji łączący zalety obu podejść. Wskazuje to na lukę naukową, która ma duży potencjał dla rozwoju modeli kondensacyjnych i wskazuje potrzebę dalszych badań.

Podsumowując, wyniki przedstawionych eksperymentalnej i numerycznej analizy przemian fazowych wskazują na istotny wpływ tego zjawiska na charakter przepływów

okołodźwiękowych. Zjawiska przemiany fazowej prowadzą do lokalnej zmiany parametrów płynu oraz charakteru przepływu, co wpływa na cały układ przepływowy. Zarówno jednorodna, jak i niejednorodna kondensacja może prowadzić do obniżenia sprawności maszyn i urządzeń, co jest solidną podstawą do stwierdzenia, że w badaniach i projektowaniu układów przepływowych należy brać pod uwagę zjawiska przemian fazowych.